Dissertation zur Erlangung des Doktorgrades

der Fakultät für Chemie und Pharmazie

der Ludwig-Maximilians-Universität München

Protein Transduction by Lipo-Oligoaminoamide Nanoformulations

Peng Zhang

aus

Taian, Shandong, China

2017

Erklärung

Diese Dissertation wurde im Sinne von § 7 der Promotionsordnung vom 28. November 2011 von Herrn Prof. Dr. Ernst Wagner betreut.

Eidesstattliche Versicherung

Diese Dissertation wurde eigenständig und ohne unerlaubte Hilfe erarbeitet.

München, 01.06.2017

.....

Peng Zhang

Dissertation eingereicht am 01.06.2017

1. Gutachter: Prof. Dr. Ernst Wagner

2. Gutachter: Prof. Dr. Wolfgang Frieß

Mündliche Prüfung am 25.07.2017

Meiner Familie

子曰：“知之者不如好之者，好之者不如乐之者。”

——《论语•雍也》

The Master said, "They who know the truth are not equal to those who love it, and they who love it are not equal to those who delight in it."

—— *Confucian Analects-Yong Ye*

translated by James Legge

Table of Contents

1 Introduction

Section 1.4 has been partly adapted from: Peng Zhang and Ernst Wagner, History of Polymeric Gene Delivery Systems. Topics in Current Chemistry 375 (2):26.

1.1 Proteins as therapeutic agents

Proteins have been evolutionarily chosen to perform specific functions in human body, including composing cell structures or tissue scaffolds, catalyzing various biochemical reactions, regulating immune responses, and transporting biomolecules in single cell or among organs [1]. Many diseases derive from the abnormal structures or undesirable expression level of proteins. Therefore, protein therapeutics present great potency in the treatment of various diseases [1, 2]. The advantages of protein therapeutics include higher functional specificity and less adverse effects over small-molecule drugs [1], meanwhile, protein therapeutics will not elicit permanent or random genetic alterations in cell genome, and have lower genetic risk, which make protein therapeutics a safer alternative to gene therapy [3]. Since the introduction of human insulin (the first recombinant protein therapeutic) in 1982, a considerable number of protein therapeutics have been developed and applied in disease therapy, such as metabolic and endocrine disorders, autoimmune diseases and malignant tumors [1, 2].

Among the protein therapeutics, monoclonal antibodies came out as outstanding and promising representatives for the protein-based therapy since the approval of CD3-specific monoclonal antibody in 1986 [4, 5]. The number of approved monoclonal antibody in the Europe and US had dramatically increased to forty-seven by 2014 for the treatment of various diseases [5]. For example, bevacizumab [6-9], a humanized monoclonal antibody that could bind a variety of isoforms of vascular endothelial growth factor A (VEGFA), could be used to treat non-small-cell lung cancer and colorectal cancer; Adalimumab [10, 11], a human monoclonal antibody, could block

the interaction between tumor necrosis factor α (TNFα) and its receptors, inhibit inflammatory responses, and then improve rheumatoid arthritis. Especially, the recent approval of Pembrolizumab and Nivolumab which target the programmed cell death protein 1 (PD-1) and the approval of Atezolizumab which targets the programmed death-ligand 1 (PD-L1) by the US Food and Drug Administration (FDA) were considered as great successes in the cancer immunotherapy [12].

Besides antibody-based protein drugs, other molecular types of proteins are also used for therapy and diagnostic of human diseases. For instance, human albumin [13] has been used to treat hypoproteinaemia or nephrotic syndrome via increasing the osmolarity of circulating plasma and sustaining circulating blood volume; Interferon-γ1b (IFNγ) [14-18] could enhance antimicrobial response and inflammatory response, and has been applied in the treatment of osteopetrosis and granulomatous disease. Human follicle-stimulating hormone (FSH) [19, 20] has been used to assist reproduction by augmenting ovulation. Collagenase [21, 22] could be used to debride the necrotic tissues of wounds such as dermal ulcers or burn via digesting collagen; Recombinant hirudin [23, 24] could inhibit the bioactivity of thrombin, and has been used to treat heparin-induced thrombocytopaenia. Noninfectious surface antigen of hepatitis B virus [25, 26] has been widely used as vaccine for hepatitis B vaccination to prevent hepatitis B infection. The diagnosis of abnormal GH secretion could be performed with recombinant growth hormone releasing hormone (GHRH) [27, 28] fragment. Additionally, HIV antigens [29-31] could be used to diagnose HIV infection by the detection of HIV antibodies in human body.

As mentioned above, notably, clinically applied proteins therapeutics are limited to those exerting bioactivities extracellularly, a large number of protein biologics which perform functions intracellularly have not been well developed or widely applied in clinical trials. Therefore, any technology to delivery specifically intact and functional proteins into cytosol or subcellular targets presents a tremendous potential for future

development of novel protein therapeutics and has great commercial significance [32]. In light of this, a variety of delivery technologies have been developed and optimized towards a safe and efficient targeted intracellular protein delivery system, such as lipid nanoparticles [33-35], nanocapsules [36-39], polymersomes [40, 41], nanogels [42, 43], polymer micelles [44, 45], or coupling with cell-penetrating peptides [46-48]. While great effort has been made, the clinical development of intracellular protein delivery technologies is still in its infancy. However, with the continuous progress of nanobiotechnology and the development of novel intracellular protein delivery approaches, it is predictable that targeted intracellular protein delivery will be applied in the clinical treatment of human diseases with higher safety and efficacy.

1.2 Barriers for protein delivery

Many protein therapeutics have been successfully applied in the treatment of various human diseases [1, 2]. However, some challenges limit the development and application of potential protein therapeutics. For example, the scale up production of bioactive proteins with precise post-translational modifications [49] should be gained to meet the demand of research and marketing. Meanwhile, the development of commercial protein expression systems which have the capacity of large-scale expression of appropriately modified proteins, such as bacteria, yeast and mammalian cells [50-52], requires enormous time and fund. The intrinsic properties of proteins also make the way rocky to their therapeutic applications, such as the large sizes, fragile and complicated tertiary structures, varying surface charges and susceptibility to protease degradation [1, 53-55]. Therefore, appropriate formulation of protein biologics should be investigated and developed, improper formulation or modification of native proteins can provoke denaturation, degradation or precipitation of the protein molecules [55]. Regard to in vivo application, the native proteins can also be recognized by immune system, and then lose the bioactivities if neutralized by neutralizing antibodies or degraded by endolysosomal proteases after internalization

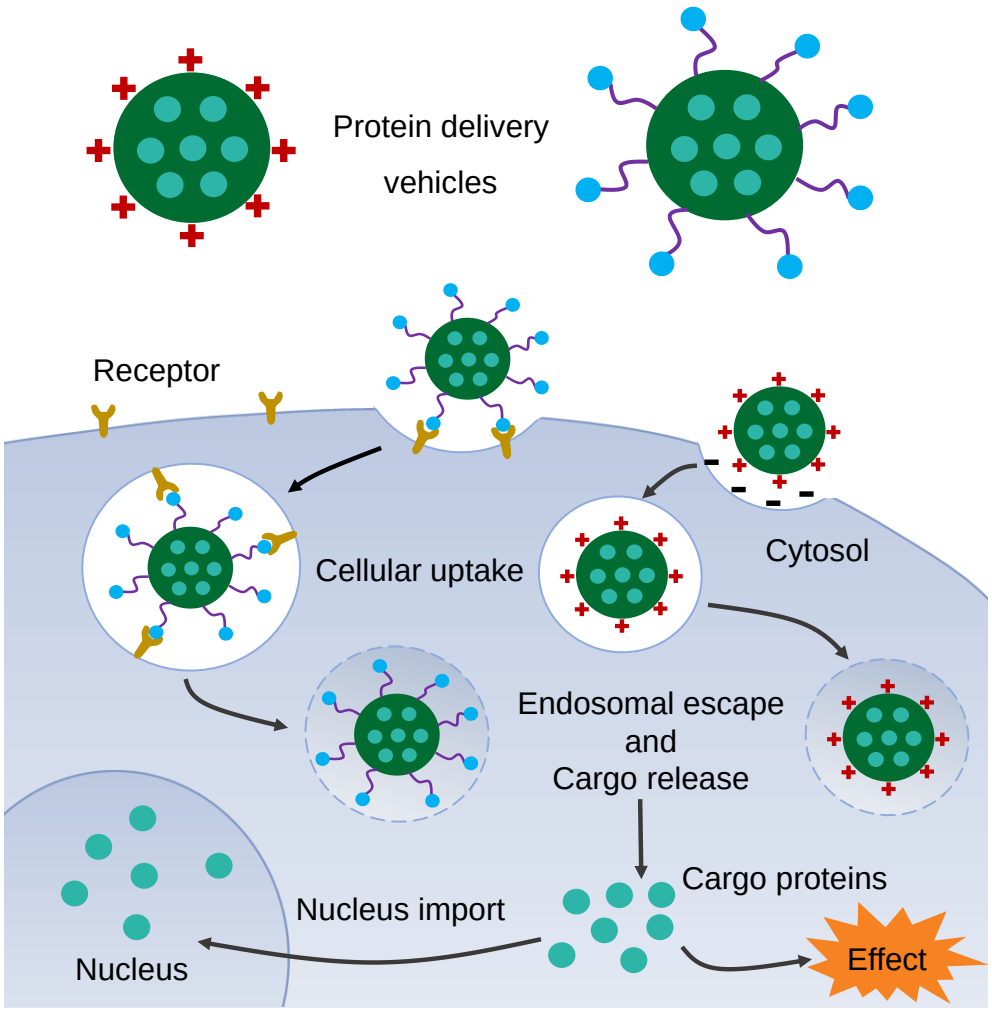

Scheme 1.1 Cellular barriers for intracellular protein delivery.

by phagocytes [1, 56]. Proteins with small molecular weight could suffer from the rapid renal clearance from the blood circulation, and may not reach the target cells, tissues or organs [1, 53]. Meanwhile, unlike the hydrophobic small-molecule drugs, most of the native proteins cannot diffuse into the cell because of their large sizes and electrostatic repulsions to cell membrane [57, 58]. Another barrier for intracellular protein delivery is the endosomal sequestration, if the internalized proteins cannot escape from the endolysosomes, they will be degraded by the proteases in the lysosomes [36, 58]. Therefore, to maintain the bioactivity in the cytosol or reach the targeted subcellular organelles, such as the nucleus or the mitochondria, the delivered proteins must escape from the endolysosomes [59]. To cope with these

barriers, appropriate protein delivery platforms or strategies should be developed [54]. These delivery systems should appropriately formulate the proteins without affecting the native bioactivities of proteins, protect the protein in the blood circulation from dissociation from the delivery platform or inactivation by the immune system, decrease renal clearance to prolong the circulation half-life, meanwhile specifically deliver proteins to the targeted cells, tissues or organs, and then mediate precise “on demand” release of cargo protiens to decrease the side effects and improve efficacy of protein therapeutics [54, 55, 58, 60]. For the development of intracellular protein therapeutics, these systems must also mediate highly efficient targeted cellular internalization, effective endolysosomal escape to avoid being degraded by lysosomal proteases, timely release of proteins into the cytosol from the delivery systems responding to intracellular stimuli like reducing cytosolic enviroment and following subcellular traffic to specific subcellular sites to exert biological functions (Scheme 1.1) [54, 58, 61].

1.3 Strategy for intracellular protein delivery

Intracellularly functional proteins present a promising subclass of protein therapeutics. However, due to limited efficiency of delivery technologies, the therapeutic application of intracellularly functional proteins is still in its infancy. Immunotoxins [62, 63] have been investigated in the treatment of cancer patients [64]. Onconase [65] is a member of the ribonuclease A (RNase A) superfamily [64, 66, 67], which can degrade the cytosolic RNA after internalization by cancer cells and induce tumor cell killing, has been also evaluated in clinical trials. In general, inefficient cellular uptake and especially endolysosomal sequestration hinder effective protein delivery into the cellular cytosol. Cargo proteins are mostly trapped and degraded in the endolysosomes without reaching the subcellular target sites to exert subsequent biological actions. Therefore, novel and potential delivery technologies are highly demanded to deal with the encouraging future opportunities of intracellular protein transduction [68].

Among the traditional methods, electroporation and microinjection could directly deliver proteins into the cellular cytosol. These methods are invasive and will damage the cell membrane [69, 70], which make them difficult for in vivo application to unaccessible targeted cells, tissues or organs [61]. Cell-penetrating peptides (CPPs) mediated protein delivery is another most widely used method for intracellular protein transduction [71, 72]. CPPs can be conjugated to cargo proteins via recombinant protein technology or chemical post-modification [71, 72]. A variety of CPPs [73] have been developed and investigated for their potency in intracellular delivery of various protein cargoes [74, 75], such as cytokines and enzymes [61]. The main obstacle of CPP-mediated intracellular protein delivery is the endolysosomal sequestration of CPP-tagged cargo proteins [76, 77].

Benefitting from the advances of nanotechnology, nanocarrier-based [78, 79] intracellular protein delivery has been considerably developed and presents several advantages as protein carriers [68]. First, nanocarriers can protect cargo proteins from denaturation or enzymatic degradation in biological environment [78, 80, 81]. Second, nanocarriers can prolong the half-life of proteins in blood circulation by increasing the size of the protein formulations and reducing renal clearance [78, 82, 83]. Third, nanocarriers provide higher flexibility of chemical synthesis and modifications to improve the physical and chemical properties of the nanoparticles, such as the size, zeta-potential, and allow ligand modification for targeted delivery to specific cells, tissues or organs [84-86]. Cargo proteins can be loaded into the nanocarrieers by covalent conjugation, encapsulation and physical adsorption [68]. Among these nanocarriers, inorganic nanoparticles [68, 87], liposomes [88, 89], lipid nanoparticles [33-35], nanocapsules [36-39], polymersomes [40, 41], nanogels [42, 43], polymer micelles [44, 45], or protein-based carriers [90-93], have been pursued.

Inorganic materials, such as carbon nanotubes [87, 94], quantum dots [95], gold nanoparticles [96], silica nanoparticles [97, 98] or magnetic nanoparticles [99], have

been used as nanocarriers for intracellular protein delivery. For example, Dai and colleagues first used single-walled carbon nanotubes (SWNTs) to deliver streptavidin into a variety of cell lines [94]. They also used this platform to deliver cytochrome c into NIH-3T3 cells, resulting in programmed cells death [100]. However, inorganic materials usually have low endosomal escape, and cannot be degraded in vivo, which may result in cumulative toxicity.

Liposomes are among the commonly used lipid-based nanoparticles and have been investigated as nanocarriers for various protein delivery [61]. For example, oligoarginine-modified liposomes effectively delivered β-galactosidase into the cytosol with a bioactive form [101]. Lysine containing cationic liposomes could mediate effective transduction of antibodies and albumin into cytosol through coveolae-mediated endocytosis [102].

Xu et al. developed a novel protein delivery system based on the combinatorial library chemistry, the synthesized cationic lipid-like nanoparticles could efficiently delivery reversibly chemically modified proteins including RNase A and saporin into the cancer cells, resulting in both in vitro and in vivo antitumor activities [34]. They also developed combinatorial bioreducible lipid nanoparticles as the delivery platform for genome-deiting proteins. With this platform, they successfully delivered the Cas9:sgRNA complexes and Cre recombinase into human cells enabling effective genome editing and gene recombination with higher efficiencies than 70%. Meanwhile, they demonstrated effective gene recombination in mouse brain after in vivo Cre recombinase delivery [33]. Liu et al. used common cationic lipids to deliver genome-editing proteins such as Cas9:sgRNA complexes and Cre recombinase, and achieved efficient genome editing both in vitro and in vivo [35].

As mentioned above, endolysosomal sequestration is a main barrier for effective intracellular protein delivery, therefore, direct delivery of cargo proteins into the cytosol is supposed as an efficient method to conquer endosomal entrapment. Rotello

and colleagues developed nanoparticle-stabilized nanocapsules to deliver directly the green fluorescent protein and caspase-3 protein into the cytosol via a membrane fusion-like pathway, where the GFP presented homogeneous green fluorescence throughout the cells and CASP3 mediated effective cell apoptosis, validating effective cytosolic delivery of proteins as bioactive forms [36]. With GIPA AuNPs-stabilized nanocapsules, they could also directly deliver high molecular weight proteins including dsRed (112 kD) and β-galactosidase (464 kD) into the cytoplasma without blocking their biocativites, avoiding endosomal sequestration [103].

Yan et al. recently developed an intracellular protein transduction method using in situ polymerization-based encapsulation that occurs on the surface of single protein molecule to form single-protein nanocapsules [38]. With this platform, they could efficiently encapsulate various proteins into the nanocapsules, such as enhanced green fluorescent protein (EGFP), bovine serum albumin (BSA), horseradish peroxidase (HRP), caspase-3 (CAS) and superoxide dismutase (SOD). The EGFP nanocapsules mediated efficient cellular uptake, and a 50 h retention of intense fluorescence after injection into the mice. Gu et al. further improved the preparation of single-protein nanocapsules by encapsulating the single protein molecule with enzymatically degradable polymer shell, which could be degraded by proteases. They also used the physical adsorption instead of the covalent pre-modification on the surface of proteins to perform in situ polymerization. The degradable caspase-3 nanocapsules could induce cell apoptosis in tested cancer cells [39].

Polymersomes provide another type of carrier for efficient intracellular protein delivery, which consists of amphipathic block copolymers and separate the aqueous interior from the outside solution through hydrophobic membranes [104-106]. Zhong et al. synthesized novel biodegradable chimaeric polymersomes with asymmetric poly (ethylene glycol)-b-poly(ε-caprolactone)-b-poly(2-(diethylamino) ethyl methacrylate) (PEG-PCL-PDEA) triblock copolymers using varying molecular weights of PDEA

blocks. Different from the outer longer PEG block (M_n= 5 kg/mol), the inside shorter PDEA cationic blocks (M_n= 1.1-4.1 kg/mol) are supposed to facilitate the protein encapsulation efficiency. Meanwhile, the hydrophobic PCL blocks are biodegradable and present no cytotoxicity. As a result, the polymersome with the PDEA blocks having a molecular weight of 2700 presented highest protein loading efficiency and could efficienly deliver FITC labeled cytochrome into the cytosol of RAW 264.7 cells [40]. In order to achieve cancer-targeting protein delivery systems, they further developed a Acupa modified pH-responsive chimaeric polymersomes (Acupa-CPs) based on Acupa-PEG-PTMBPEC-PSAC triblock copolymers, namely, 2-[3-[5-amino-1-carboxypentyl]-ureido]-pentanedioic acid-poly(ethylene glycol)-b-poly(2,4,6-trimethoxybenzylidene-pentaerythritol carbonate)-b-poly (succinic acid carbonate). With PSMA-targeting Acupa-CPs, they efficiently deliver therapeutic cargo proteins including cytochrome C and granzyme B into the PSMA over-expressed prostate cancer cell line, LNCaP cells, resulting in specific anticancer effects [41].

Zhong et al. also developed a hyaluronic acid based nanogel platform for intracellular protein delivery by the combination of “tetrazole-alkene” photoclick reaction and inverse nanoprecipitation. This protein delivery platform showed effective growth inhibition of orthotopic A549 human lung tumor or MCF-7 human breast tumor after treatment with granzyme B or cytochrome c loaded hyaluronic acid nanogels [42, 43].

Kataoka et al. developed a new protein delivery method based on a core-shell structured charge-conversional polyionic complex (PIC) micelles with a size of 50 nm by electrostatic interactions between the cationic block copolymer PEG-pAsp(DET), namely, PEG-poly[N-(N'-(2-aminoethyl)-2-aminoethyl)aspartamide] and the cis-aconitic anhydride or citraconic anhydride modified cationic protein cytochrome c. The modifications of cytochrome c were supposed to tune the surface charge of proteins to decrease the pI value. The PIC micelles presented a charge-conversional

property because the cis-aconitic amides and citraconic amides are labile at the acidic endosomal pH 5.5 but keep stable at the physiological pH 7.4. The PIC micelles exhibited efficient endosome escape and effectively delivered the cytochrome c protein into the cysosol of HuH-7 cells [107].

Supercharged proteins are a kind of naturally occurring or engineered proteins, they have unusually high negative or positive net theoretical charge (typically more than 1 net charge unit per kD of protein molecular weight) [61]. Superpositively charged engineered GFP variants have been reported in the previous studies for the intracellular delivery of bioactive proteins into the mammalian cells both in vitro and in vivo based on their potent membrane penetrating ability [108]. Also, a variety of naturally occurring superpositively charged human proteins have the capacity to deliver bioactive proteins into the mammalian cells both in vitro and in vivo [109, 110]. Virus-like particles (VLPs) provide another strategy for intracellular protein delivery. VLPs consist of viral capsid proteins and have no virus genome, replicating ability and pathogenicity [92]. Cargo proteins can be encapsulated into VLPs via fusing with the anchoring protein [90, 91]. Reiser and colleagues efficiently encapsulated foreign proteins into polyomavirus-like particles and achieved effective intracellular delivery of GFP [111].

1.4 Development of sequence defined oligomers for protein delivery

Although a variety of strategies have been developed and investigated for their efficiency on therapeutic delivery of protein biologics. One always should keep in mind that the final destination of our design on macromolecule (nucleic acids or proteins) delivery system is for clinical application. Therefore, pharmaceutical precision of the protein delivery system has great significance and needs to be carefully considered. Inspired by the natural organisms that synthesize proteins in defined sequences based on the genetic sequence information stored in nucleic acids, also benefit from the great advances of macromolecular chemistry based on solid-phase-assisted

synthesis, sequence-based macromolecular synthesis can be realized via sequenced assembly of artificial subunits or nature-derived amino acids or lipids [112, 113]. In light of this, Schaffert and colleagues designed and synthesized novel artificial amino acid building blocks (e.g. succinoyl tetraethylene pentamine, Stp; succinoyl pentaethylene hexamine, Sph) [114, 115]. These artificial oligoamino acids protected by Fmoc and tBoc contain a few repeats of the effective aminoethylene motif that mediate the proton sponge effect in PEI [116, 117]. Using these artificial oligoamino acids, and combined with commercial Fmoc-protected amino acids or fatty acids, a variety of sequence defined cationic oligomers were assembled into precise sequences using solid-phase-assisted synthesis technology with high pharmaceutical precision, which are defined and reproducible in size, topology (linear, two-arm, three-arm, four-arm, or PEGylated two-arm architectures with targeting liagnads), coupling order and sites of subunits [114, 118]. All these elements play a crucial role in the transfection efficiency of oligomers. Therefore, in addition to pharmaceutical precision, synthesis of sequence defined oligomers is also significant for the investigation of structure–activity relationships. These sequence defined cationic oligomers presented efficient ability in the pDNA and siRNA delivery [114, 115]. Therefore, they are supposed to have the potency as delivery domains in conjugates of proteins or other drugs [119]. In initial work, one sequence-defined three-arm cationic oligomer had been conjugated with proteins by bioreducible disulfide linkage [120] or a pH-sensitive traceless click linker [121], and resulted in successful delivery of nlsEGFP or β-galactosidase into cells.

1.5 Aim of thesis

Protein therapeutics [1] have gained increasing attention due to their great potential in the treatment of many diseases. For cancer, they may provide a higher functional specificity and less genetic risks than standard nontargeted chemotherapies. Clinically applied proteins therapeutics however are limited to those exerting bioactivities extracellularly, intracellularly active proteins as a therapeutic subclass still is in its early stage due to delivery problems. The particular crucial barriers include specific delivery to the targeted cells, highly efficient cellular internalization, effective endolysosomal escape, timely release of proteins from the delivery system and following subcelluar traffic to specific subcellular sites [54, 58, 61]. Among these barriers, especially endolysosomal entrapment hampers effective protein transduction into the cytosol. Cargo proteins are largely trapped and degraded in the endolysosomes without access to the subcellular target sites for subsequent biological actions. Therefore, novel delivery technologies are required to cope with these barriers via combing multiple functions. Precise sequence-defined oligomers have been designed and synthesized and contain various moieties and functions in our laboratory using solid-phase synthesis technology [114, 115]. In light of this, the thesis focuses on the development of novel nanoformulations for targeted intracellular protein delivery based on sequence-defined mutifunctional lipo-oligoaminoamides.

The first aim of the thesis was to screen sequence-defined oligomers for enhanced targeted intracellular protein transduction and cancer therapy with effective endosomal escape and investigate the structure-activity relationships. For this purpose, 16 PEGylated two-arm or four-arm oligomers optionally containing folic acid for cell receptor targeting were selected and had to be evaluated for targeted intracellular protein transduction. Different artificial amino acid building blocks, as well as protonatable histidines, or oleic acids were included to enhance endosomolytic ability. All these oligomers had to be coupled to nlsEGFP or RNase A by disulfide

bonds, respectively. The disulfide linkages are supposed to be cleaved in the reducing cytosolic environment after endolysosomal escape [122-126]. The targeted intracellular transduction efficiency of nlsEGFP and RNase A via these oligomers had to be evaluated and compared to identify the potent transduction carrier, meanwhile, structure-activity relationships of these oligomers were also investigated.

The second aim of the thesis was to screen and optimize the lipo-oligomer nanoformulations by formulating the most effective oligomer-protein conjugates with various lipids. To this end, novel nanoformulations should be developed by bioreversible coupling of cargo protein with the sequence defined lipo-oligomer ***728*** followed by self-assembly with a variety of helper lipids (DOPS; DOPE; or linoleic acid), cholesterol, PEGylated lipids (DMPE-PEG2000 or DSPE-PEG2000) and optionally a folic acid-PEG conjugated lipid analog ***1042*** for targeting. Protein cargos RNase A or nlsEGFP were covalently coupled to lipo-oligomer ***728*** via disulfide linkages before nanoformulation. The colloidal stability of the nanoparticles in various conditions and targeted cytosolic delivery efficiency of cargo proteins by these nanoformulations should be evaluated and compared to identify the most potent nanoformulations.

2. Materials and Methods

2.1 Materials

2.1.1 Chemicals and reagents

Dichloromethane (DCM) was purchased from Bernd Kraft (Germany). Trifluoroacetic acid (TFA) were purchased from Acros Organics (USA). Syringe microreactors were obtained from Multisyntech GmbH (Witten, Germany). 2-Chlorotrityl chloride resin, Fmoc or Boc protected α-amino acids, N,N-diisopropylethylamine (DIPEA), peptide grade dimethylformamide (DMF), piperidine,benzotriazol-1-yl-oxy-tris-pyrrolidino-phosphonium hexafluorophosphate (Pybop), and 1-hydroxy-benzotriazole (HOBt) were purchased from Iris Biotech (Marktredwitz, Germany). Hydrazine from Merck (Darmstadt, Germany). 25% ammonia solution from Carl Roth (Karlsruhe, Germany). N^{10}-(Trifluoroacetyl)pteroic acid was obtained from Niels Clauson-Kaas A/S (Farum, Denmark), Fmoc-N-amido-dPEG$_{24}$-acid from Quanta Biodesign (Powell, USA). Cholesterol, linoleic acid (LinA), N-succinimidyl 3-(2-pyridyldithio) propionate (SPDP), ethylenediaminetetraacetic acid (EDTA), DL-dithiothreitol (DTT), triisopropylsilane (TIS), dimethyl sulfoxide (DMSO), 3,6-dioxa-1,8-octanedithiol (DODT), 5,5'-dithio-bis(2-nitrobenzoic acid) (DTNB), FITC, L-glutathione reduced (GSH), folic acid, dimethylsulfoxide (DMSO), 3-(4,5-dimethylthiazol-2-yl)-2,5-diphenyltetrazolium bromide (MTT), ninhydrin, phenol, potassium cyanide (KCN), sodium hydroxide (NaOH), hydrochloric acid solution (HCl, 1M) were purchased from Sigma-Aldrich (Munich, Germany). Acetonitrile (ACN, HPLC grade) was obtained from VWR (Darmstadt, Germany). Deuterium oxide (D_2O) from Euriso-Top (Saint-Aubin Cedex, France). n-hexane and methyl-tert-butyl ether (MTBE) from Brenntag (Mülheim/Ruhr, Germany). 1,2-dioleoyl-sn-glycero-3-phosphoethanolamine (DOPE), 1,2-dimyristoyl-sn-glycero-3-phosphoethanolamine-N-[methoxy(polyethylene glycol)-2000] (DMPE-PEG2000), 1,2-dioleoyl-sn-glycero-3-phospho-L-serine (DOPS),1,2-distearoyl-sn-

glycero-3-phosphoethanolamine-N-[methoxy(polyethylene glycol)-2000] (DSPE-PEG2000) were bought from Avanti Polar Lipids, Inc. HEPES from Biomol GmbH. BCA protein assay reagents were purchased from Thermo Scientific. Antibiotics, fetal bovine serum (FBS) and cell culture media were bought from Life Technologies or Sigma-Aldrich.

2.1.2 Proteins

Recombinant nlsEGFP was produced as previously reported [121]. RNase A from bovine pancreas were purchased from Sigma-Aldrich.

2.1.3 Bacteria strain

E.coli protein expression strain BL21(DE3)plysS was purchased from Novagen (Merck4biosciences, Darmstadt, Germany).

2.1.4 Oligomers

K-ε(PEG_{24}-A)-K-α,ε[K-α,ε(Sph_3-C)$_2$]$_2$ (***706***), K-ε(PEG_{24}-FolA)-K-α,ε[K-α,ε(Sph_3-C)$_2$]$_2$ (***707***), K-ε(PEG_{24}-E)-K-α,ε[H-K-α,ε(H-Sph)$_3$-H-C)$_2$]$_2$ (***712***), K-ε(PEG_{24}-FolA)-K-α,ε[H-K-α,ε(H-Sph)$_3$-H-C)$_2$]$_2$ (***713***), K-ε(PEG_{24}-E)-K-α,ε(Sph_3-Y_3-C)$_2$ (***714***), K-ε(PEG_{24}-FolA)-K-α,ε(Sph_3-Y_3-C)$_2$ (***715***), K-ε(PEG_{24}-E)-K-α,ε(Stp_4-C-K-OA_2)$_2$ (***728***), K-ε(PEG_{24}-FolA)-K-α,ε(Stp_4-C-K-OA_2)$_2$ (***729***), K-ε(PEG_{24}-E)-K-α,ε[K-α,ε(Stp_3-C)$_2$]$_2$ (***732***), K-ε(PEG_{24}-FolA)-K-α,ε[K-α,ε(Stp_3-C)$_2$]$_2$ (***733***), K-ε(PEG_{24}-E)-K-α,ε[H-K-α,ε((H-Stp)$_3$-H-C)$_2$]$_2$ (***761***), K-ε(PEG_{24}-FolA)-K-α,ε[H-K-α,ε((H-Stp)$_3$-H-C)$_2$]$_2$ (***762***), K-ε(PEG_{24}-E)-K-α,ε[(H-Stp)$_4$-H-Y_3-C]$_2$ (***794***), K-ε(PEG_{24}-FolA)-K-α,ε[(H-Stp)$_4$-H-Y_3-C]$_2$ (***795***) were designed and provided by Dr. Dongsheng He. K-ε(PEG_{24}-FolA)-K-α,ε(Stp_4-C)$_2$ (***737***), K-ε(PEG_{24}-GlutA)-K-α,ε(Stp_4-C)$_2$ (***937***) were designed and provided by Philipp Klein. K-ε(PEG_{36}-FolA)-K-α,ε($SteA)_2$ (***1042***) was designed and provided by Benjamin Steinborn and Dr. Ulrich Lächelt. C-(STP)$_3$-K-α,ε[(STP)$_3$-C]$_2$ (***386***) was synthesized as reported before[114, 117].

2.2 Methods

2.2.1 Synthesis of the cationic building block Fmoc-Stp(Boc)$_3$-OH

The cationic building block Fmoc-Stp(Boc)$_3$-OH was synthesized as reported before [117]. Briefly, the two primary amines of TEPA were selectively protected by ethyl trifluoroacetate, and then the three secondary amines of TEPA were protected by di-tert-butyl dicarbonate. Subsequently, the two primary amines were deprotected with NaOH, followed by the asymmetric functionalization of the two terminal primary amines with Fmoc-Osu and succinic anhydride, respectively. After purification with dry column chromatography, the cationic building block Fmoc-Stp(Boc)$_3$-OH was obtained.

2.2.2 Loading of 2-chlorotrityl chloride resin with Fmoc-Cys(Trt)-OH.

2-chlorotrityl chloride resin (500 mg, chloride loading 1.55 mmol/g) was swelled in dry DCM for 10 min for two times. Subsequently, 0.4 eq mmol Fmoc-Cys(Trt)-OH and 0.9 eq mmol DIPEA were added to the resin and incubated at RT for 1 h. After removing the reaction solvents, the resin was incubated with a mixture of DCM/MeOH/DIPEA (80/15/5 v/v/v) for 10 min for two times at RT. After removal of the reaction mixture, the resin was washed 5 times with DCM and about 30 mg of the resin was separated for the loading determination. Therefore, an exact amount of resin was treated with 1 mL deprotection solution (20% piperidine in DMF) for 1 h. Afterwards, the solution was diluted and absorption was measured at 301 nm. The loading was then calculated according to the equation: resin load [mmol/g] = (A*1000)/(m [mg]*7800*d_f) with d_f as dilution factor. The rest resin was washed 3 times with DMF, and then was treated 5 times for 10 minutes with 20 % piperidine in DMF. Reaction progress was monitored by Kaiser test. Finally, the resin was washed

3 times with DMF, 3 times with DCM, 3 times with n-hexane and dried under vacuum.

2.2.3 Loading of 2-chlorotrityl chloride resin with Dde-Lys(Fmoc)-OH

The loading was performed analogously to the loading of 2-chlorotrityl chloride resin with Fmoc-Cys(Trt)-OH. Instead of Fmoc-Cys(Trt)-OH, Dde-Lys(Fmoc)-OH was used as amino acid.

2.2.4 Kaiser test

Kaiser test was used to quantify the presence of free amines on the resin [127]. A small amount of DCM washed resin was transferred to an Eppendorf tube. One drop of each 80 % (w/v) phenol in EtOH, 5 % (w/v) ninhydrin in EtOH and 20 µM potassium cyanide (KCN) in pyridine were added into the Eppendorf tube. The Eppendorf tube was incubated for 4 min at 99 °C under shaking. For the positive Kaiser test, the presence of free amines was proved by blue colored resin beads and solution. For the negative Kaiser test, the absence of free amines was indicated by colorless resin beads and light yellow solution.

2.2.5 General solid-phase synthesis process

Solid-phase synthesis was carried out by a sequential cycle process of coupling and deprotection. Generally, in Fmoc-based solid-phase synthesis, the deprotected amino acid pre-loaded resin was incubated with a 4-fold excess of the pre-activated Fmoc-protected amino acids identified by the desirable sequence of oligomer at RT for 1 h. The pre-activation of Fmoc-protected amino acids was performed by incubation with an equimolar amount of HOBt, PyBOP and twice molar amount of DIPEA. Fmoc-deprotection was usually performed by a 10 min incubation with 20% piperidine in DMF for several times. Kaiser test was carried out to detect the presence of free amines after each coupling and deprotection step [127]. In case of unexpected

results (positive after coupling or negative after deprotection) of the Kaiser test, the last coupling or deprotection step was repeated, respectively. After full assembly of the oligomer sequence, the products were cleaved from the resin, purified by SEC, and characterized by RP-HPLC and ^{1}HMR.

2.2.6 Oligomer cleavage

The completely assembled oligomers were cleaved from the resin by an incubation with a mixture of TFA/DODT/TIS/H_2O (94:1:2.5:2.5 v/v/v) for 90 min under shaking. The cleavage solution was collected in a round-bottom flask and the resin was washed 3 times with TFA, 3 times with DCM. The combined solution was concentrated under reduced pressure to a final volume of approximately 1 mL and added dropwise to a pre-cooled 50 mL mixture of MTBE/n-hexane (1/1 v/v), then the precipitated crude product was obtained. After a centrifugation for 30 min at 4000 rpm and 4 °C, the supernatant was discarded and the precipitate was dried under a nitrogen stream.

2.2.7 Synthesis of 386

The three-arm oligomer ***386*** was synthesized as reported before [114]. Generally, 2-Chlorotrityl chloride resin was preloaded with Fmoc-Cys(Trt)-OH, and then the cationic building block Fmoc-Stp(Boc)$_3$-OH, Fmoc-Lys(Fmoc)-OH and Boc-Cys(Trt)-OH were stepwise coupled based on the desirable sequence via the general solid-phase synthesis process.

2.2.8 Synthesis of 728 and 729

2-Chlorotrityl chloride resin preloaded with Dde-Lys(Fmoc)-OH was used for the synthesis of ***728*** and ***729***. After Fmoc-deprotection, Fmoc-N-amido-dPEG$_{24}$-OH and Fmoc-Glu-OtBu were stepwise coupled to the ε-amino group of the preloaded lysines. After another Fmoc-deprotection, the resin was separated into two parts for the further

synthesis of ***728*** and ***729***, respectively. For ***728*** synthesis, the amino group of Fmoc-deprotected glutamic acid was protected by di-tert-butyl dicarbonate. For ***729*** synthesis, the amino group of Fmoc-deprotected glutamic acid was coupled with N^{10}-(Trifluoroacetyl)pteroic acid to generate folic aicd. After finishing assembly of the folic acid (or glutamic acid) ligand, the Dde protection groups of α-amino groups of the preloaded lysines were removed by treating the resin of both ***728*** and ***729*** for 20-30 times with 4% hydrazine in DMF (v/v), the deprotection process was monitored by checking absorption of the reaction solution at 290 nm. Subsequently, Fmoc-Lys(Fmoc)-OH, Fmoc-Stp$(Boc)_3$-OH, Fmoc-Cys(Trt)-OH and oleic acid were coupled stepwise to the deprotected α-amino group of the preloaded lysine based on the desirable sequence via the general solid-phase synthesis process. Finally, a deprotection of the trifluoroacetyl-group of pteroic acid was carried out using 25% aqueous ammonia solution/DMF (1:1) four times for 30 min. After each deprotection cycle, the resin was washed with DMF. After completion of the reaction, the resin was washed with DMF, DCM and n-hexane and dried in vacuo. The crude product was purified by SEC after cleavage.

2.2.9 Size-exclusion chromatography

All oligomers were purified by size exclusion chromatography using an Äktapurifier 10 platform (GE Healthcare Bio-Sciences AB, Uppsala, Sweden) with a P-900 solvent pump module, a pH/C-900 conductivity module, a UV-900 UV/VIS multi-wavelength detector and a Frac-950 automated fractionator. Sephadex G-10 column was used for purification and 10 mM hydrochloric acid solution / acetonitrile (7:3) was used as eluent. The desirable fractions were collected, pooled and lyophilized.

2.2.10 RP-HPLC

The purity of the synthesized oligomers was analyzed by RP-HPLC using a Waters HPLC system equipped with a Waters 600E multisolvent delivery system, a Waters

996 PDA detector and a Waters 717plus autosampler. As indicated, the compounds were analyzed using a Waters Sunfire C18 or Xbridge C18 column (5 µm, 4.6 x 150 mm) and a water/acetonitrile gradient (95:5 – 0:100) containing 0.1 % TFA. For the detection, the extinction at 214 nm was monitored.

2.2.11 ^{1}H-NMR

^{1}H NMR spectra was performed using a Jeol JNMR-GX 400 (400 MHz) or JNMR-GX 500 (500 MHz) without TMS as internal standard. Deuterium oxide (D_2O) was used as solvent. All chemical shifts were calibrated to the residual proton signal of the solvent and are reported in ppm. Data are presented as s = singlet, d = doublet, t = triplet, m = multiplet. The spectra were analyzed with MestReNova (MestReLab Research).

2.2.12 Expression and purification of nlsEGFP

Recombinant nlsEGFP was produced as previously reported [121]. E. coli BL21(DE3)plysS containing nlsEGFP plasmid were grown in LB Medium (50 µg/mL ampicillin, 50 µg/mL chloramphenicol) at 37 °C with constant shaking to an optical density of 0.6-0.8 (600 nm). After cool down to room temperature, protein expression was induced by adding 1 mM IPTG and then incubated at 32 °C over night with constant shaking. Subsequently, the bacteria were harvested by centrifugation (30 min, 4000 x g, 4 °C). The supernatant was discarded and the pellet was resuspended in lysis buffer (20 mM Tris, 20% sucrose, 0.2 M NaCl, 10 mM MgCl2, pH 7.5). RNase (10 µg/mL), DNase (30 µg/mL), lysozyme (1 mg/mL) and 1 mM PMSF were added into the lysis buffer. The solutions were frozen and thawed and sonicated (3 x 20 sec on ice, full power). The bacterial lysate was ultracentrifuged (30 min, 20000 rpm, 4 °C) and the supernatant was filtered using a 0.45 µm syringe filter. The proteins were purified by nickel chromatography using a gradient from binding buffer (50mM sodium hydrogenphosphate, 300 mM sodium chloride, 20 mM imidazole) to elution buffer (50mM sodium hydrogen phosphate, 500 mM sodium chloride, 250 mM imidazole).

The purified protein was dialyzed over night against PBS buffer (pH 7.4) using a dialysis membrane (14000 MWCO) from Carl Roth (Karlsruhe, Germany), and then the concentration of purified protein was quantified using BCA assay.

2.2.13 Fluorescein-modified RNase A

RNase A (6 mg, 0.438 μmol) was dissolved in sodium carbonate-bicarbonate buffer (2 mL, 0.1 M pH 9.0). Then FITC (1.314 μmol) was dissolved in DMSO (5 mg/mL) and added to the RNase A solution. After a 2 h incubation at 25 °C, the FITC modified RNase A was purified by size-exclusion chromatography via a Sephadex G25 superfine column using PBS buffer (1 mM EDTA, pH 7.4) as the mobile phase. The purified RNase A-FITC was concentrated by Amicon Ultra centrifugal filter units (Millipore; MWCO 3000 Da). Protein concentration was measured by BCA assay as instructions. The whole experiment process was protected from light.

2.2.14 SPDP modification of nlsEGFP

nlsEGFP (6 mg, 0.19 μmol) was dissolved in PBS buffer (2 mL, pH 7.4) containing 1 mM EDTA. Then SPDP (1.14 μmol) was dissolved in DMSO (50 μL) and added to the nlsEGFP solution. After a 2 h incubation at 37 °C, the resulting SPDP modified nlsEGFP was purified by size exclusion chromatography on a Sephadex G25 superfine column using HEPES buffer (pH 8.5, 0.3 M) as the mobile phase. Protein concentration was measured by BCA assay as instructions. The molar ratio of SPDP to nlsEGFP could be quantified by calculating the change in absorbance at 343 nm after reducing samples of the SPDP modified nlsEGFP with DTT using an extinction coefficient of 8080 M^{-1} cm^{-1} .

2.2.15 SPDP modification of RNase A or RNase A-FITC

RNase A (6 mg, 0.438 μmol) or RNase A-FITC (6 mg) was dissolved in PBS buffer (2 mL, pH 7.4) containing 1 mM EDTA. Then SPDP (2.19 μmol) was dissolved in DMSO

(100 µL) and added to the RNase A solution or RNase A-FITC solution. After a 2 h incubation at 37 °C, the resulting SPDP modified proteins were purified respectively by size-exclusion chromatography on a Sephadex G25 superfine column using HEPES buffer (pH 8.6, 0.1 M) as the mobile phase. Protein concentration was measured by BCA assay as instructions. The molar ratio of SPDP to RNase A or RNase A-FITC could be quantified by calculating the change in absorbance at 343 nm after reducing samples of the SPDP modified RNase A with DTT using an extinction coefficient of 8080 M^{-1} cm^{-1}.

2.2.16 Conjugation of proteins with oligomers

Oligoaminoamides of the oligomer library were synthesized by solid phase-assisted synthesis using the properly fmoc, tboc-protected artificial oligoamino acids (Stp and Sph) [116, 117] as reported before. [114, 116, 117, 125, 128, 129] The SPDP modified nlsEGFP was divided into 0.25 mg per aliquot and dissolved in HEPES buffer (0.5 mL, pH 8.5, 0.3 M). For SPDP modified RNase A or RNase A-FITC, the proteins were divided into 0.25 mg per aliquot and dissolved in HEPES buffer (0.25 mL, pH 8.6, 0.1 M). Various oligomers dissolved in water (50 mg/mL; for 728 and 729, 25 mg/mL) were added to the above modified protein solutions, respectively, as twice the molar quantity of covalently attached SPDP. This ratio was empirically found as optimum oligomer/cargo ratio. After a 15 min incubation at 20 °C, the formed conjugates were shock-frozen in liquid nitrogen and stored at −80 °C or used for further experiments immediately.

For the formulation of lipo-oligomer nanoformulations, The SPDP modified RNase A was divided into 0.1 mg portions per aliquot and dissolved in HEPES buffer (0.2 mL, pH 7.4, 20 mM). The SPDP modified nlsEGFP was divided into 0.1 mg portions per aliquot and dissolved in HEPES buffer (0.2 mL, pH 8.5, 0.3 M). Lipo-oligomer ***728*** dissolved in water (20 mg/mL) was added to the above modified protein solutions respectively at a twofold excess relative to covalently attached SPDP. This ratio was

empirically found as optimum oligomer/cargo ratio. After a 15 min incubation at 20 °C, the formed conjugates were immediately used for further experiments.

2.2.17 Preparation of lipo-oligomer nanoformulations

Lipo-oligomer nanoformulations were prepared using the lyophilization and rehydration method. Briefly, the aqueous solutions of protein conjugate (produced as described above), or corresponding free protein, or free ***728*** lipo-oligomer were added to the dry lipid mixtures with different defined molar ratios. After vortexing, the solutions were rapidly frozen in liquid nitrogen and lyophilized overnight. During lyophilization, the mixtures of protein conjugate and lipids were protected from light. Then, the mixtures were rehydrated with water by vortexing. The resulting solutions were sonicated at 40 ℃ for 5 min (ultrasonic bath USC THD/HF) and left at room temperature for 48 h to make sure all free thiols were oxidized. The formulated nanoparticles were then characterized by DLS measurement or TEM imaging.

2.2.18 Cell culture

Human cervix carcinoma cells (KB) or murine lymphocytic leukemia cells (L1210) were grown in folic acid free RPMI-1640 medium, supplemented with 10% FBS, 100 U/mL penicillin, 100 µg/mL streptomycin and 4 mM stable glutamine. Neuro 2A cells were grown in Dulbecco's modified Eagle's medium (DMEM), supplemented with 1 g/L glucose, 10% FBS, 100 U/mL penicillin, 100 µg/mL streptomycin and 4 mM stable glutamine. MCF-7 cells were grown in DMEM, supplemented with 4.5 g/L glucose, 10% FBS, 1 mM sodium pyruvate, 100 U/mL penicillin, 100 µg/mL streptomycin and 4 mM stable glutamine. All cells were cultured at 37 °C in an incubator with 5 % CO_2 and humidified atmosphere.

2.2.19 Cellular association

KB cells were seeded into 24-well plates at a density of 50 000 cells per well. After 24 h, the 500 µL medium was replaced with fresh serum-containing medium. Then, the various nlsEGFP nanoparticles (final concentration 1 µM) or 729-SS-RNase A-FITC conjugate (final concentration 2 µM) were added into each well and incubated on ice for 45 min. For competition experiments with free folic acid, the KB cells were pretreated with 1 mM free folic acid for 30 min on ice before adding nanoparticles. Then, the cells were washed with 500 µL PBS, detached with trypsin/EDTA and diluted with PBS containing 10% FBS. After centrifugation, the cells were taken up in 600 µL PBS containing 10% FBS. The cellular fluorescence was assayed by excitation of nlsEGFP or FITC at 488 nm and detection of emission at 510 nm with a Cyan ADP flow cytometer (Dako, Hamburg, Germany). Cells were appropriately gated by forward/sideward scatter and pulse width for exclusion of doublets, and counterstained with DAPI (4′,6-diamidino-2- phenylindole) to discriminate between viable and dead cells. Minimum ten thousand gated cells per sample were collected. Data were recorded with Summit software (Summit, Jamesville, NY). Analysis was done by FlowJo 7.6.5 flow cytometric analysis software. All experiments were performed in triplicates.

2.2.20 Cellular internalization

KB cells were seeded into 24-well plates at a density of 50 000 cells per well. After 24 h, the 500 µL medium was replaced with fresh serum-containing medium. Then, the various nlsEGFP conjugates (final concentration 1 µM) or ***729***-SS-RNase A-FITC conjugate (final concentration 2 µM) was added into each well and incubated at 37 °C for 45 min or incubated at 37 °C for 24 h, followed by an incubation of 24 h in fresh media. Then, the cells were washed with 500 µL PBS, detached with trypsin/EDTA, and diluted with PBS containing 10% FBS. After centrifugation, the cells were taken up in 600 µL PBS (pH 4.0) to extinguish the outside fluorescence or in 600 µL PBS

containing 10% FBS. The cellular fluorescence was assayed by excitation of nlsEGFP or FITC at 488 nm and detection of emission at 510 nm with a Cyan ADP flow cytometer (Dako, Hamburg, Germany). Cells were appropriately gated by forward/sideward scatter and pulse width for exclusion of doublets, and counterstained with DAPI (4′,6-diamidino-2-phenylindole) to discriminate between viable and dead cells. Minimum 10 000 gated cells per sample were collected. Data were recorded with Summit software (Summit, Jamesville, NY). Analysis was done by FlowJo 7.6.5 flow cytometric analysis software. All experiments were performed in triplicates.

2.2.21 Particle size and zeta potential

Particle size and zeta potential of protein conjugates were measured by dynamic laser-light scattering using a Zetasizer Nano ZS (Malvern Instruments, Worcestershire, UK). For particle size measurement, nanoparticles were measured in 100 µL HEPES buffer (pH 7.4, 20 mM) at a concentration of 0.25 mg/mL. Then the nanoparticle suspension was diluted to 800 µL for zeta potential measurement.

2.2.22 Transmission electron microscopy (TEM)

Formvar-carbon 300 mesh copper grids (Ted Pella Inc., Redding, USA) were activated by mild plasma cleaning. Afterwards, the grids were incubated with 20 µL of lipo-oligomer nanoformulations solution for 3 min. Excess liquid was blotted off using filter paper until the grid was almost dry. Before staining, the grids were washed with 5 µL of staining solution for 5 seconds. Then, the grids were incubated with 5 µL of a 2% aqueous uranyl formate solution for 10 seconds, excess liquid was blotted off using filter paper, followed by air-drying for 20 min. Samples then were analyzed using JEM 1011 (JEOL, Japan) at 80 kV.

2.2.23 Ellman's assay

DTNB (5,5'- dithiobis(2-nitrobenzoic acid)) stock solution (60 µL, 4 mg/mL) was dissolved in 2440 µL of Ellman's buffer (0.2 M Na_2HPO_4 with 1 mM EDTA, pH 8.0) as DTNB-working solution. 30 µL of protein nanoparticles or standard cysteine solution were diluted in 170 µL DTNB-working solution and incubated for 15 min at 37 °C. The absorbance of solutions was measured at 412 nm. Concentration of the free thiol group was calculated via the calibration curve.

2.2.24 Turbidity assay

To compare the serum stability of various nanoparticles, an initial absorbance at 660 nm was measured after 90 µL per well of the nanoparticle solutions (50 µg/mL) was added into the 96-well plates. The wavelength of 660 nm was selected to be sufficiently high to avoid absorbance by serum proteins. After this, half of the nanoparticles were mixed with 10 µL of FBS per well, the other half nanoparticles were mixed with 10 µL per well of PBS as controls. The plates were immediately placed at 37 ℃ for 2 h, afterwards, the absorbance at 660 nm of each well was measured. All readings were normalized to the above initial absorbance. All experiments were performed in triplicates.

2.2.25 Calcein release assay

RNase A nanoformulations containing calcein (0.1 M) were prepared analogously as described above, but with rehydrating the dry lipids mixtures with PBS (pH 7.4) containing 0.1 M calcein. Untrapped calcein were removed from the calcein containing nanoparticles by size exclusion chromatography using Sephadex G25 column and PBS (pH 7.4) as elution buffer. After PBS (pH 7.4) or 3% triton X-100 treatment, the change in fluorescence intensity due to calcein release from the nanoparticles was monitored by a multimode microplate reader (Spark 10M, Tecan, Switzerland) at 485 nm excitation and 535 nm emission, respectively. The

fluorescence intensities were normalized regarding the fluorescence intensity of the samples treated with PBS (pH 7.4).

2.2.26 Erythrocyte leakage assay

Preserved human red blood cells (obtained from LMU Clinics—Campus Grosshadern, Munich, Germany) were washed with PBS for several times. After centrifugation, the erythrocyte pellet was diluted to 5×10^7 erythrocytes per mL with PBS (buffered to the indicated pH). The protein conjugates or plain oligomers were diluted to 75 µL with above PBS, respectively, and added to a V-bottom 96-well plate (NUNC, Denmark). Control wells had buffer with 1% Triton X-100 for 100% lysis. Then, 75 µL erythrocyte suspension was added to each well, resulting in a final concentration of 1 µM nlsEGFP conjugates or 2 µM RNase A conjugates or 5 µM plain oligomers per well. The plates were incubated under constant shaking for 1 h at 37 °C. After centrifugation, 80 µL supernatant was analyzed for hemoglobin release at 405 nm with a microplate reader (Tecan Spectrafl uor Plus, Tecan, Switzerland). PBS with different indicated pH was used as negative control. Relative hemolysis was defined as hemolysis (%) = (A 405 (conjugate treated) − A 405 (PBS treated))/ (A 405 (Triton X treated) − (A 405 (PBS treated)) × 100.

2.2.27 Fluorescence microscopy

KB cells were seeded into 8 well Nunc chamber slides (Thermo Scientific, Germany) coated with collagen at a density of 10 000 cells per well. After 24 h, the 300 µL medium was replaced with fresh medium. Subsequently, the various nlsEGFP nanoparticles were added into each well (final concentration 1 µM) and incubated at 37 °C for 24 h, followed by a 24 h incubation in fresh media. Then, the live cells were observed on a Zeiss Axiovert 200 fluorescence microscope (Jena, Germany). For ***729***-SS-RNase A-FITC transfection, the same experiment was performed, but the final concentration was 2 µM and incubation was at 37 °C for 45 min. Then, the cells

were washed with 300 µL PBS and fixed with 4% paraformaldehyde, followed by nuclei staining with DAPI (1 µg/mL). A 63× magnification DIC oil immersion objective (Plan-APOCHROMAT) and appropriate filter sets for analysis of EGFP or DAPI were used. Data were analyzed and processed by AxioVision Rel. 4.8 software (Zeiss, Jena, Germany).

2.2.28 RNase A transfection

For the screening experiment of various RNase A conjugates, KB cells were seeded into 96-well plates at a density of 10 000 cells per well. After 24 h, the medium was replaced with 80 µL fresh medium. Subsequently, the various RNase A conjugates (final concentration 4 µM), RNase A-PDP (final concentration 4 µM), polymers (final concentration 16 µM), and mixtures of free RNase A (final concentration 4 µM) and polymers (final concentration 16 µM) were diluted to 20 µL with PBS, respectively, added to each well and incubated at 37 °C for 4 h, followed by a 44 h incubation in fresh media. Afterward, MTT solution (10 µL per well, 5.0 mg/mL) was added. After incubation for 2 h, the medium was removed and the 96-well plates were stored at −80 °C for at least 1 h. 100 µL DMSO per well were added to dissolve the purple formazan product. The optical absorbance was measured at 590 nm, with a reference wavelength of 630 nm, by a microplate reader (Tecan Spectrafl uor Plus, Tecan, Switzerland). The relative cell viability (%) related to control wells treated only with 20 µL PBS was calculated as ([A] test/[A] control) × 100%. All experiments were performed in triplicates.

For investigation of protein concentration-dependent cytotoxicity of RNase A conjugates on folate-receptor-positive or negative cells and the structure–activity relationship, KB cells, MCF-7 cells, or Neuro-2a cells were seeded into 96-well plates at a density of 10 000 cells per well. After 24 h, the medium was replaced with 80 µL fresh medium. Subsequently, the RNase A conjugates (final concentration 0.25; 0.5; 1.0; 2.0; 4.0 µM), RNase A-PDP (final concentration 0.25; 0.5; 1.0; 2.0; 4.0 µM),

oligomers (final concentration 1.0; 2.0; 4.0; 8.0; 16.0 µM) were diluted to 20 µL with PBS, respectively, added to each well and incubated at 37 °C for 4 h, followed by a 44 h incubation in fresh media. Afterward, cell viability was measured by the MTT assay as describe above.

For lipo-oligomer nanoformulations, KB cells, Neuro 2A or MCF-7 were seeded into 96-well plates at a density of 10 000 cells per well. After 24 h, the medium was replaced with 80 µL fresh medium. Subsequently, the various RNase A nanoparticles (final concentration 2 µM), corresponding nanoparticles without RNase A or ***728***, mixtures of nanoparticles with free RNase A (final concentration 2 µM) and RNase A-PDP (final concentration 2 µM), were diluted to 20 µL with PBS respectively, added to each well and incubated at 37 °C for 4 h in 10% FBS containing media (for serum stability test, 0 % FBS and 20% FBS containing media were used), followed by a 44 h incubation in fresh media. For competition experiments with free folic acid, the KB cells were pretreated with 1 mM free folic acid for 30 min on ice before adding nanoparticles. Afterward, cell viability was measured by the MTT assay as describe above.

For investigation of protein concentration-dependent cytotoxicity of lipo-oligomer RNase A nanoformulations on folate receptor positive KB cells, the cells were seeded into 96-well plates at a density of 10 000 cells per well. After 24 h, the medium was replaced with 80 µL fresh medium. Subsequently, the RNase A nanoparticles (final concentration 0.1; 0.5; 1.0; 1.5; 2.0 µM), RNase A-PDP (final concentration 0.1; 0.5; 1.0; 1.5; 2.0 µM) and corresponding nanoparticles without RNase A were diluted to 20 µL with PBS respectively, added to each well and incubated at 37 °C for 4 h, followed by a 44 h incubation in fresh media. Afterwards, cell viability was measured by the MTT assay as describe above.

2.2.29 Cell viability assay of nlsEGFP nanoparticles

KB cells were seeded into collagen coated 96-well plates at a density of 10 000 cells per well. After 24 h, the medium was replaced with 80 μL fresh medium. Subsequently, the nlsEGFP nanoparticles (final concentration 0.1; 0.25; 0.5; 1.0; 1.5 μM) and nlsEGFP-PDP (final concentration 0.1; 0.25; 0.5; 1.0; 1.5 μM) were diluted into 20 μL with PBS, respectively, added into each well, and incubated with cells at 37 °C for 24 h, then the medium was replaced with 100 μL fresh medium, followed by another 24 h incubation. Afterward, cell viability was measured by the MTT assay as describe above.

2.2.30 Statistical analysis

The statistical significance of experiments were analyzed using the Tukey test, $p < 0.05$ was considered statistically significant in all analyses (95% confidence interval).

3. Results

3.1 Enhanced intracellular protein transduction by sequence defined tetra-oleoyl oligoaminoamides targeted for cancer therapy

Section 3.1 has been adapted from: Peng Zhang, Dongsheng He, Philipp Michael Klein, Xiaowen Liu, Ruth Röder, Markus Döblinger, and Ernst Wagner, Adv. Funct. Mater. 2015, 25, 6627–6636.

As mentioned above, protein therapeutics [130, 131] have gained increasing attention due to their great potential in the treatment of many diseases. For cancer, they provide a higher functional specificity and less genetic risks than standard nontargeted chemotherapies. Clinically applied proteins therapeutics however are limited to those exerting bioactivities extracellularly, intracellularly active proteins as a therapeutic subclass still is in its early stage due to delivery problems. The particular crucial barriers include specific delivery to the targeted cells, highly efficient cellular internalization, effective endolysosomal escape, timely release of proteins from the delivery system and following subcelluar traffic to specific subcellular sites [54, 58, 61]. Among these barriers, especially endolysosomal entrapment hamper effective protein transduction into the cytosol. Cargo proteins are largely sequestrated and degraded in the endolysosomes without access to the subcellular target sites for subsequent biological actions. Therefore, novel delivery technologies are required to cope with these barriers via combing multiple functions. Amongst other technologies, biodegradable microgel encapsulation [132], nanocapsules [133], polymer micelles [134], lipid-like nanoparticles [135], virus-like protein nanoparticles [136], cationic oligomer and polymer formulations [120, 121, 137-140] or coupling with peptide transduction domains [141, 142] have been pursued. Here we present bioreversible conjugation of the cargo protein with precise sequence-defined oligoaminoamide carriers as an alternative encouraging option, which have been designed and

syntesized and contain various moieties and functions in our laboratory using solid-phase synthesis technology.

We recently synthesized such cationic oligomers based on artificial amino acid blocks (e.g., succinoyl tetraethylene pentamine, Stp; succinoyl pentaethylene hexamine, Sph) which were assembled into precise sequences, and demonstrated their efficient capacity in delivery of pDNA and siRNA polyplexes [114, 115]. Furthermore, receptor ligand and polyethylene glycol (PEG) modified oligomers were successfully generated for targeted nucleic acid delivery [129, 143]. This work revealed the endolysosomal barrier as a critical hurdle, and resulted in the design of endosomolytic domains such as fatty acids [114, 128] or endosomally protonatable units [129]. These units, when incorporated into oligomers, dramatically increased nucleic acid transfection. We hypothesized that the novel precise carriers might be useful also as delivery domains in conjugates of proteins or other drugs [119]. In initial work, one sequence-defined three-arm cationic oligomer had been conjugated with proteins by bioreducible disulfide [120] linkage for delivery of nlsEGFP or β-galactosidase into cells. In this work, 16 PEGylated two-arm and four-arm oligomers optionally containing folic acid for cell receptor targeting were selected and evaluated for targeted intracellular protein transduction. Different artificial amino acid building blocks, as well as protonatable histidines, or oleic acids were included to enhance endosomolytic ability. All these oligomers were coupled to nlsEGFP or RNase A by disulfide bonds, respectively. The disulfide linkages are supposed to be cleaved in the reducing cytosolic environment after endolysosomal escape [122-126]. Our new results show that the oleic acid modified targeted sequence-defined oligomers very potently transducer nlsEGFP and RNase A into the cytosol, where nlsEGFP undergoes efficient delivery into the nucleus, and RNase A triggers most effective killing of folate-receptor-positive cancer cells.

3.1.1 Synthesis of oligoaminoamide–protein conjugates

From an existing library of more than 900 precise cationic oligoaminoamides, sixteen candidates were chosen for in-depth evaluation of intracellular protein delivery. Sequences and topology are shown in Table 3.1. Two representative proteins, nlsEGFP and RNase A, were employed to evaluate targeted intracellular protein delivery. The conjugation process of the various oligomers to the model proteins (nlsEGFP, RNase A) is shown in Figure 3.1 A. Biologically reducible N-succinimidyl 3-(2-pyridyldithio)propionate (SPDP) linkers were utilized to covalently attach oligomers to nlsEGFP or RNase A through disulfide bonds. On average, every nlsEGFP molecule was modified with three SPDP linkers, for RNase A, two SPDP

Table 3.1 Oligoaminoamide oligomers for protein conjugation.

Sequence (C to N Terminal)	ID	Topology
K- ε (PEG_{24}-E)-K- α,ε (Sph_3-Y_3-C)$_2$	***714***	2-arm
K- ε (PEG_{24}-FolA)-K- α,ε (Sph_3-Y_3-C)$_2$	***715***	
K- ε (PEG_{24}-E)-K- α,ε (Stp_4-C-K-OA_2)$_2$	***728***	
K- ε (PEG_{24}-FolA)-K- α,ε (Stp_4-C-K-OA_2)$_2$	***729***	
K- ε (PEG_{24}-GlutA)-K- α,ε (Stp_4-C)$_2$	***937***	
K- ε (PEG_{24}-FolA)-K- α,ε (Stp_4-C)$_2$	***737***	
K- ε (PEG_{24}-E)-K- α,ε [(H-Stp)$_4$-H-Y_3-C]$_2$	***794***	
K- ε (PEG_{24}-FolA)-K- α,ε [(H-Stp)$_4$-H-Y_3-C]$_2$	***795***	
C-(STP)$_3$-K- α,ε [(STP)$_3$-C]$_2$	***386***	3-arm
K- ε (PEG_{24}-A)-K- α,ε [K- α,ε (Sph_3-C)$_2$]$_2$	***706***	4-arm
K- ε (PEG_{24}-FolA)-K- α,ε [K- α,ε (Sph_3-C)$_2$]$_2$	***707***	
K- ε (PEG_{24}-E)-K- α,ε [H-K- α,ε (H-Sph)$_3$-H-C)$_2$]$_2$	***712***	
K- ε (PEG_{24}-FolA)-K- α,ε [H-K- α,ε (H-Sph)$_3$-H-C)$_2$]$_2$	***713***	
K- ε (PEG_{24}-E)-K- α,ε [K- α,ε (Stp_3-C)$_2$]$_2$	***732***	
K- ε (PEG_{24}-FolA)-K- α,ε [K- α,ε (Stp_3-C)$_2$]$_2$	***733***	
K- ε (PEG_{24}-E)-K- α,ε [H-K- α,ε ((H-Stp)$_3$-H-C)$_2$]$_2$	***761***	
K- ε (PEG_{24}-FolA)-K- α,ε [H-K- α,ε ((H-Stp)$_3$-H-C)$_2$]$_2$	***762***	

Abbreviations: FolA: folic acid; GlutA: glutaric acid; OA: oleic acid; E: glutamic acid; C: cysteine; H: histidine; K: branching lysine selectively modified at α and ε amines; Y: tyrosine; A: alanine; PEG_{24}: polyethylene glycol containing 24 ethylene oxide monomer units. PEGylated oligomer syntheses were performed by Dongsheng He and Philipp Klein (PhD students, Pharmaceutical Biotechnology, LMU Munich).

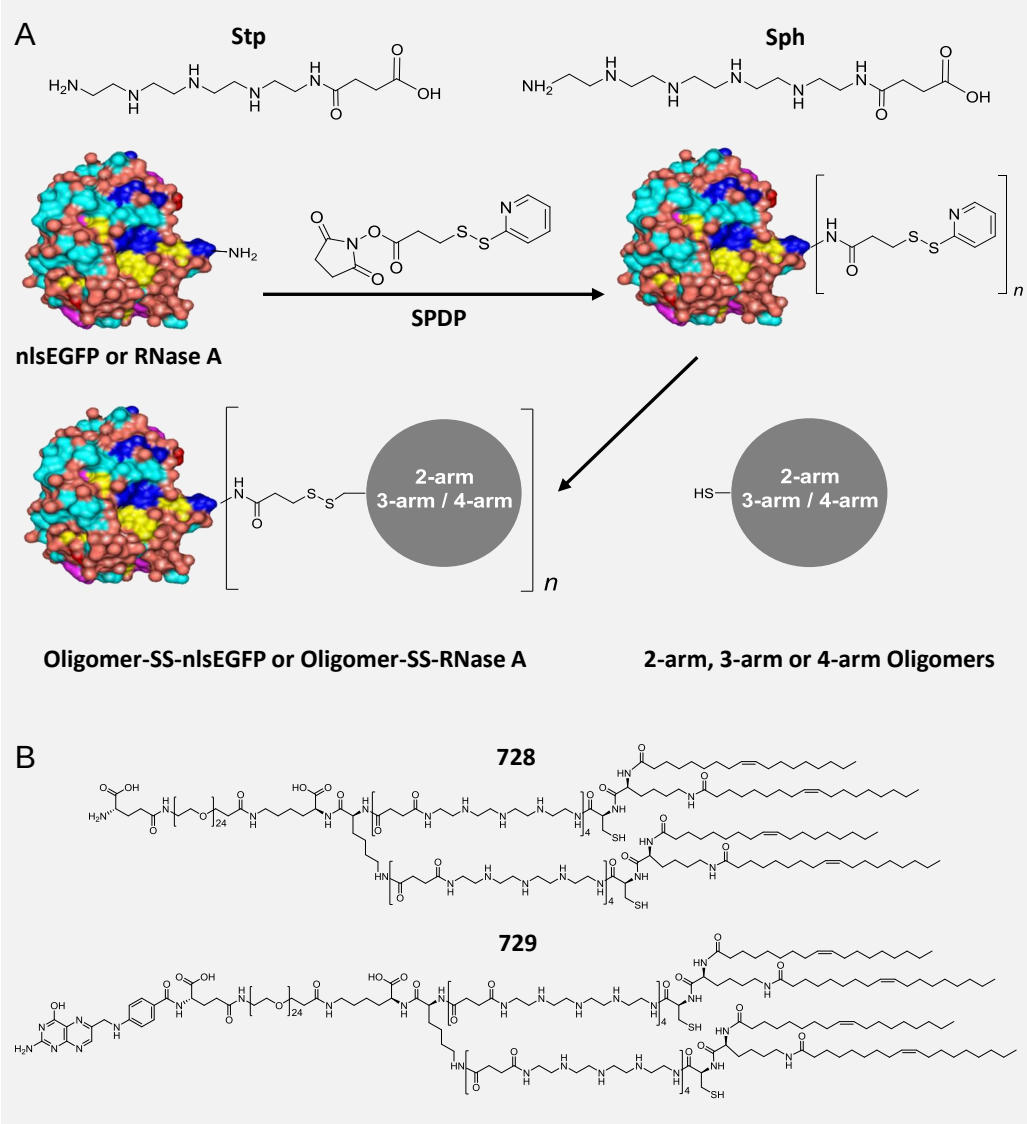

Figure 3.1 (A) Modification of nlsEGFP or RNase A with Stp or Sph containing 2-, 3-, or 4-arm oligomers (Table 3.1) via bioreducible SPDP linkers. Number of oligomers (n) covalently coupled to the protein: *n* = 3 (in average) for nlsEGFP, n = 2 (in average) for RNase A. Conjugates spontaneously form nanoparticles. (B) Chemical structures of oleic acid modified 2-arm oligomer ***728*** and ***729***.

linkers were introduced per protein molecule. As shown in Figure 3.2, nlsEGFP and RNase A were successfully modified with representative oligomers (***728, 729, 937, 737)***. The treatment of nlsEGFP and RNase A conjugates with reducing GSH at cytosolic concentration (5 µM) generated oligomer free nlsEGFP or RNase A. The other oligomers also exhibited successful modification of proteins and biological reversibility of disulfides linkages (data not shown). In aqueous solution, the protein conjugates spontaneously form nanoparticles, with the sizes and surface charges

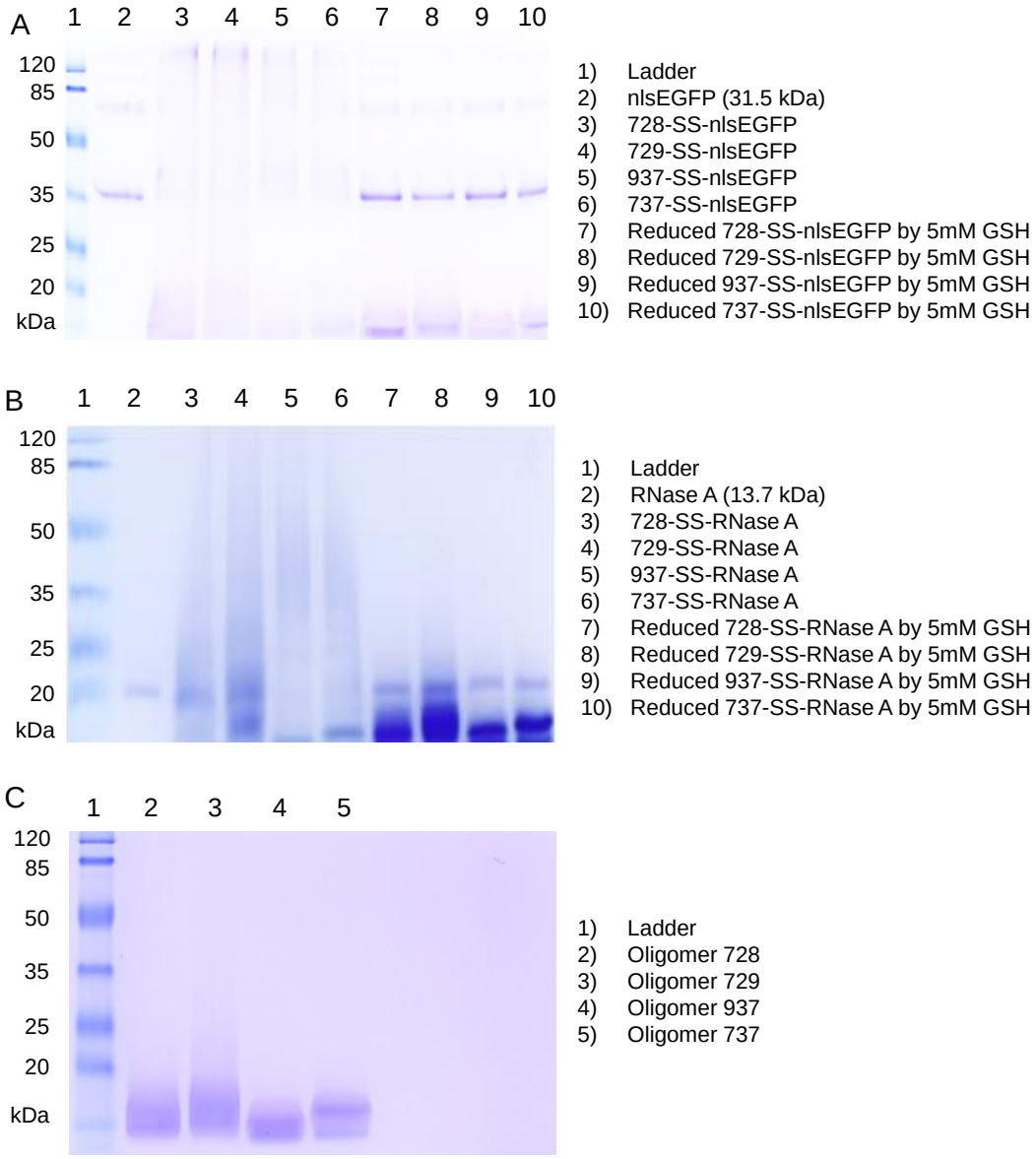

Figure 3.2 SDS-PAGE analysis of successful modification of (A) nlsEGFP and (B) RNase A with representative oligomers (***728, 729, 937, 737***) and the bioreversibility of the disulfide bonds (5 µg protein). (C) Free oligomers control. Note: While nlsEGFP well separates in the SDS-PAGE from the oligomers (Figure 3.2 A), the small RNase A protein overlaps with the oligomers (Figure 3.2 B), with the FolA-PEG linked lipo-oligomer ***729*** (lane 4) and to some extent also ***728*** (lane 3). As described in the experimental section, oligomers are included into the conjugation step at twice molar quantity. Therefore it is likely that not all free lipo-oligomers will incorporate into the lipo-protein-nanoparticles by covalent disulfide linkage, and a small fraction remains in noncovalent form and detectable in the SDS-PAGE. We do not assume that this is unconjugated RNase A protein. Please note that the band migration like RNase A is not visible with the conjugates of lipid-free oligomers ***937/737*** (lanes 5 and 6) prepared in the analogous manner.

determined by dynamic light scattering (DLS, see Table 3.2 for nlsEGFP; Table 3.3 for RNase A) strongly depending on the selected oligomer. The conjugates of RNase A

Table 3.2 Particle size (Z-average) and zeta potential of nlsEGFP conjugates in HEPES buffer determined by DLS. Variations refer to the median of three measurements of the same sample.

nlsEGFP Conjugate	Z-average (nm)	Mean zeta potential (mV)	Topology
714	359.8 ± 18.2	7.69 ± 0.20	2-arm
715	514.4 ± 38.1	7.59 ± 0.22	
728	29.7 ± 0.5	13.07 ± 0.71	
729	36.6 ± 1.0	15.00 ± 0.70	
937	189.6 ± 17.0	3.71 ± 0.14	
737	234.9 ± 25.2	3.75 ± 0.72	
794	529.7 ± 11.0	7.49 ± 0.26	
795	637.4 ± 103.1	7.63 ± 0.29	
706	190.6 ± 0.8	14.50 ± 0.35	4-arm
707	512.2 ± 64.3	15.27 ± 0.50	
712	79.0 ± 9.0	16.60 ± 0.78	
713	163.1 ± 77.1	10.59 ± 1.94	
732	353.1 ± 4.3	9.25 ± 0.85	
733	970.8 ± 49.0	8.67 ± 0.76	
761	1724.3 ± 138.1	6.30 ± 0.60	
762	1190.5 ± 173.4	5.65 ± 0.55	

Table 3.3 Particle size (Z-average) and zeta potential of RNase A conjugates in HEPES buffer determined by DLS. Variations refer to the median of three measurements of the same sample.

RNase A conjugate	Z-average (nm)	Mean zeta potential (mV)	Topology
714	630.6 ± 162.3	9.58 ± 0.82	2-arm
715	263.0 ± 85.7	13.77 ± 2.55	
728	22.5 ± 0.2	18.30 ± 1.18	
729	25.4 ± 0.7	21.27 ± 1.01	
937	256.1 ± 29.0	14.57 ± 1.04	
737	317.8 ± 13.5	17.33 ± 1.86	
794	119.2 ± 42.0	1.80 ± 1.17	
795	141.9 ± 101.8	2.91 ± 1.72	
386	182.6 ± 25.0	3.81 ± 2.57	3-arm
706	123.4 ± 18.9	6.20 ± 0.73	4-arm
707	276.9 ± 110.8	10.01 ± 3.11	
712	309.8 ± 51.5	16.50 ± 1.04	
713	299.6 ± 30.5	20.53 ± 0.60	
732	180,9 ± 47,9	5.43 ± 0.76	
733	366.0 ± 63.3	11.70 ± 1.06	
761	249.1 ± 117.5	5.00 ± 1.42	
762	92.0 ± 28.1	4.86 ± 1.03	

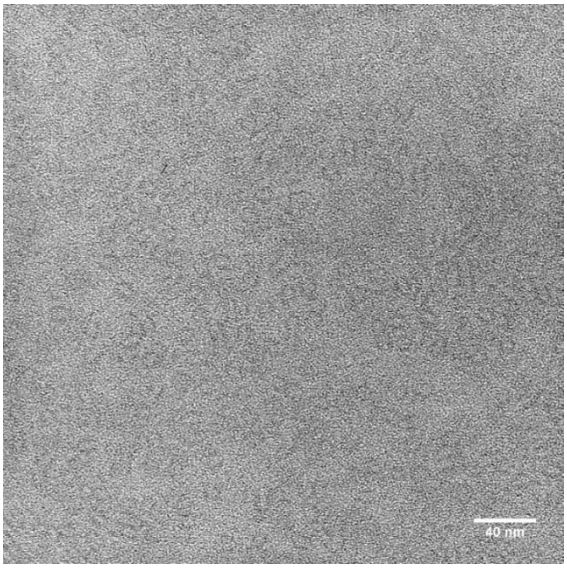

Figure 3.3 TEM image of ***729***-SS-RNAse A conjugates, performed with a Titan Themis TEM at 120 kV. Before observation, conjugates were negatively stained with 1% pH 7.0 phosphotungstic acid solution. Experiment performed by Dr. Markus Döblinger (Department of Chemistry, LMU Munich).

formed slightly smaller (23–600 nm) and more positively charged (zeta potential up to +22 mV) nanoparticles as compared to the nlsEGFP conjugates (30 nm to >1 µm; zeta up to 14 mV). Notably, only the lipo-oligomers ***728*** and ***729*** (chemical structures shown in Figure 3.1 B) mediated the formation of small nanoparticles with average sizes of 23–25 nm and +20 mV zeta potential for RNase A conjugates, and 30–36 nm and +14 mV zeta for nlsEGFP conjugates. The transmission electron microscopy (TEM) image of representative ***729***-SS-RNase A conjugates (Figure 3.3) showed a homogeneous distribution of the nanosized conjugates, with a uniform size of an average diameter of ≈10 nm and elliptical or worm-like shape (length >10 nm).

3.1.2 Screening of oligomer–nlsEGFP conjugates reveals oleoyl-modified oligomer *729* as potent transduction carrier

To evaluate the protein delivery efficiency and folate receptor specificity of the targeted oligomers, cells were transfected with nlsEGFP conjugates in standard serum-containing medium as described in the experimental section. Flow cytometry

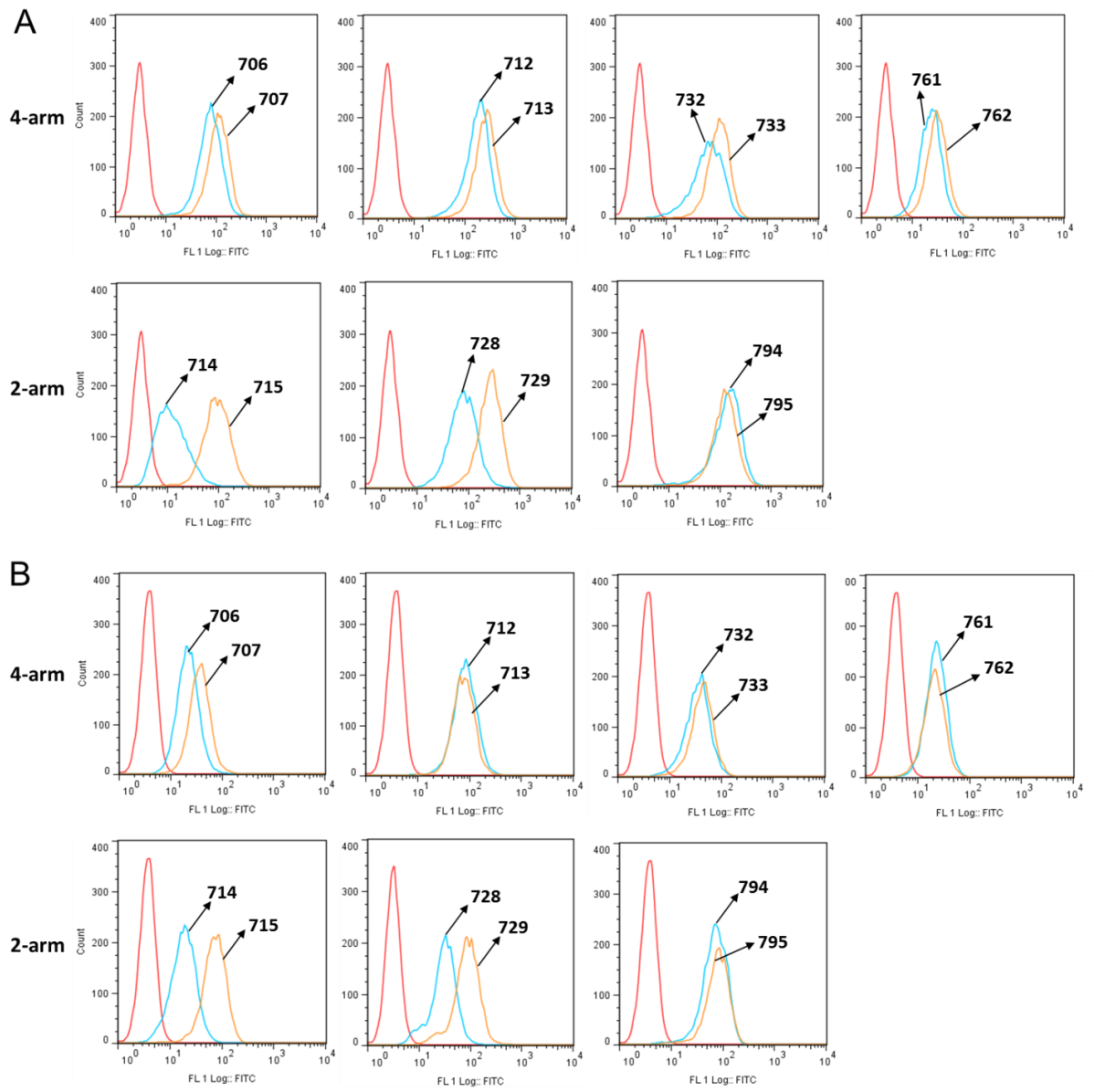

Figure 3.4 Cellular association (A) and cellular internalization (B) of various nlsEGFP conjugates (1 µM, oligomers indicated by ID number) after 45 min incubation with KB cells determined by flow cytometry. Orange: targeted oligomer conjugates; Light blue: non-targeted control oligomer conjugates; Red: PBS treated cell control.

was used to quantify the fluorescence intensity. Figure 3.4 demonstrates that all the conjugates showed nice cellular association and internalization already after a short 45 min incubation. The four-arm targeted oligomerconjugates (***707, 713, 733, 762***) did not display significantly better association and internalization compared with the conjugates of their nontargeted control oligomers. The two-arm targeted oligomer conjugates, ***715*** and ***729***, manifested far higher cell binding and uptake than their

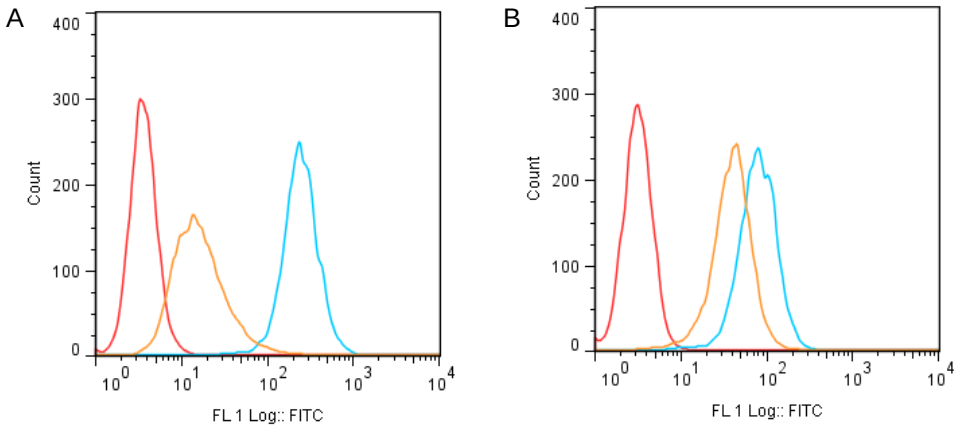

Figure 3.5 Free folic acid competition results for ***729*-**SS-nlsEGFP delivery. (A) Cellular association of ***729***-SS-nlsEGFP conjugates (1 μM) after 45 min incubation with KB cells determined by flow cytometry. (B) Cellular internalization of ***729***-SS-nlsEGFP conjugates (1 μM) after 45 min incubation with KB cells determined by flow cytometry. The experiment was performed by pre-treatment of the KB cells with 100 μM free folic acid on ice for 30 min before adding conjugates. Orange: with free folic acid competition; Light blue: without free folic acid competition; Red: PBS treated cell control.

nontargeted controls. Free folic acid competition experiment was also performed to further confirm the folate receptor specificity of ***729***-SS-nlsEGFP. The results (Figure 3.5) revealed that free folic acid competition significantly inhibited the cellular association and slightly inhibited the cellular internalization of ***729***-SS-nlsEGFP.

Furthermore, the fluorescence intensity was investigated after incubating the cells with the nlsEGFP conjugates for 24 h, followed by an additional 24 h incubation in fresh media (Figure 3.6). Cells treated with ***712, 713, 728, 729, 794***, and ***795*** nlsEGFP conjugates however remained (22%–92%) enhanced green fluorescent protein (EGFP) fluorescence-positive, whereas the cells treated with the other conjugates (***706, 707, 714, 715, 732, 733, 761, 762***) had lost nlsEGFP fluorescence (<10%). Compared with ***706*** and ***707***, respectively, ***712*** and ***713*** nlsEGFP conjugates had a higher recovery of EGFP fluorescence. It is noteworthy that ***729***-SS-nlsEGFP showed the highest percentage of fluorescence-positive cells (92%) among all the conjugates.

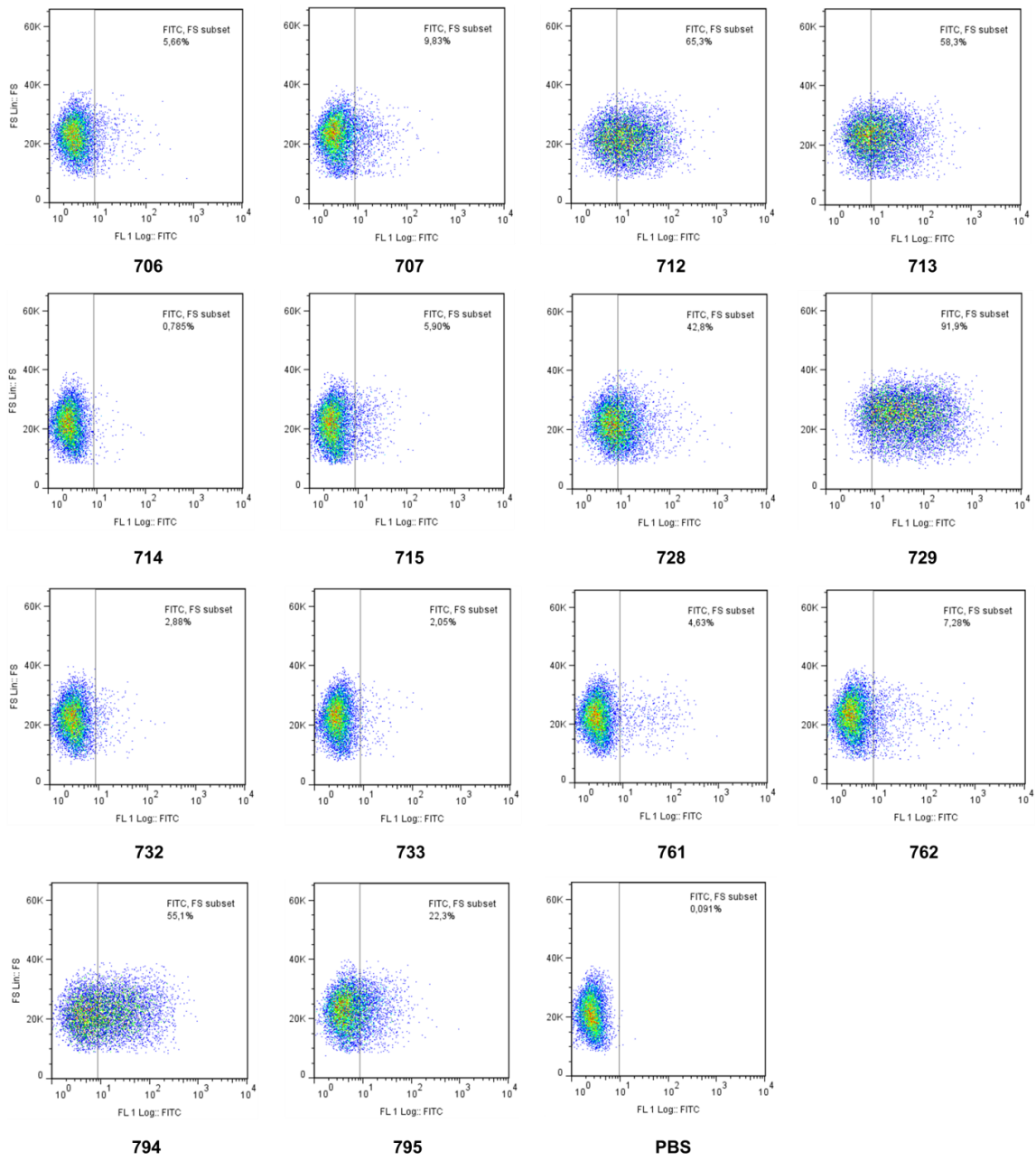

Conjugates	706	707	712	713	714	715	728	729	732	733	761	762	794	795
GFP pos. / (%)	5.7	9.8	65.3	58.3	0.8	5.9	42.8	91.9	2.9	2.1	4.6	7.3	55.1	22.3

Figure 3.6 Representative results of cellular internalization of various nlsEGFP conjugates (1 µM, indicated by ID number) after 24 h incubation with KB cells, followed by an additional incubation of 24 h in fresh media determined by flow cytometry. PBS: PBS treated cell control.

Fluorescence microscopy confirmed the capacity of these oligomers to deliver nlsEGFP into cells, promote endolysosomal escape, and subsequent subcellular trafficking into the nucleus. Figure 3.7 A displays that ***729***-SS-nlsEGFP and ***728***-SS-nlsEGFP treated cells presented homogeneous fluorescence throughout the

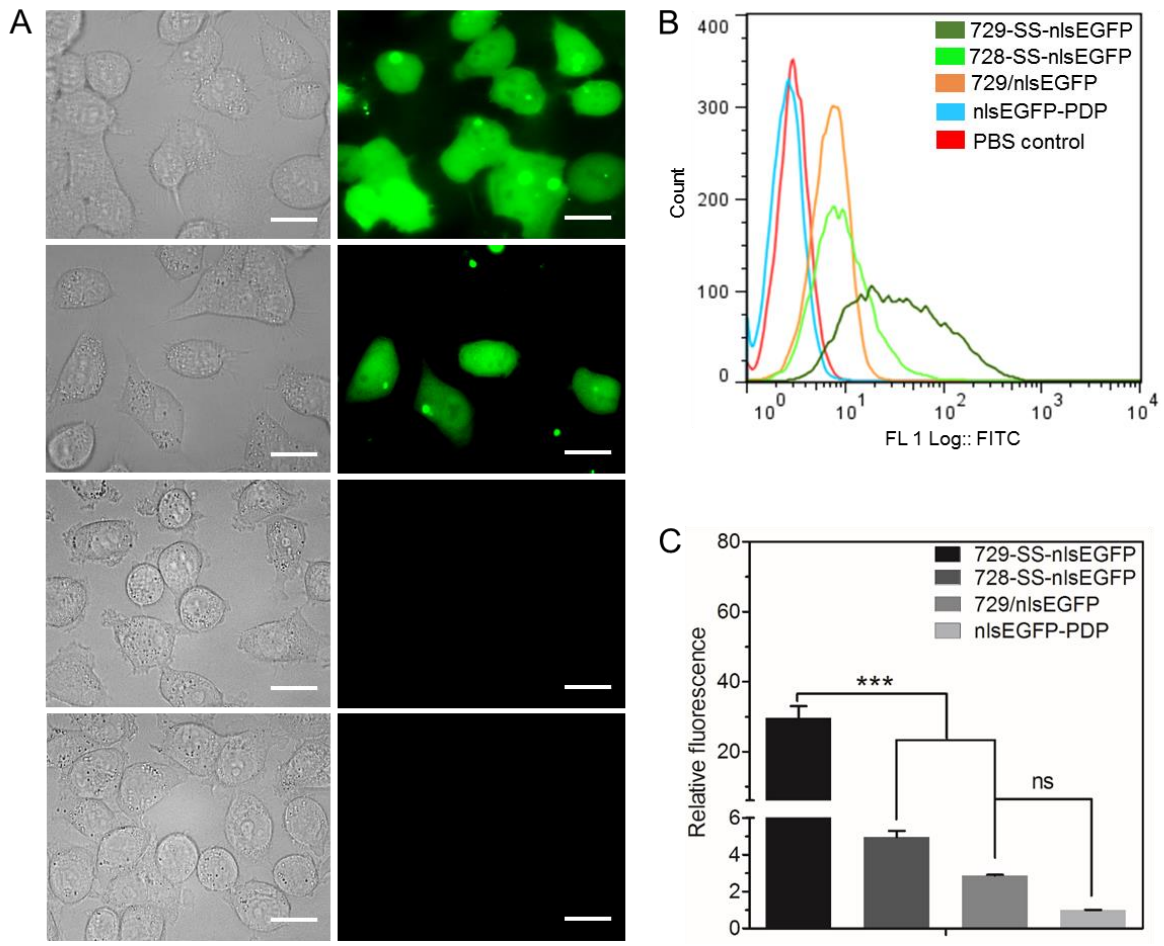

Figure 3.7 Transduction of KB cells with ***729***-SS-nlsEGFP (FolA-targeting) compared to ***728***-SS-nlsEGFP (non-targeted) mediated protein transduction. (A) Fluorescence microscopy of the live KB cells treated with 1 µM ***729***-SS-nlsEGFP (row 1), 1 µM ***728***-SS-nlsEGFP (row 2), mixtures of 6 µM ***729*** and 1 µM free nlsEGFP (row 3) and 1 µM nlsEGFP-PDP (row 4) for 24 h, followed by a 24 h incubation in fresh media. Left column: bright-field images of the treated cells. Right column: EGFP fluorescence of the treated cells. (B) Cellular internalization of each sample incubated with KB cells as described in (A). (C) Relative fluorescence intensities of cells treated with each sample as described in (A). The intensities were normalized regarding to the mean fluorescence intensity of the cells treated with nlsEGFP-PDP. ****p* < 0.001; ns: no significant difference. Data are shown as mean ± SD (n=3). Scale bar = 20 µm.

cells for 24 h after an incubation time of 24 h. However, cells treated with the other conjugates showed no fluorescence or just punctate fluorescence under the fluorescence microscope (data not shown). Moreover, nlsEGFP was found imported into the cell nuclei. In contrast, SPDP modified nlsEGFP and the mixture of ***729*** and free nlsEGFP without covalent attachment had very low efficiency to enter the treated cells (not detectable by fluorescence microscopy). More EGFP positive cells were

Table 3.4 Summary of the intracellular nlsEGFP delivery efficacy of various targeted nlsEGFP conjugates (indicated by oligomer ID number)

Conjugates (Oligomer-SS-nlsEGFP)	Cellular association	Cellular internalization	Target specificity	EGFP positive cells (48h, %)	Nuclear import
707	+	+	-	10	-
713	+	+	-	58	-
715	+	+	+	6	-
729	+	+	+	92	+
733	+	+	-	2	-
762	+	+	-	7	-
795	+	+	-	22	-

[a)]+ : positive; [b)]- : negative

observed in the fluorescence microscope images of ***729***-SS-nlsEGFP treated than ***728***-SS-nlsEGFP treated cells. This was confirmed by flow cytometry. Cells treated with SPDP modified nlsEGFP present almost the same fluorescence background intensity as phosphate buffered saline (PBS) treated cells (Figure 3.7 B). Cells incubated with a mixture of ***729*** and free nlsEGFP display only slightly higher fluorescence. Importantly, ***729***-SS-nlsEGFP treated cells displayed a significantly higher mean fluorescence intensity, sixfold higher than that of cells treated with nontargeted ***728***-SS-nlsEGFP, and tenfold higher than that of cells treated with the mixture of ***729*** and free nlsEGFP (Figure 3.7 C). In conclusion, it is noteworthy that ***729***-SS-nlsEGFP is the only conjugate presenting nice cellular association, cellular internalization, folate receptor specificity, long-term (48 h) survival of nlsEGFP activity, and subcellular nuclear import among all the targeted oligomers (Table 3.4).

3.1.3 Folate-PEG-oleoyl containing two-arm oligomer *729*-SS-RNase A conjugate triggers potent KB carcinoma cell killing

To further compare their protein delivery efficiency, oligomers were conjugated with RNase A as therapeutic cargo protein at a molar ratio of 4:1. This oligomer/cargo protein ratio was empirically found as most effective. Successful delivery of RNase A

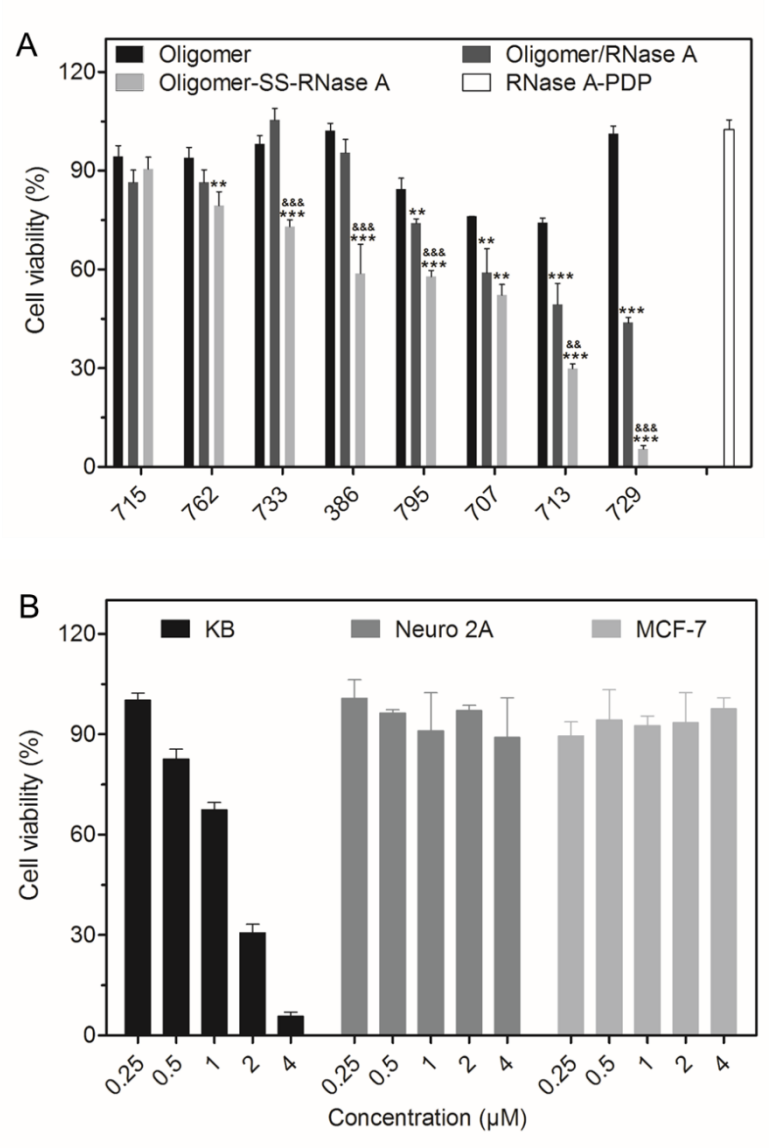

Figure 3.8 A) Evaluation of RNase A transfection efficiency with various RNase A conjugates on KB cells presented as % cell metabolic activity of control cells (MTT assay). Cells were incubated with the indicated agents under standard culture conditions for 4 h, followed by a 44 h incubation with fresh media. Black: oligomer control (16 μM); deep grey: mixtures of oligomer (16 μM) and free RNase A (4 μM); grey: RNase A conjugates (4 μM); white: RNase A-PDP (4 μM). B) Protein concentration-dependent cytotoxicity of ***729*** mediated RNase A transfection on folate receptor positive KB cells in comparison to folate receptor negative cells (MCF-7 and Neuro 2A). *: compared with oligomer; &: compare with oligomer/RNase A. $^{**}p < 0.01$, $^{***}p < 0.001$, $^{\&\&}p < 0.01$, $^{\&\&\&}p < 0.001$. Data are shown as mean ± SD (n=3).

into the cytosol was expected to elicit degradation of cytosolic RNA, thereby inducing cell killing. KB cells were treated with the various oligomers, the corresponding oligomer/RNase A noncovalent mixtures as controls, or the oligomer–RNase A conjugates, and the metabolic cell activity after 48 h was determined using an

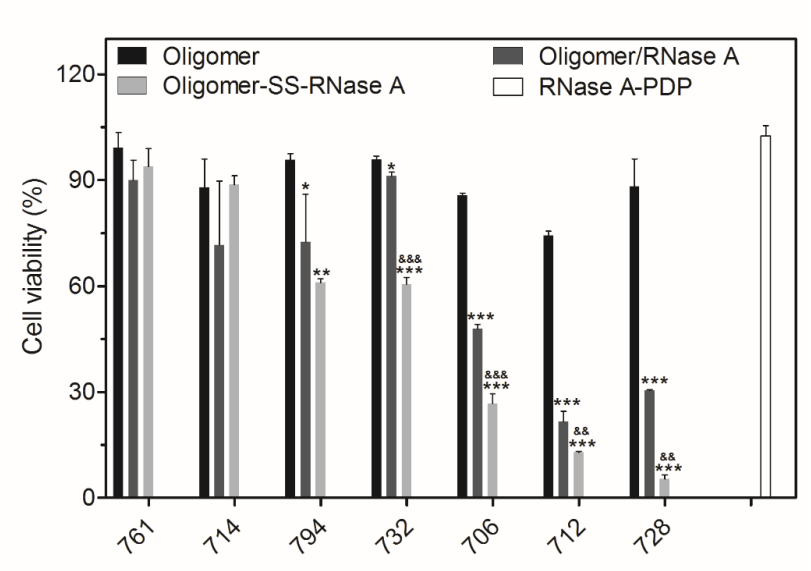

Figure 3.9 Evaluation of RNase A transfection efficiency with various non-targeted RNase A conjugates on KB cells by a cell metabolic activity assay (MTT assay). Black: oligomer control (16 μM); Deep grey: mixtures of oligomer (16 μM) and free RNase A (4 μM); Grey: RNase A conjugates (4 μM); White: RNase A-PDP (4 μM). *: compared with oligomer; $^{\&}$: compare with oligomer/RNase A. *p < 0.05, **p < 0.01, ***p < 0.001, $^{\&\&}p$ < 0.01, $^{\&\&\&}p$ < 0.001. Data are shown as mean ± SD (n=3).

dimethylthiazolyldiphenyltetrazolium bromide (MTT) assay (Figure 3.8 A). Cells treated with oligomers only showed no or only low (up to 25%) reduction in metabolic activity. The corresponding dose of SPDP linker modified RNase A did also not result in any detectable change of cell viability. Unmodified RNase A was also nontoxic (data not shown). In contrast, the RNase A conjugates formed with various oligomers exhibited cytotoxicity. Five targeted oligomers (***707, 713, 729, 733, 795***) and their nontargeted control oligomers (***706, 712, 728, 732, 794*** in Figure 3.9) could successfully deliver RNase A into tumor cells and reduce their viability. The three-arm oligomer ***386***, previously reported as carrier for nlsEGFP delivery, could transduce RNase A into cells resulting in moderate (40%) reduction of cell viability. Cells treated with the mixtures of free RNase A and oligomers also presented appreciable reduction of metabolic activity. The covalent conjugates, however, always displayed a far higher cytotoxicity than the mixtures. Consistent with the nlsEGFP transfection results, the RNase A conjugates of histidinylated oligomers ***712*** and ***713*** showed higher cytotoxicity than those of the histidine lacking analogs ***706*** and ***707***, respectively.

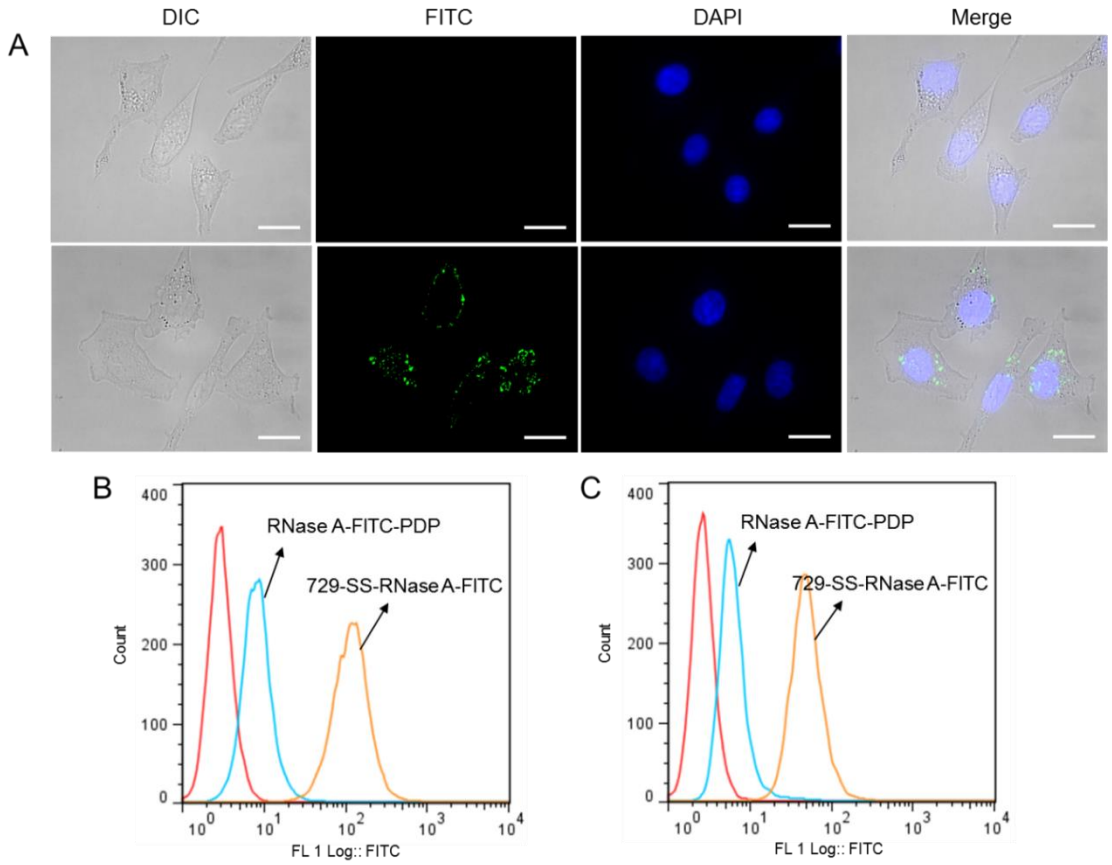

Figure 3.10 Transduction of KB cells with ***729***-SS-RNase A-FITC. (A) Fluorescence microscopy of the KB cells treated with 2 µM RNase A-FITC-PDP (row 1), or 2 µM ***729***-SS-RNase A-FITC (row 2) for 45 min short incubation. (B) Cellular association and (C) cellular internalization after 45 min incubation with KB cells as determined by flow cytometry. Scale bar = 20 µm.

Among all the tested conjugates, ***729***-SS-RNase A (Figure 3.8 A) and its nontargeted ***728*** analog (Figure 3.9) mediated the by far highest cytotoxicity, decreasing the viability of KB cells down to 5%, whereas the toxicity of the free oligomer was negligible. Based on the promising RNase A delivery efficiency, ***729***-SS-RNase A was evaluated in more detail. Figure 3.8 B presents the protein dose dependence of cytotoxicity. Interestingly, no significant decrease in cell viability was observed in folate-receptor-negative cells (MCF-7 and Neuro-2a) after incubation with ***729***-SS-RNase A conjugate at the same concentrations.

The cellular internalization and intracellular distribution of 729-SS-RNase A in KB cells was also investigated using fluorescein isothiocyanate (FITC) labeled RNase A to

obtain ***729***-SS-RNase A-FITC conjugates. Fluorescence microscopy (Figure 3.10 A) showed that free RNase A-FITC-PDP could not efficiently enter cells, as evidenced by lack of green fluorescence. In contrast, for ***729***-SS-RNase A-FITC treated cells, already after a relatively short 45 min incubation, a remarkable cellular uptake of ***729***-SS-RNase A-FITC and intracellular accumulation in endosomes was visible as green punctuate fluorescence. The different cell association and internalization efficiencies of ***729***-SS-RNase A-FITC and free RNase A-FITC-PDP were also confirmed and quantified by flow cytometry evaluation (Figure 3.10 B,C), revealing again that ***729*** is a potent nanocarrier for protein delivery.

3.1.4 The key role of oleic acids in oligomer *729*—facilitating enhanced cytosolic entry via lipid membrane destabilization and subsequent cell killing by RNase A

The former results clearly demonstrate that ***729*** outperformed other oligomers with endosomal escape function, such as the four-arm oligomer comprising Sph and histidines, in protein delivery. We conclude that the oleic acids as the endosomolytic unit in ***729*** play a crucial role in the enhanced intracellular protein delivery. Therefore, based on this hypothesis, control oligomers (***937, 737***) with the same sequence,

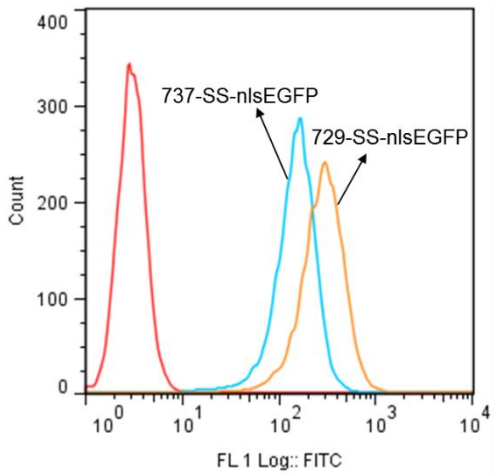

Figure 3.11 Cellular association of nlsEGFP conjugates (1 µM) formed with ***729*** or ***737*** (analog without oleic acid modification) after 45 min incubation with KB cells determined by flow cytometry. Red: PBS treated cell control.

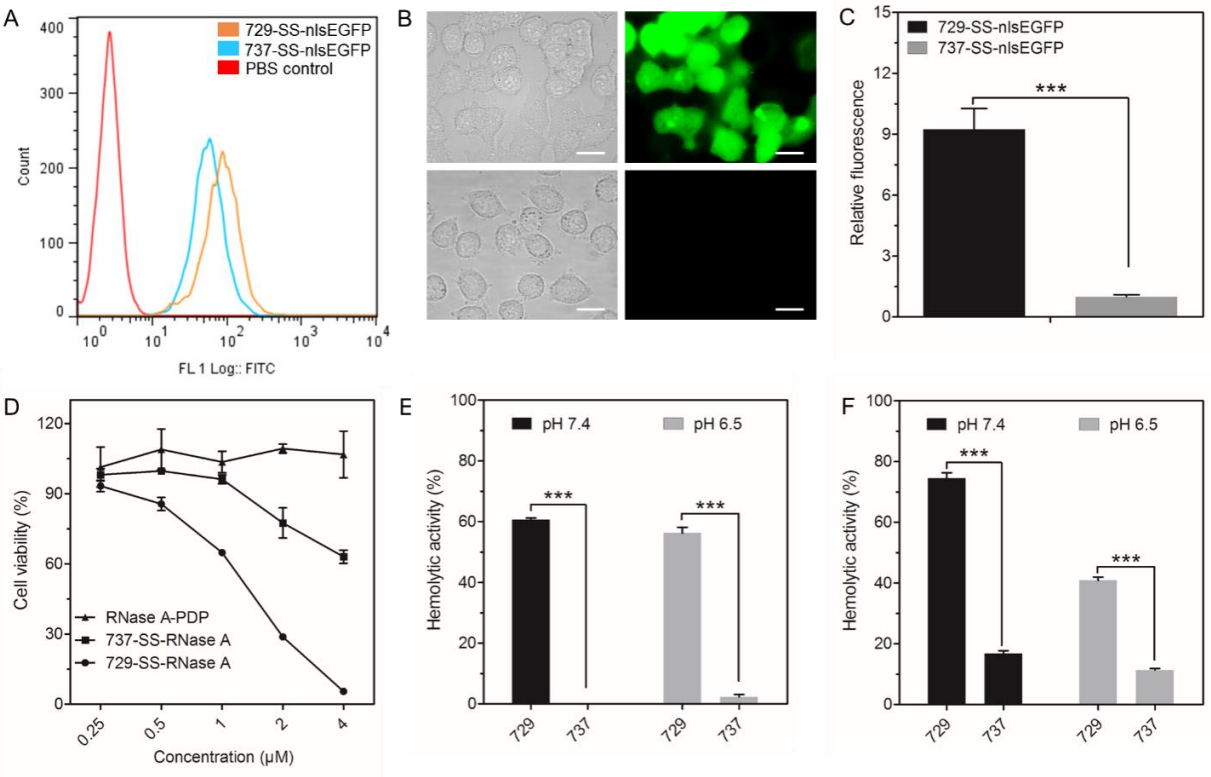

Figure 3.12 Structure-activity relationship of ***729*** enhanced intracellular protein delivery. (A) Cellular internalization of 1 μM ***729*** (oleic acid modified) or ***737*** (lacking oleic acids) targeted nlsEGFP conjugates after 45 min incubation with KB cells as determined by flow cytometry. (B) Fluorescence microscopy of live KB cells treated with 1 μM ***729***-SS-nlsEGFP (row 1) or 1 μM ***737***-SS-nlsEGFP (row 2) for 24 h, followed by an incubation of 24 h in fresh media. Left column: bright-field images of the treated cells. Right column: EGFP fluorescence of the treated cells. (C) Relative fluorescence intensities per cell after in total 48 h after treatment as described in (B). The intensities were normalized regarding to the mean fluorescence intensity of cells treated with ***737***-SS-nlsEGFP. (D) Evaluation of RNase A transduction with ***729*** or ***737*** RNase A conjugates on KB cells by using a cell metabolic activity (MTT) assay. (E) Lytic activity of ***729*** or ***737*** nlsEGFP conjugates (1 μM) at physiological pH 7.4 and early endosomal pH 6.5 in an erythrocyte leakage assay. (F) Lytic activity of ***729*** or ***737*** RNase A conjugates (2 μM) at pH 7.4 and pH 6.5. ***$p < 0.001$. Data are shown as mean ± SD (n=3). Scale bar = 20 μm.

without or with folate targeting ligand, PEG and topology as in ***728*** or ***729*** except the oleic acids were synthesized, analyzed, and compared for protein delivery efficiency. After a 45 min incubation, folate-targeted ***737***-SS-nlsEGFP in comparison to the ***729***-SS-nlsEGFP conjugate displayed an only slightly reduced cell association (Figure 3.11) and intracellular uptake (Figure 3.12 A) as analyzed by flow cytometry. However, as Figure 3.12 B reveals, after cell exposure to ***729***-SS-nlsEGFP for 24 h

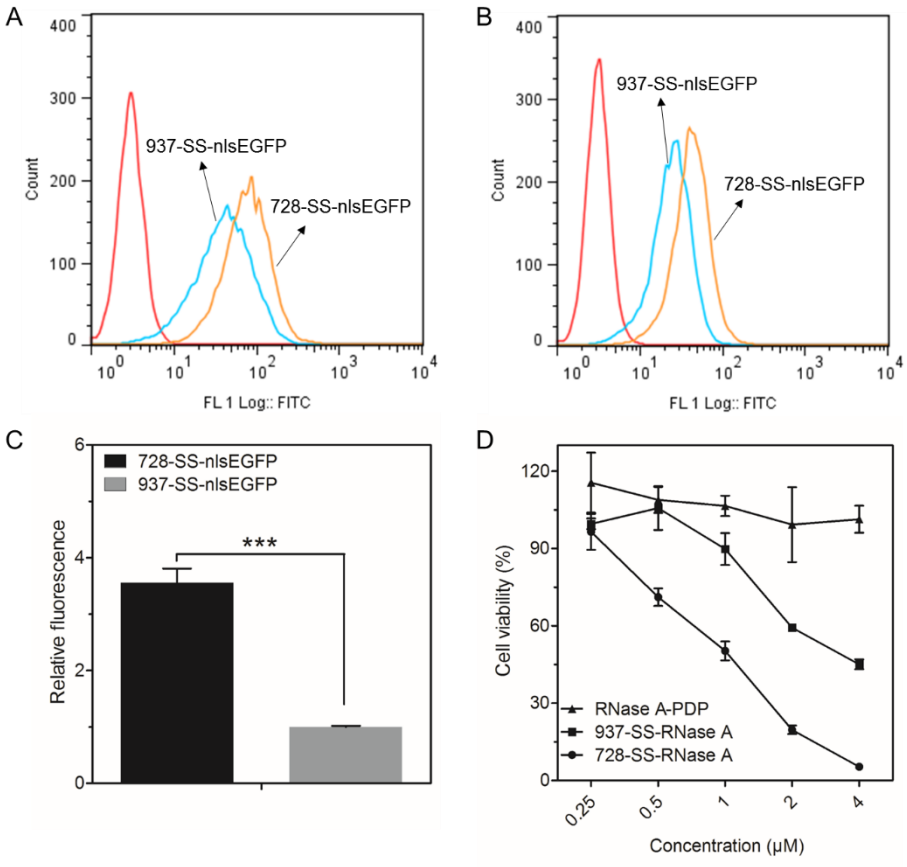

Figure 3.13 Structure - intracellular protein delivery relationship of ***728*** and ***937*** (analog without oleic acid modification). (A) Cellular association of ***728*** or ***937*** formed nlsEGFP conjugates (1 µM) after 45 min incubation with KB cells determined by flow cytometry. (B) Cellular internalization of 728 or 937 formed nlsEGFP conjugates (1 µM) after 45 min incubation with KB cells determined by flow cytometry. (C) Relative fluorescence intensities of per cell treated with each sample for 24h, followed by another 24 h incubation in fresh media. The intensities were normalized regarding to the mean fluorescence intensity of the cells treated with ***937***-SS-nlsEGFP. (D) Evaluation of RNase A transfection efficiency with ***728*** or ***937*** RNase A conjugates on KB cells by a cell metabolic activity assay (MTT assay). ****p* < 0.001. Data are shown as mean ± SD (n=3).

under standard culture conditions, followed by another 24 h incubation in fresh media, the cells showed green fluorescence of nlsEGFP distributed throughout the cytosol and nucleus, whereas no nlsEGFP was observable in the ***737***-SS-nlsEGFP treated cells. Flow cytometry results (Figure 3.12 C) demonstrate a nine times higher meanfluorescence intensity for ***729***-SS-nlsEGFP treated cells compared with ***737***-SS-nlsEGFP treated cells. An analogous comparison of the RNase A delivery efficiency of ***729***-SS-RNase A and ***737***-SS-RNase A gave consistent results (Figure

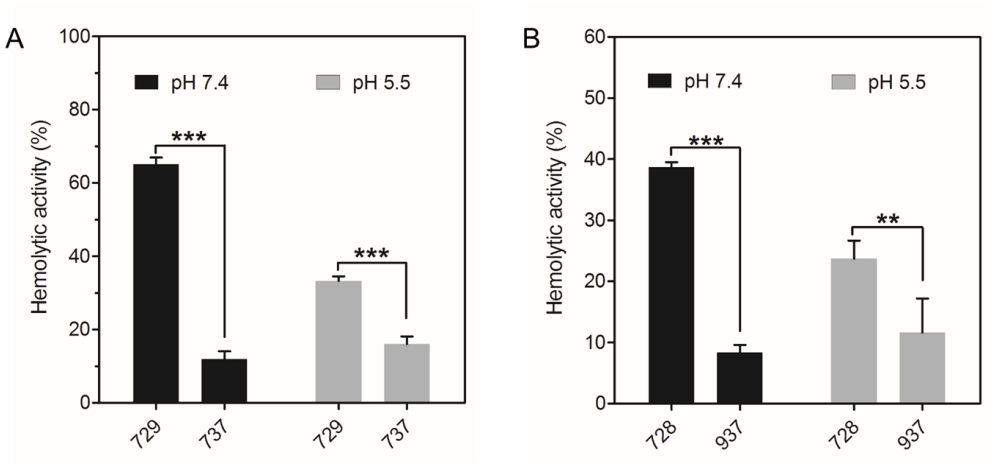

Figure 3.14 Erythrocyte leakage assay of plain oligomers (5 µM) at different pH values. (A) Leakage assay of ***729*** and ***737*** (analog without oleic acid modification). (B) Leakage assay of ***728*** and ***937*** (analog without oleic acid modification). ***p* < 0.01, ****p* < 0.001. Data are shown as mean ± SD (n=3).

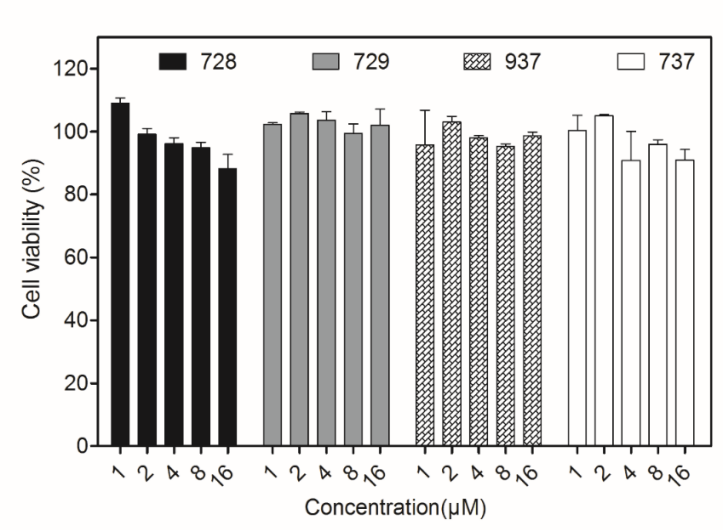

Figure 3.15 Cell viability evaluation of the cells treated with different oligomers at different concentration. Data are shown as mean ± SEM (n=3).

3.12 D). KB cells treated with ***729***-SS-RNase A experienced significantly higher cytotoxicity compared with cells treated with ***737***-SS-RNase A. To further verify this conclusion, an erythrocyte leakage assay was performed to compare the lytic effects of ***729***-SS-nlsEGFP and ***737***-SS-nlsEGFP (Figure 3.12 E) or ***729***-SS-RNase A and ***737***-SS-RNase A (Figure 3.12 F) on lipid membranes. A potent lytic activity was observed for ***729***-SS-nlsEGFP both at physiological pH and early endosomal pH, whereas, in sharp contrast, ***737-***SS-nlsEGFP displayed no significant hemolysis under these conditions (Figure 3.12 E). Similar findings were made in hemolysis

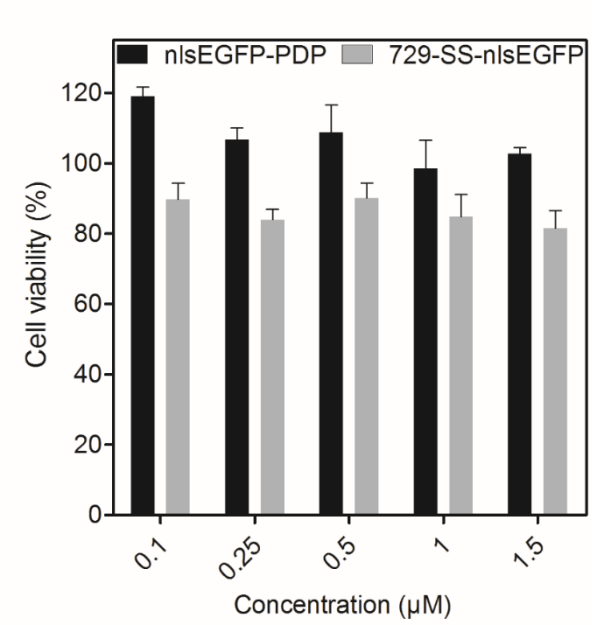

Figure 3.16 Metabolic cell activities (in % of untreated controls) of KB cells treated with ***729***-SS-nlsEGFP or nlsEGFP-PDP at indicated concentration. Data are shown as mean ± SD (n=3).

studies of the RNase A conjugates; again, ***729***-SSRNase A caused far more erythrocyte lysis than ***737***-SS-RNase A (Figure 3.12 F). These results are well consistent with the cell metabolic activity assays (Figure 3.12 D) after RNase A transductions. Also the oleic acid modified nontargeted oligomer ***728*** presented higher nlsEGFP and RNase A delivery efficiency than the control oligomer ***937*** **(**Figure 3.13). The erythrocyte leakage assay of plain oligomers (without protein conjugation, Figure 3.14) also showed a higher lytic activity of the oleic acid modified oligomers (***728, 729***) than the oligomers without oleic acid (***937, 737***). A direct effect of the oligomers on cell viability however could be excluded (Figure 3.15). Furthermore, analogous oligomer conjugates of the nontoxic nlsEGFP protein did not mediate cytotoxicity (more than 80% metabolic activity of treated cells; Figure 3.16).

3.2 Lipo-oligomer nanoformulations for targeted intracellular protein delivery

Section 3.2 has been partly adapted from: Peng Zhang, Benjamin Steinborn, Ulrich Lächelt, Stefan Zahler, and Ernst Wagner, Biomacromolecules DOI: 10.1021/acs.biomac.7b00666.

In our previous research, a series of sequence-defined cationizable oligoaminoamides was synthesized via precise assembly of artificial amino acid blocks such as succinoyl tetraethylene pentamine (Stp), which presented efficient and effective pDNA and siRNA transfection capacities [112, 114, 116, 117]. Furthermore, some of these oligomers were also found to be favorable for delivery of protein into the cytosol of cells [120, 121, 137, 138, 144]. Especially the amphiphilic triblock lipo-oligomers ***728*** and ***729*** displayed high protein transduction activity ([144] and previous chapter), containing eight units of cationizable Stp for endosome escape, two terminal cysteines for reversible covalent protein conjugation and stabilizing of formed nanoparticles, a tetra-oleic acid block for providing hydrophobicity and endosomolytic activity, and a polyethylene glycol (PEG) unit for shielding optionally with folate (in case of ***729***) for targeting. For ***729*** protein conjugates first encouraging demonstration of receptor targeted delivery was obtained, the formulation however presented micellar protein nanorod structures (diameter 10 nm by TEM, hydrodynamic diameter 25-35 nm by DLS) with limited stability [144]. Therefore, aim of the current work has been the optimization of the formulation by combining the previously reported lipo-oligoaminoamide ***728*** – protein conjugates with various lipids, optionally including a novel folic acid-PEG conjugated lipid ***1042*** for folate receptor targeting. RNase A and nlsEGFP were applied as two representative cargo proteins, which were first coupled to ***728*** via disulfide bonds. These linkages are supposed to be reduced within the reducing cytosolic environment after the escape of conjugates from endolysosomes. [144, 145] We found that optimized proteoliposome nanoparticles including ***728***, DOPS, cholesterol, DMPE-PEG2000 and ***1042*** can

effectively deliver RNase A or nlsEGFP into cells in the presence of serum, where RNase A induces highest targeted cell killing on folate-receptor-positive KB carcinoma cells, and nlsEGFP undergoes highly efficient targeted delivery into the cytosol and nucleus of KB cells.

3.2.1 Formation and characterization of lipo-oligomer nanoformulations

A novel targeted intracellular protein delivery platform (Figure 3.17 A) was developed through the self-assembly of ***728***, a sequence-defined amphiphilic triblock oligoaminoamide lipo-oligomer, which was bioreversibly conjugated with the cargo protein, together with various helper lipids at defined molar ratios into proteo-lipidic nanoparticles. Three different helper lipids, DOPS (anionic lipid), DOPE (neutral lipid), LinA (fatty acid) were applied to help to form stable nanoparticles and neutralize the positive charges on the nanoparticle surfaces. Cholesterol was applied to stabilize lipid bilayers and enhance the stability of the lipidic protein nanoparticles. Three PEGylated lipids, DMPE-PEG2000, DSPE-PEG2000, or the novel folate-PEGconjugated lipid analog ***1042*** (see below) were also used to reduce the zeta potential, enhance the serum stability, and provide optional targeting capacity (Figure 3.18). Figure 3.17 A also displays the molar ratios of the optimized protein formulations and hypothetical liposomal or micellar structures depending on the helper lipid content (see below).

Figure 3.19 presents the chemical structures of sequence-defined oligomers which were applied in the current study and generated by solid-phase synthesis [116, 117]. Oligomer ***728*** (Figure 3.19) [144] contains a monodisperse PEG chain (24 ethylene oxide units), coupled to the cationic backbone to decrease unspecific protein binding and providing a hydrophilic block. The cationizable backbone of ***728*** was assembled with a two-arm topology containing eight Stp units in total. Stp is an artificial amino acid building block, supposed to enhance endosomal escape of internalized nanomaterial by the proton-sponge effect [146]. Oleic acids were included into ***728*** to

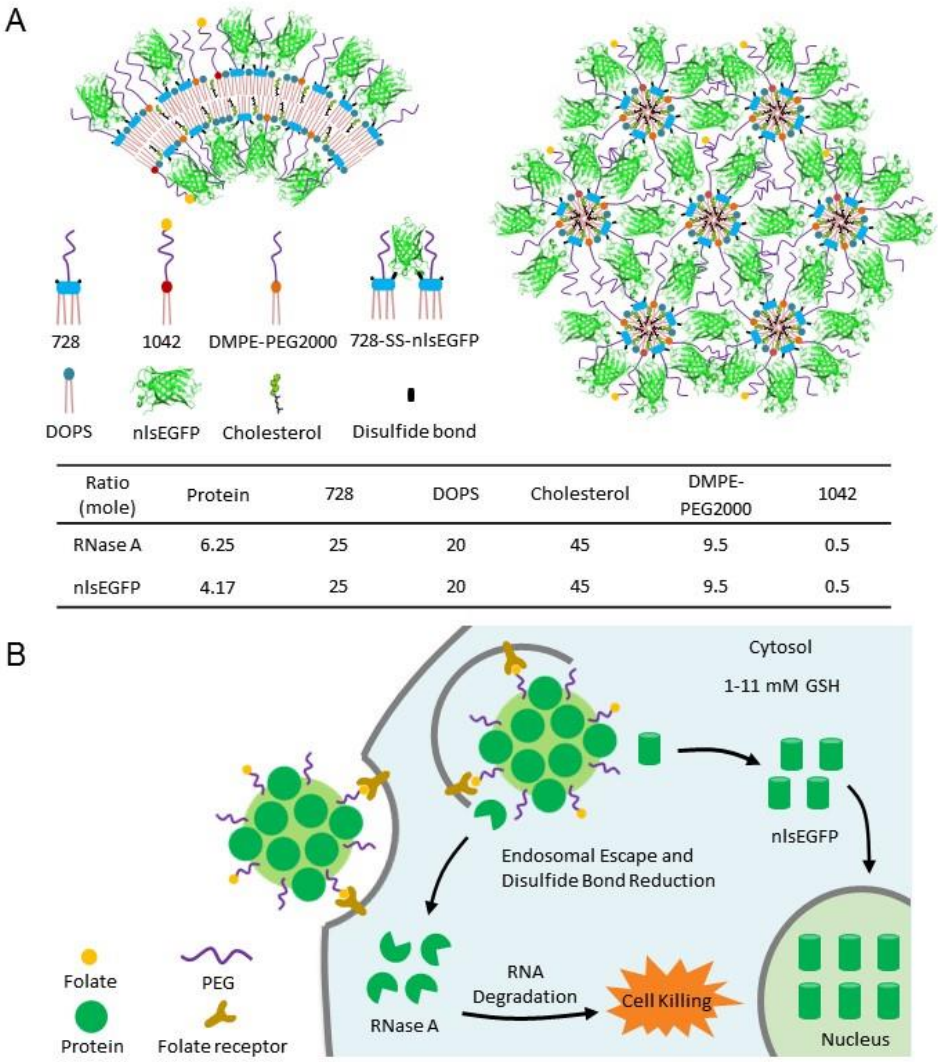

Ratio (mole)	Protein	728	DOPS	Cholesterol	DMPE-PEG2000	1042
RNase A	6.25	25	20	45	9.5	0.5
nlsEGFP	4.17	25	20	45	9.5	0.5

Figure 3.17 A) Formulation components (bottom; molar ratios of optimized formulations) and hypothetical structures of nanoformulations (left, proteo-liposomal; right proteo-micellar, displayed for EGFP). B) Targeted intracellular protein delivery meditated by lipo-oligomer nanoformulations.

provide a hydrophobic block for nanoparticle stabilization and endosomal membrane destabilization. Additionally, natural amino acids are integrated in ***728***: glutamic acid at the distal end of PEG; lysines serving as branching points of the two-arm topology via the modification of α- and ε-amino groups; cysteines for conjugation to the cargo proteins by reducible disulfide bonds and further crosslink-stabilization of the nanoformulations. The novel folate-PEG conjugated lipid analog ***1042*** (Figure 3.19) was designed as optional targeting component, with folate incorporated at the distal end of polyethylene glycol (containing 36 ethylene oxide units) linked with two stearic acids via a lysine spacer. Two cargo proteins, RNase A and nlsEGFP, were applied to

Cholesterol	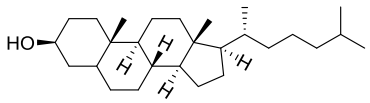
Linoleic acid	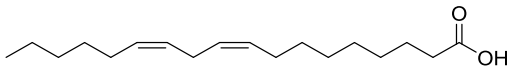
DOPS	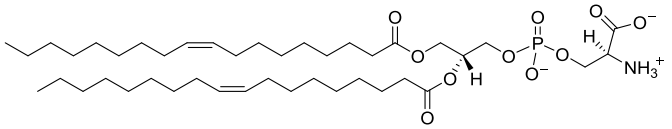
DOPE	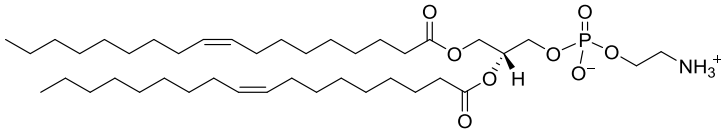
DMPE-PEG2000	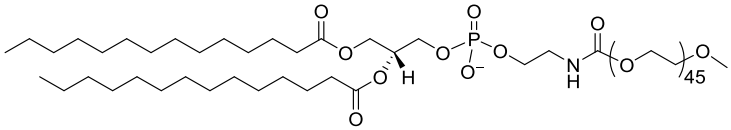
DSPE-PEG2000	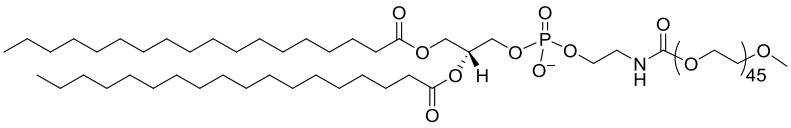

Figure 3.18 Chemical structures of involved lipids.

728	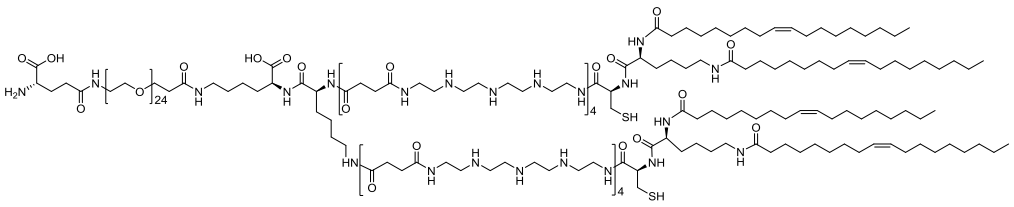 K- ε (PEG_{24}-E)-K- α,ε (Stp_4-C-K-OA_2)$_2$
1042	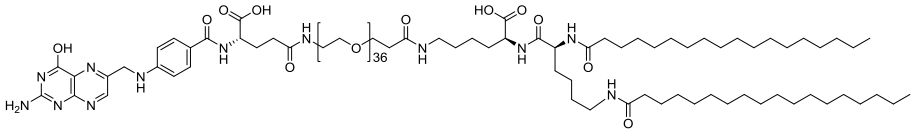 K- ε (PEG_{36}-FolA)-K- α,ε ($SteA$)$_2$

Figure 3.19 Chemical structure of lipo-oligomer ***728*** and the folic acid-PEG conjugated lipid analog ***1042***. Sequences are shown from C to N terminus. Abbreviations: E: glutamic acid; OA: oleic acid; C: cysteine; K: branching lysine selectively modified at α and ε amines; PEG_{24}: polyethylene glycol containing 24 ethylene oxide monomer units; FolA: folic acid; SteA: stearic acid; PEG_{36}: polyethylene glycol containing 36 ethylene oxide monomer units. The novel FolA-PEG lipid ***1042*** was designed and synthesized by Benjamin Steinborn and Dr. Ulrich Lächelt (PhD study, Pharmaceutical Biotechnology, LMU Munich).

Table 3.5 Composition (ratios in molar %) of lipo-oligomer nanoformulations.

Protein	Formulation	***728***	Helper lipids	Cholesterol	DM/SPE-PEG2000	***1042***
RNase A	FA-***728***-DOPS-DMPE-RNase A	25	20	45	9.5	0.5
	FA-***728***-DOPE-DMPE-RNase A	25	20	45	9.5	0.5
	FA-***728***-LinA-DMPE-RNase A	25	20	45	9.5	0.5
	FA-***728***-DOPS-DSPE-RNase A	25	20	45	9.5	0.5
	FA-***728***-DOPE-DSPE-RNase A	25	20	45	9.5	0.5
	FA-***728***-LinA-DSPE-RNase A	25	20	45	9.5	0.5
	728-DOPS-DMPE-RNase A	25	20	45	10	
nlsEGFP	FA-***728***-DOPS-DMPE-nlsEGFP	25	20	45	9.5	0.5
	728-DOPS-DMPE-nlsEGFP	25	20	45	10	

investigate the targeted protein delivery (Figure 3.17 B). RNase A, if internalized into the cytosol, can efficiently kill cancer cell through degrading the cellular RNA. [66, 147] nlsEGFP contains a nuclear localization sequence derived from SV40 large T-antigen which helps to transport EGFP into the nucleus after cytosolic delivery. [121] To prepare the lipo-oligomer nanoformulations, RNase A (MW 13.7 kDa) or nlsEGFP (MW 31.5 kDa) were first covalently coupled to ***728*** via disulfide bonds using N-succinimidyl 3-(2-pyridyldithio) propionate (SPDP) linkers. On average, RNase A or nlsEGFP molecules were modified with two or three SPDP linkers, respectively. Then, the PDP-modified protein was reacted with 4 (in case of RNase A) or 6 (for nlsEGFP) molar equivalents of ***728***. Subsequently, the resulting ***728***-SS-protein conjugates were added as aqueous solution to the dry lipid mixtures (various molar ratio as described in Table 3.5). After lyophilization and rehydration, [148, 149] as well as sonication, [150, 151] small and uniformly sized nanoparticles were formed. The nanoparticles were incubated for 48 h at room temperature, to make sure that the free

Table 3.6 Particle size (Z-average) and zeta potential of protein nanoparticles in HEPES buffer determined by DLS. Variations refer to the median of three measurements of the same sample.

Nanoparticle Formulation	Z-average(nm)	PDI	Zeta Potential(mV)
FA-***728***-DOPS-DMPE-RNase A	111,7 ± 1,2	0,29 ± 0,00	13,6 ± 0,2
FA-***728***-DOPE-DMPE-RNase A	94,6 ± 1,0	0,29 ± 0,01	18,9 ± 0,9
FA-***728***-LinA-DMPE-RNase A	96,8 ± 6,1	0,45 ± 0,02	22,3 ± 2,8
FA-***728***-DOPS-DSPE-RNase A	116,7 ± 0,5	0,28 ± 0,01	14,3 ± 0,6
FA-***728***-DOPE-DSPE-RNase A	101,3 ± 0,5	0,42 ± 0,03	20,3 ± 1,4
FA-***728***-LinA-DSPE-RNase A	154,5 ± 3,4	0,50 ± 0,01	20,5 ± 1,0
728-DOPS-DMPE-RNase A	86,2 ± 1,5	0,39 ± 0,01	15,9 ± 0,2
FA-***728***-DOPS-DMPE-nlsEGFP	119.2 ± 2.8	0.27 ± 0.01	6.09 ± 0.30
728-DOPS-DMPE-nlsEGFP	76.9 ± 5.8	0,36 ± 0.01	8.37 ± 0.74

thiols were fully oxidized via disulfide crosslinkage formation. Upon intracellular delivery, the disulfide bonds are supposed to be reduced in the cytosol through glutathione (GSH) resulting in release of oligomer-free proteins (Figure 3.17 B**)**. The reversibility of conjugation between RNase A or nlsEGFP and ***728*** has been demonstrated in our previous work. [144]

Dynamic light scattering (DLS) measurements of the prepared lipo-oligomer nanoformulations showed that their average sizes varied from 80 nm to 150 nm (Table 3.6). The zeta potential of the proteoliposomes nanoparticles varied from 6 mV to 22 mV (Table 3.6). The RNase A nanoparticles exhibited higher zeta potential than nlsEGFP nanoparticles. Helper lipid-containing nanoformulations like FA-***728***-DOPS-DMPE-RNase A and FA-***728***-DOPS-DMPE-nlsEGFP showed bigger particle sizes of ~100 nm compared to the sizes ~25-35 nm of their previously described control conjugates ***728***-SS-RNase A or ***728***-SS-nlsEGFP without helper lipids, respectively (Figure 3.20 A). Meanwhile, the zeta potential was decreased from 20 mV to 13 mV for RNase A nanoparticles, 11 mV to 6 mV for nlsEGFP nanoparticles

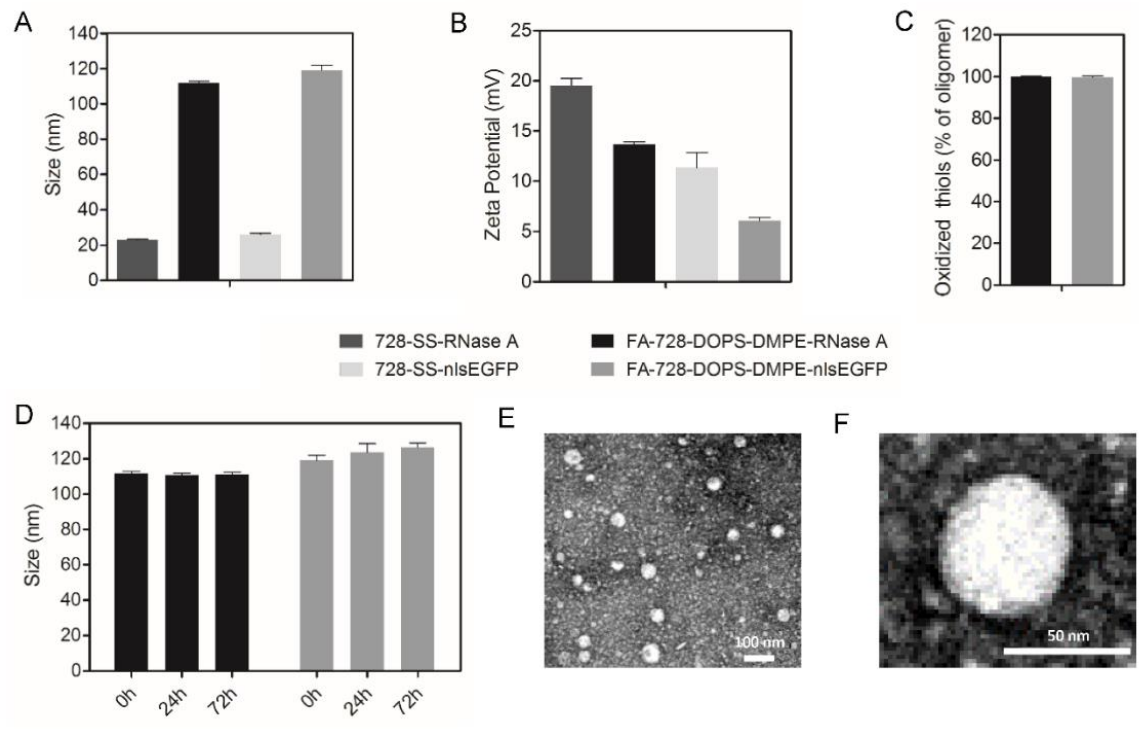

Figure 3.20 Characterization of representative lipo-oligomer nanoformulations. A) Sizes and B) Zeta potential of representative RNase A or nlsEGFP nanoparticles. C) Oxidation of free thiols in representative RNase A or nlsEGFP nanoparticles. D) Stability of representative RNase A or nlsEGFP nanoparticles. E) and F) TEM images of representative RNase A nanoparticles (FA-***728***-DOPS-DMPE-RNase A). Scale bar = 100 nm (E) or 50 nm (F). TEM images were generated by Susanne Kempter (Department of Physics, LMU Munich).

(Figure 3.20 B). Among all tested nanoparticles, only the DOPS group presents relatively obvious charge decreases (Table 3.6). The oxidation of free cysteines as an important step in the nanoparticle formation process was also investigated using the Ellman's assay. Figure 3.20 C shows that almost 100% of free thiols in FA-***728***-DOPS-DMPE-RNase A or FA-***728***-DOPS-DMPE-nlsEGFP nanoparticles were oxidized. Other tested formulations also presented almost full oxidation (Figure 3.21). The resulting disulfide crosslinkages are supposed to stabilize the formed nanoparticles. Therefore, the stabilities of FA-***728***-DOPS-DMPE-RNase A or FA-***728***-DOPS-DMPE-nlsEGFP nanoparticles were further investigated by particle size measurements after 72 h. The size of the RNase A nanoparticles was unchanged after 72 h, and only a slight but insignificant increase was observed for nlsEGFP nanoparticles (Figure 3.20 D). The transmission electron microscopy (TEM) image of

FA-***728***-DOPS-DMPE-RNase A nanoparticles showed a relatively homogeneous distribution of round shaped nanoparticles, most of them displaying an average diameter of ~50 nm (Figure 3.20 E, F).

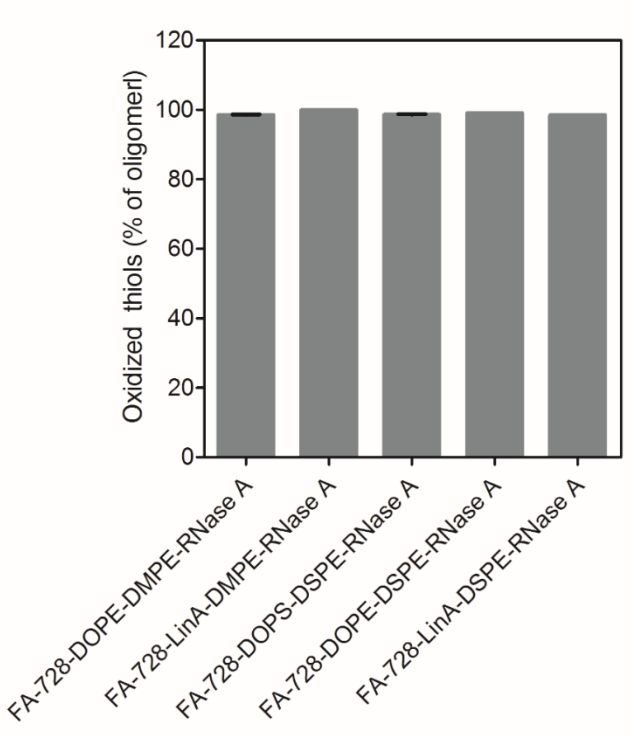

Figure 3.21 Oxidation of free thiols in representative RNase A nanoparticles. Data are shown as mean ± SD (n=3).

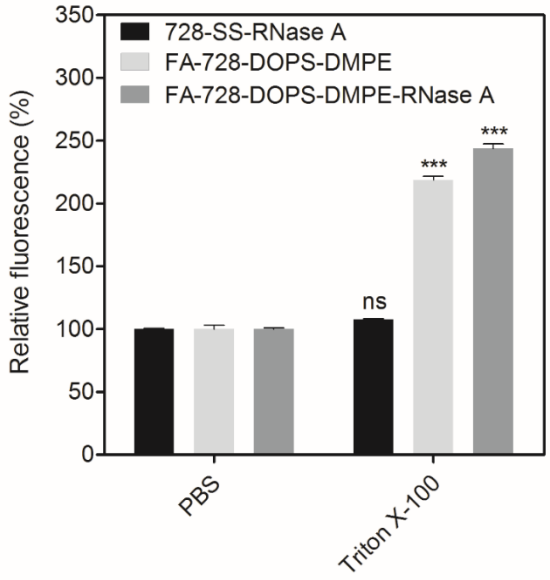

Figure 3.22 Calcein release from the RNase A nanoparticles after PBS or 3 % triton X-100 treatment. Statistical analysis in comparison with the PBS treated corresponding RNase A nanoparticles; ns: no significant difference; ***$p < 0.001$. Data are shown as mean ± SD (n=3).

Meanwhile, RNase A nanoformulations containing calcein (0.1 M) were generated by rehydrating the dry lipids mixtures with PBS (pH 7.4) containing 0.1 M calcein. Untrapped calcein was removed by size exclusion chromatography using Sephadex G25 column. Calcein is self-quenched at high concentration (0.1 M), [152, 153] and will be dequenched after release from the nanoparticles and dilution to lower concentrations. Calcein release studies by dissolving the formulations with triton X-100 resulted in calcein release and increased the fluorescence intensity in case of the helper lipid-containing RNase A nanoparticles but not for ***728***-SS-RNase A protein conjugate (Figure 3.22).

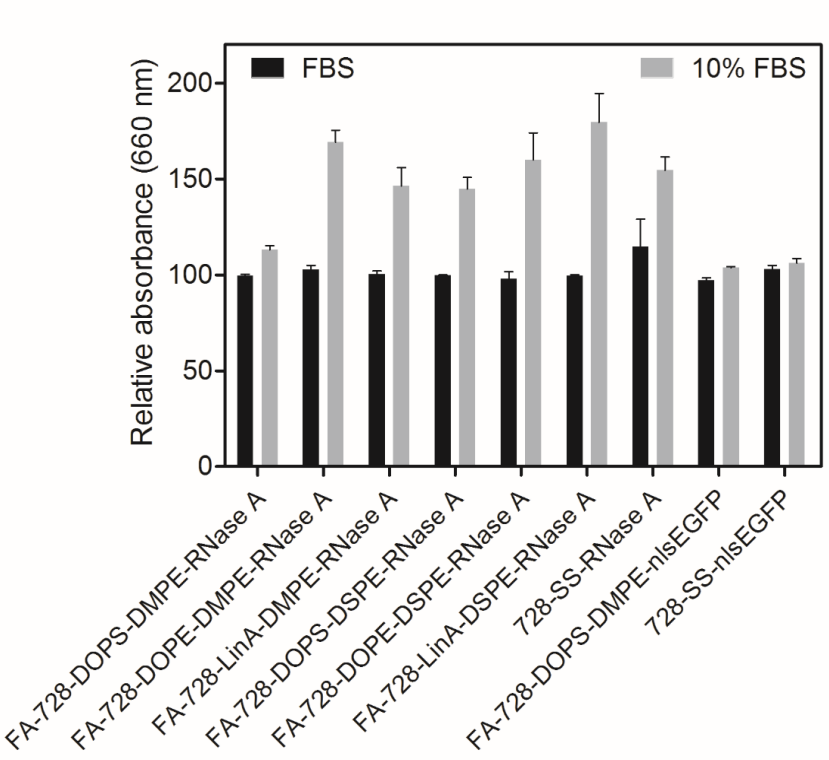

Figure 3.23 Turbidity measurements of representative protein nanoparticles after PBS or 10% FBS treatment for a 2 h incubation at 37 °C. Data are shown as mean ± SD (n=3).

Turbidity measurement results exhibited that none of the tested lipo-oligoaminoamide nanoparticles showed significant aggregation after PBS treatment for 2 h. After incubation in 10 % serum-containing buffer for 2 h, FA-***728***-DOPS-DMPE-RNase A presented highest resistance of aggregation among the RNase A nanoparticles. Also

the nlsEGFP nanoparticles were stable in 10% serum-containing buffer and resisted aggregation (Figure 3.23).

3.2.2 Comparison of cell killing effect of lipo-oligomer RNase A nanoformulations

To evaluate the protein delivery efficiency of targeted lipo-oligoaminoamide nanoformulations and intracellular protein bioactivity, RNase A were conjugated to the nanoparticles via disulfide bonds, which are supposed to increase the resistance of protein dissociation from nanoparticles under physiological environment. After being internalized into the reducing cytosol of cancer cells, the RNase A was supposed to be released from the nanoparticles and degrade the cellular RNA, thereby resulting in cancer cell killing. Folate-receptor positive KB cells were treated with the various RNase A nanoparticles, corresponding nanoparticles without RNase A or without ***728***, formulations of nanoparticles containing non-conjugated “free RNase A”, or RNase A-PDP at indicated concentration. MTT assay was used to determine the metabolic cell activity after 4 h incubation following another 44 h incubation in fresh medium. Cell treated with corresponding nanoparticles without RNase A did not show any reduction of metabolic activity. Also, cell viability reduction was not observed on the SPDP modified RNase A treated KB cells. Moreover, the cells treated with corresponding nanoparticles without ***728*** presented no cell viability reduction (Figure 3.24 A). In contrast, all the targeted RNase A nanoparticles showed significant cell killing. Cell treated with the corresponding nanoparticles containing nonconjugated “free RNase A” also exhibited appreciable decrease of cell viability (Figure 3.24 A). However, the nanoparticles conjugated with RNase A via disulfide linkage always presented higher cytotoxicity compared with the noncovalent formulations. Among all the tested targeted RNase A nanoparticles, FA-***728***-DOPS-DMPE-RNase A mediated the highest cytotoxicity, reducing the viability of KB cells down to 15%. Because of the promising performance on RNase A delivery, FA-***728***-DOPS-DMPE-RNase A was

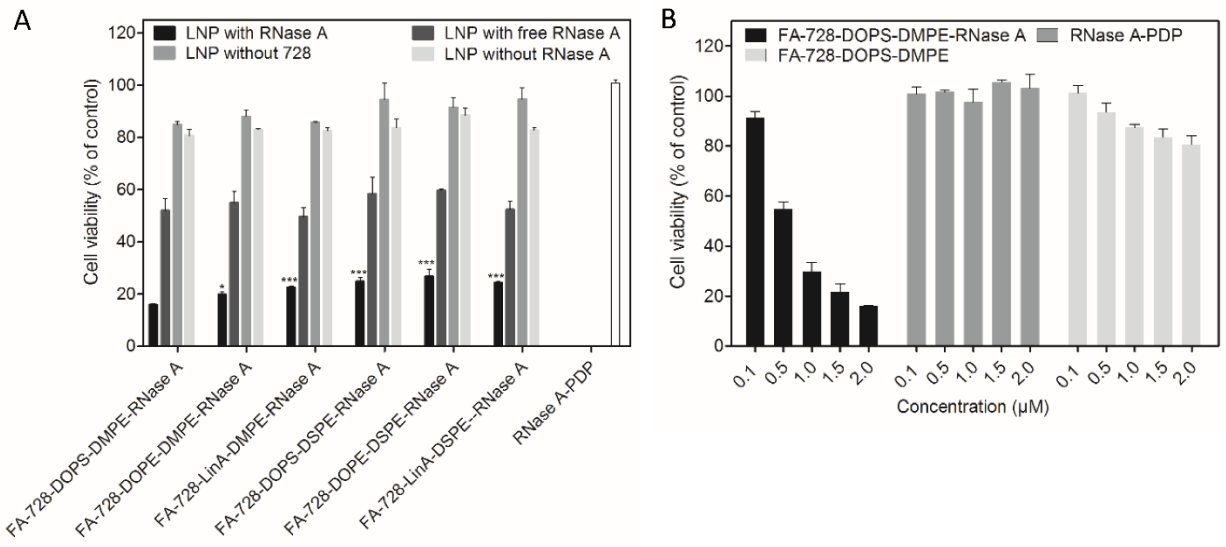

Figure 3.24 A) Evaluation of RNase A transfection efficiency with various RNase A nanoparticles on KB cells presented as % cell metabolic activity of control cells (MTT assay). Cells were incubated with the indicated agents under standard culture conditions for 4 h, followed by a 44 h incubation with fresh media. Black: RNase A nanoparticles (2 µM); deep grey: mixtures of corresponding dose of ***728***, lipids and free RNase A (2 µM); grey: mixtures of corresponding dose of lipids and free RNase A (2 µM); light grey: mixtures of corresponding dose of ***728*** and lipids without RNase A; white: RNase A-PDP (2 µM). B) RNase A protein concentration-dependent cytotoxicity of FA-***728***-DOPS-DMPE-RNase A mediated transfection on folate receptor positive KB cells. Statistical analysis in comparison with the targeted FA-***728***-DOPS-DMPE-RNase A formulation; *$p < 0.05$, ***$p < 0.001$. Data are shown as mean ± SD (n=3).

further investigated in more detail. Figure 3.24 B shows that the cell killing effect of FA-***728***-DOPS-DMPE-RNase A is protein concentration dependent. The corresponding doses of FA-***728***-DOPS-DMPE and RNase A-PDP show no distinct sign of cytotoxicity.

Next, the targeting ability of FA-***728***-DOPS-DMPE-RNase A nanoparticles was investigated in detail. As shown in Figure 3.25 A, FA-***728***-DOPS-DMPE-RNase A presented higher folate-receptor-positive KB cell killing than ***728***-DOPS-DMPE-RNase A, and 1 mM free folic acid block could efficiently reduce the KB cell killing of FA-***728***-DOPS-DMPE-RNase A to the levels of the non-targeted control. The cell killing effect of FA-***728***-DOPS-DMPE-RNase A could also be observed on folate-receptor-positive L1210 cells, however, after treatment with FA-***728***-DOPS-DMPE-RNase A, the folate-receptor-negative Neuro 2A or MCF-7 cells did

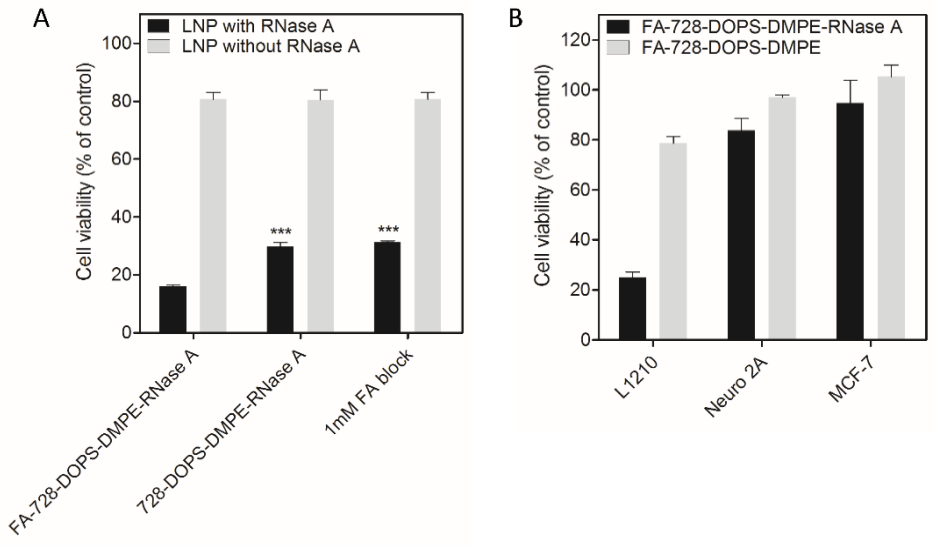

Figure 3.25 A) Evaluation of RNase A transfection efficiency with FA-***728***-DOPS-DMPE-RNase A nanoparticles and non-targeted control ***728***-DOPS-DMPE-RNase A or free folic acid competition control on KB cells presented as % cell metabolic activity of control cells (MTT assay). Cells were incubated with the indicated agents under standard culture conditions for 4 h, followed by a 44 h incubation with fresh media. For competition experiments with free folic acid, the KB cells were pretreated with 1 mM free folic acid for 30 min on ice before adding nanoparticles. B) FA-***728***-DOPS-DMPE-RNase A mediated RNase A transfection on folate receptor positive L1210 cells in comparison to folate receptor negative cells (Neuro 2A and MCF-7). Black: RNase A nanoparticles (2 µM); light grey: mixtures of corresponding dose of ***728*** and lipids without RNase A. Statistical analysis in comparison with the targeted FA-***728***-DOPS-DMPE-RNase A formulation; ***$p < 0.001$. Data are shown as mean ± SD (n=3).

not show strong reduction of cell viability (Figure 3.25 B). Moreover, free folate block could also reduce KB cell killing of other five targeted RNase A nanoparticles (Figure 3.26), which also showed effective cytotoxicity on folate-receptor-positive L1210 cells (Figure 3.27), but could not kill the folate-receptor-negative Neuro 2A or MCF-7 cells (Figure 3.28).

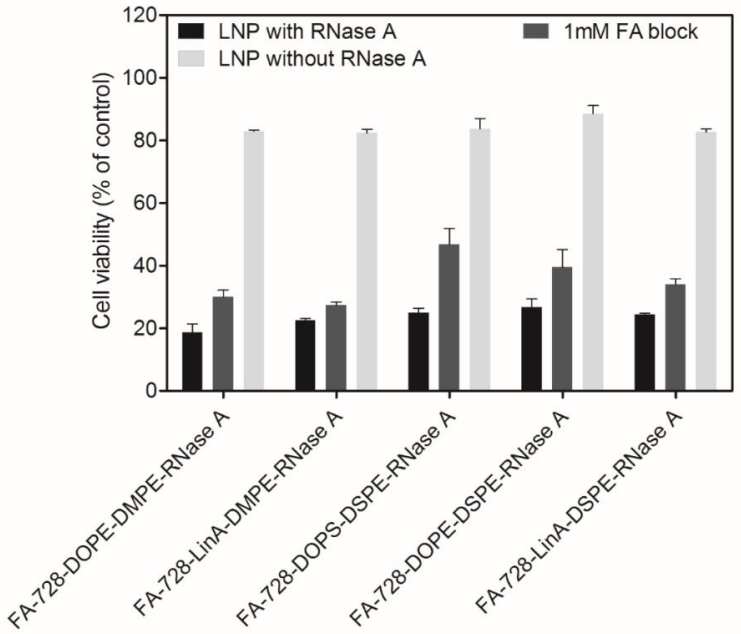

Figure 3.26 Effect of receptor competition with free folic acid on cell killing for various RNase A nanoparticles using MTT metabolic activity assay. KB cells were incubated with the indicated agents under standard culture conditions for 4 h, followed by a 44h incubation with fresh media. For competition experiments with free folic acid, the KB cells were pretreated with 1 mM free folic acid for 30 min on ice before adding nanoparticles. Black: RNase A nanoparticles (2 µM); deep grey: 1 mM free folic acid block; light grey: corresponding nanoparticles without RNase A. Data are shown as mean ± SD (n=3).

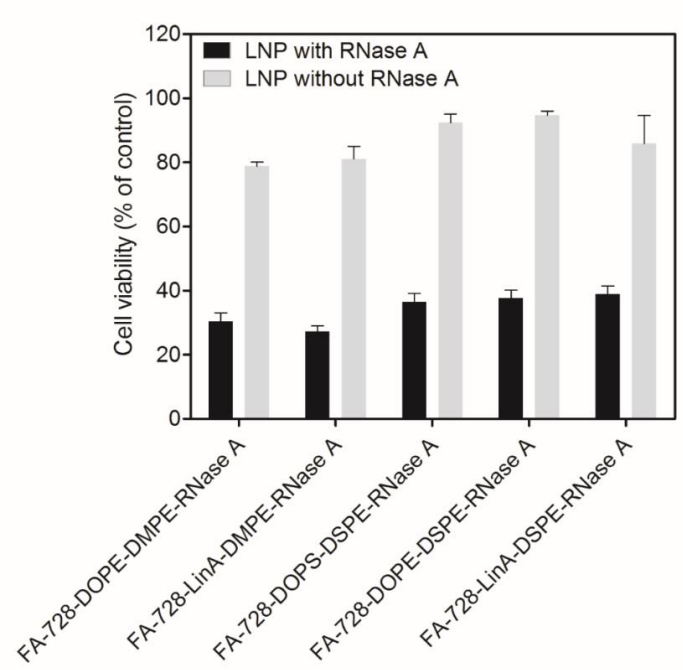

Figure 3.27 Evaluation of RNase A transfection efficiency with various RNase A nanoparticles on folate receptor positive L1210 cells presented as % of metabolic activity of control cells (MTT assay). Cells were incubated with the indicated agents under standard culture conditions for 4 h, followed by a 44 h incubation with fresh media. Black: RNase A nanoparticles (2 µM); light grey: corresponding nanoparticles without RNase A. Data are shown as mean ± SD (n=3).

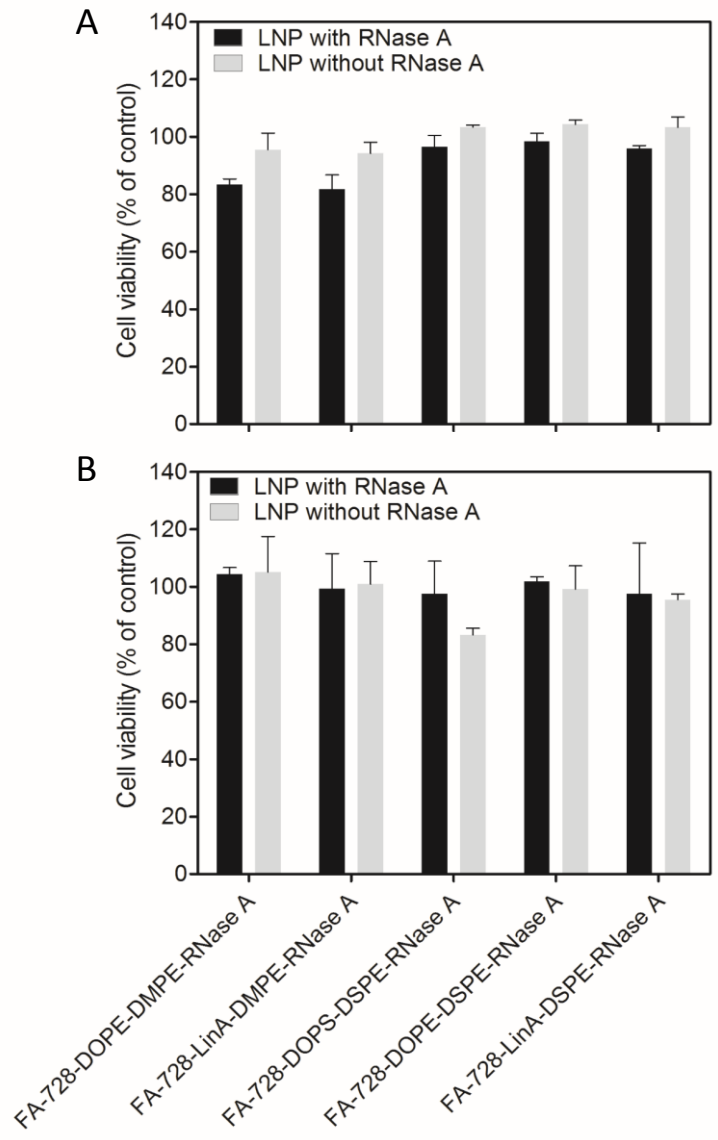

Figure 3.28 Evaluation of RNase A transfection efficiency with various RNase A nanoparticles on folate receptor negative Neuro 2A (A) or MCF-7 cells (B) presented as % cell metabolic activity of control cells (MTT assay). Cells were incubated with the indicated agents under standard culture conditions for 4 h, followed by a 44 h incubation with fresh media. Black: RNase A nanoparticles (2 µM); light grey corresponding nanoparticles without RNase A. Data are shown as mean ± SD (n=3).

The effect of co-formulation with lipids was further investigated by comparison of cell killing by different nanoformulations (FA-***728***-DOPS-DMPE-RNase A, ***728***-DOPS-DMPE-RNase A, ***728***-SS-RNase A, FA-***728***-DOPS-DMPE-free RNase A and FA-DOPS-DMPE-RNase A) testing folate-receptor-positive KB cells in 0% FBS and 20% FBS containing medium. As shown in Figure 3.29 A, after KB cells were treated with different nanoparticles in 0% FBS containing medium for 4 h followed by

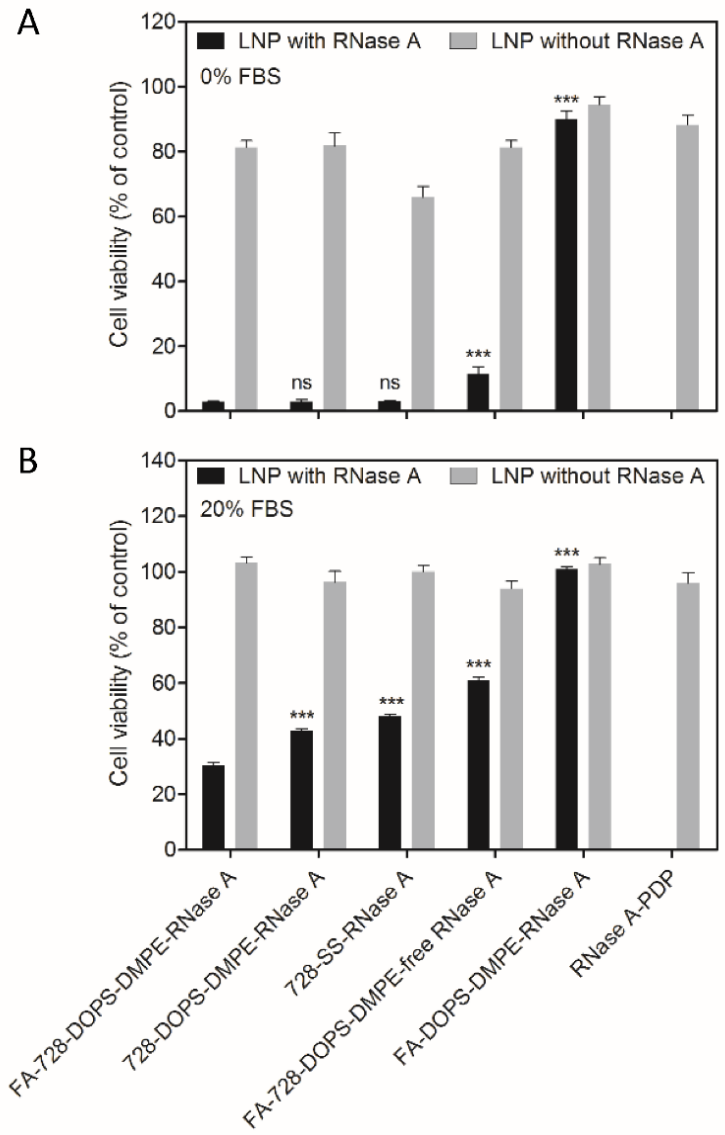

Figure 3.29 Influence of serum on KB cell killing efficiency mediated by various RNase A nanoparticles. A) Evaluation of RNase A efficacy presented as % cell metabolic activity of control KB cells (MTT assay). Cells were incubated with the indicated agents in serum-free medium for 4 h, followed by a 44 h incubation with fresh serum-containing medium. B) Evaluation of RNase A efficacy analogously as described in (A) but with incubation in medium containing 20% FBS for the first 4 h. Black: RNase A nanoparticles (2 µM); light grey: nanoparticles without RNase A. Statistical analysis in comparison with the targeted FA-***728***-DOPS-DMPE-RNase A formulation; ns: no significant difference; ****p* < 0.001. Data are shown as mean ± SD (n=3).

another 44 h incubation in fresh 10 % FBS containing medium, FA-***728***-DOPS-DMPE-RNase A presented similar cell killing as the non-targeted control or the ***728***-SS-RNase A conjugate (not significant), reducing the cellular metabolic activity of KB cells down to 3 %. FA-***728***-DOPS-DMPE-free RNase A (i.e. the formulation

containing non-conjugated RNase A) also notably decreased the metabolic activity of KB cells down to 10%, whereas nanoparticles without RNase A showed no cytotoxicity. Only KB cells treated with the plain lipo-oligomer ***728*** under serum-free conditions presented a slight 30% reduction in cellular metabolic activity. In contrast, when treating KB cells with the nanoformulations in 20% FBS containing medium for 4 h, followed by another 44 h incubation in fresh 10% FBS containing medium, FA-***728***-DOPS-DMPE-RNase A presented substantial higher KB cell killing activity than the non-targeted formulation or ***728***-SS-RNase A. Also, the cytotoxicity of FA-***728***-DOPS-DMPE-free RNase A (containing nonconjugated protein) was dramatically reduced from 90% in 0% FBS containing medium to 40% in 20% FBS containing medium (Figure 3.29 B). Both in 0% FBS and 20% FBS containing serum, the ***728***-lacking control FA-DOPS-DMPE-RNase A did not present any cytotoxicity.

3.2.3 Effective targeted intracellular delivery of nlsEGFP

Because of the superior performance of FA-***728***-DOPS-DMPE-RNase A, the same lipid composition was also applied to prepare nlsEGFP nanoformulations. Flow cytometry was applied to determine the fluorescence intensity of KB cells transfected with nlsEGFP nanoparticles in standard 10% FCS containing medium. A 45 min short incubation of these folate receptor-rich cells on ice with FA-***728***-DOPS-DMPE-nlsEGFP demonstrated a higher degree of cellular association (Figure 3.30 A) and mean fluorescence intensity (Figure 3.30 B) than with the non-targeted control ***728***-DOPS-DMPE-nlsEGFP. A competition assay with free folate was also carried out to further prove the folate receptor involvement for FA-***728***-DOPS-DMPE-nlsEGFP. The free folate block could effectively inhibit the cellular association of FA-***728***-DOPS-DMPE-nlsEGFP (Figure 3.30 A) and decrease the mean fluorescence intensity of treated cells (Figure 3.30 B). SPDP modified nlsEGFP treated cells presented almost same low fluorescence intensity as the PBS treated cell control.

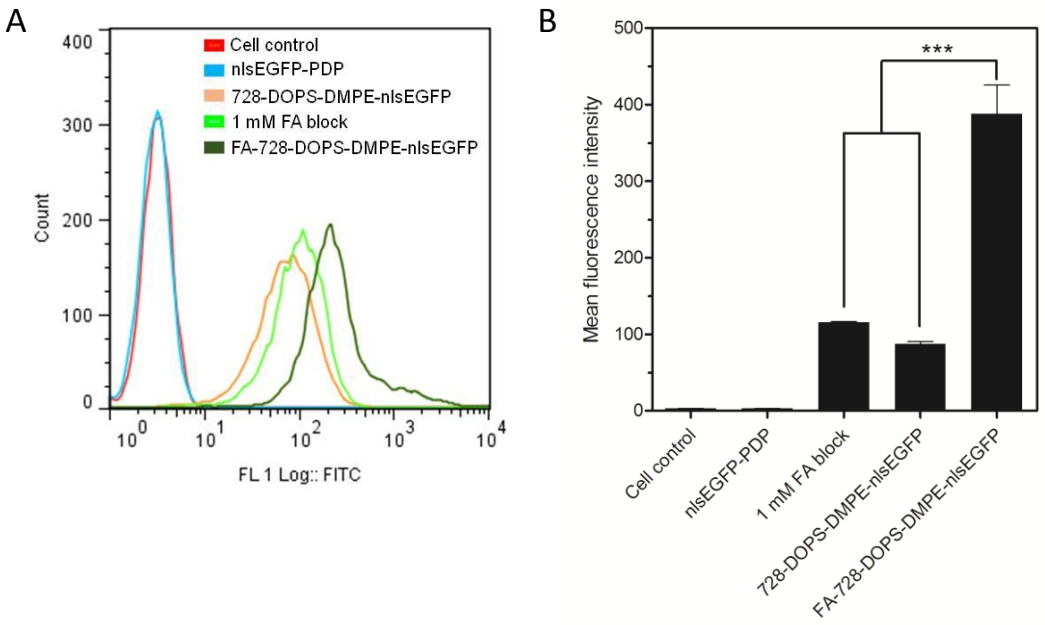

Figure 3.30 A) Cellular association of KB cells treated with various nlsEGFP nanoformulations (1 µM) on ice for 45 min by flow cytometry. For competition experiments with free folic acid, the KB cells were pretreated with 1 mM free folic acid for 30 min on ice before adding nanoparticles. Deep green: FA-***728***-DOPS-DMPE-nlsEGFP; light green: competition with free folic acid; orange: non-targeted control formulation; blue: nlsEGFP-PDP control; red: PBS treated cell control. B) Mean fluorescence intensities of cells treated with each sample as described in (A). ***$p < 0.001$. Data are shown as mean ± SEM (n=3).

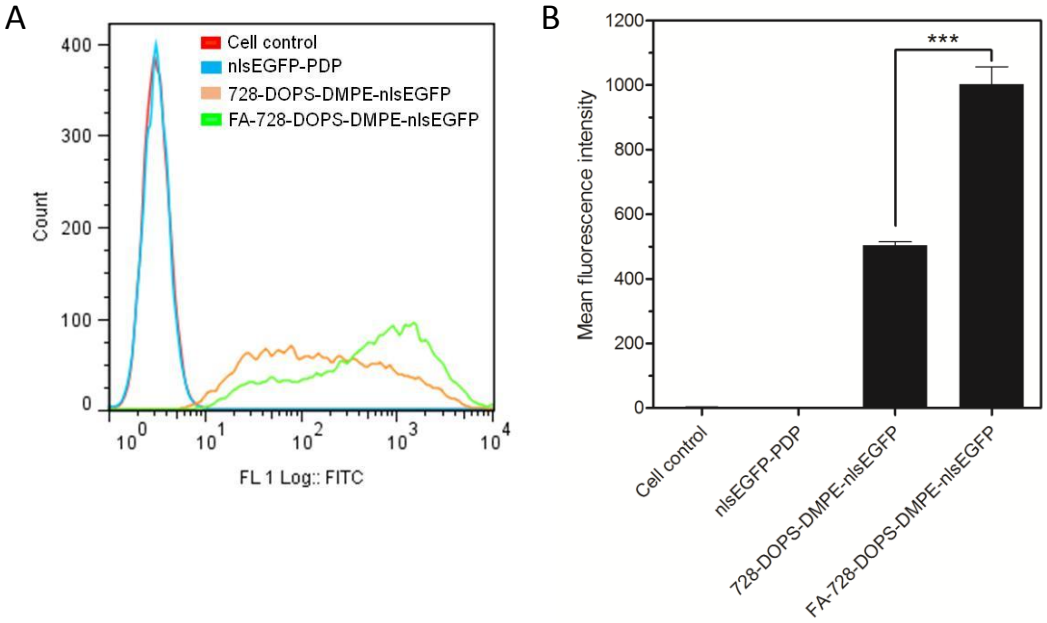

Figure 3.31 A) Cellular internalization of cells treated with various nlsEGFP nanoparticles (1 µM) for 24 h, followed by a 24 h incubation in fresh media. Green: FA-***728***-DOPS-DMPE-nlsEGFP; Orange: non-targeted control; Blue: nlsEGFP-PDP control; Red: PBS treated cell control. B) Mean fluorescence intensities of cells treated with each sample as described in (A). ***$p < 0.001$. Data are shown as mean ± SEM (n=3).

Furthermore, the cellular internalization of nlsEGFP was also studied by incubating KB cells with FA-***728***-DOPS-DMPE-nlsEGFP or ***728***-DOPS-DMPE-nlsEGFP for 24 h at body temperature, followed by another 24 h incubation in fresh medium. The results showed that both formulations presented effective nlsEGFP persistence after a long incubation, meanwhile, FA-***728***-DOPS-DMPE-nlsEGFP treated cells presented more cell internalization of nlsEGFP and higher mean fluorescence intensity than that of ***728***-DOPS-DMPE-nlsEGFP treated cells (Figure 3.31).

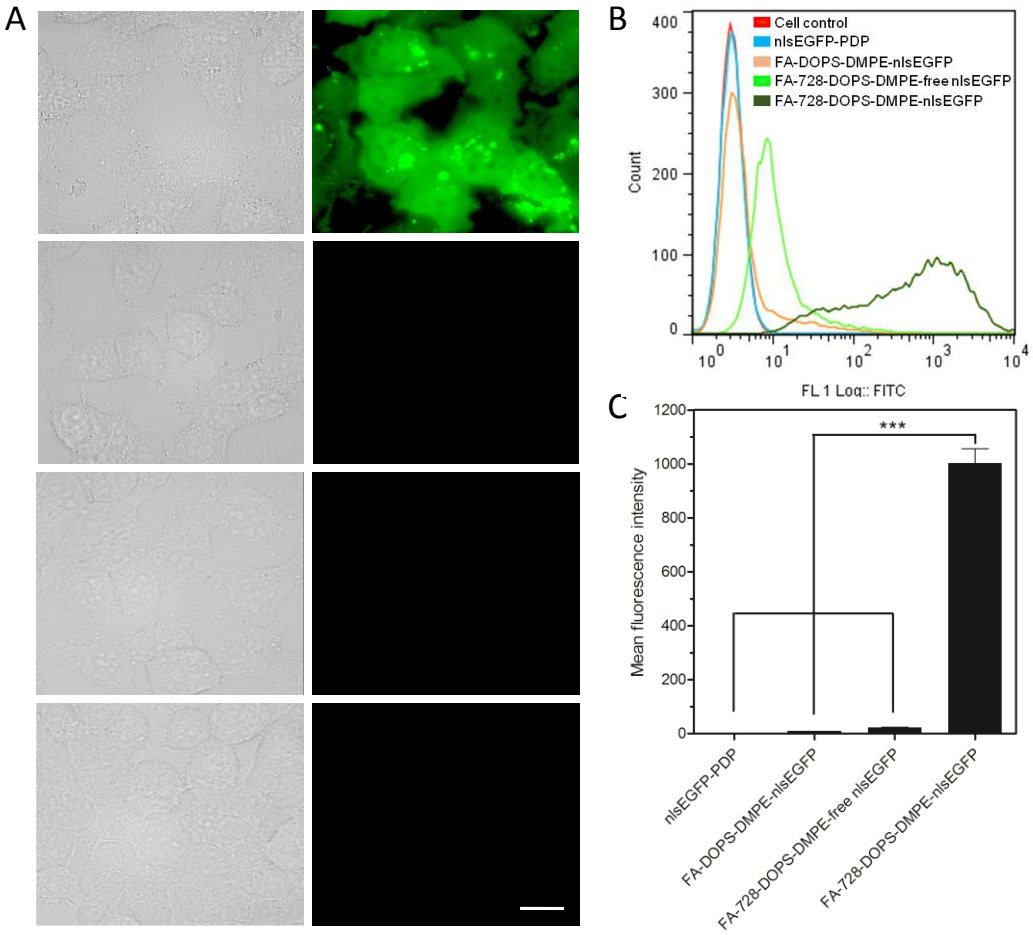

Figure 3.32 Transduction of KB cells with various nlsEGFP nanoparticles. A) Representative fluorescence microscopy of the live KB cells treated with 1 μM FA-***728***-DOPS-DMPE-nlsEGFP (row 1), 1 μM FA-***728***-DOPS-DMPE-free nlsEGFP (row 2), 1 μM FA-DOPS-DMPE-nlsEGFP (row 3) and 1 μM nlsEGFP-PDP (row 4) for 24 h, followed by a 24 h incubation in fresh media. Left column: bright-field images of the treated cells. Right column: EGFP fluorescence of the treated cells. B) Cellular internalization of each nanoformulation incubated as described in A) as determined by flow cytometry. C) Mean fluorescence intensities of cells treated with each nanoformulation. ***p < 0.001. Data are shown as mean ± SEM (n=3). Scale bar = 20 μm.

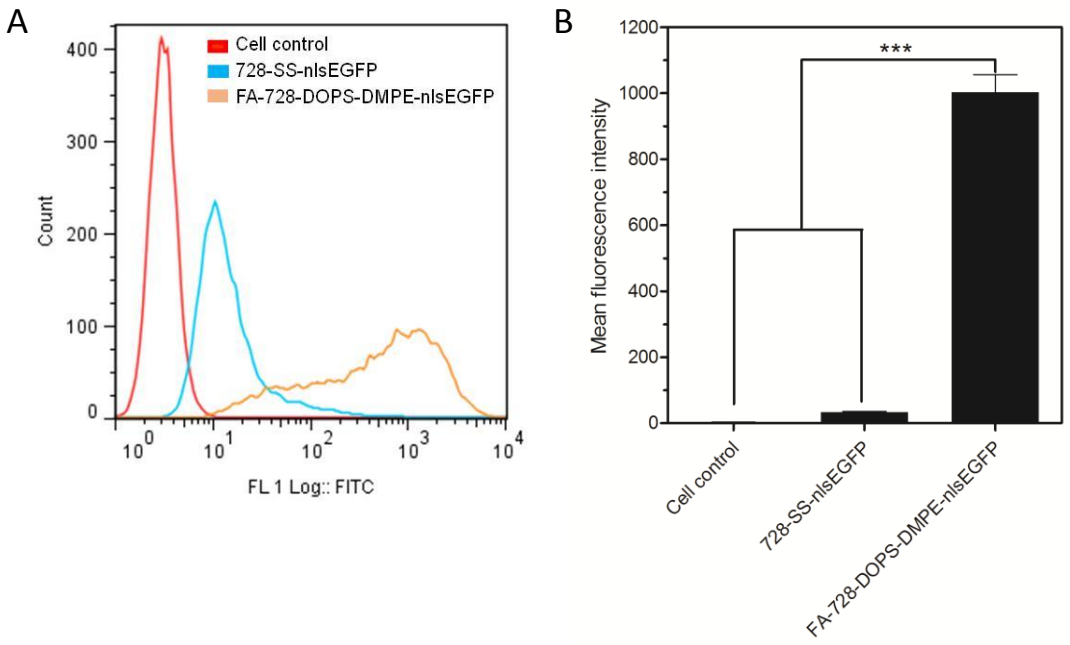

Figure 3.33 A) Cellular internalization of cells treated with various nlsEGFP nanoparticles (1 µM) for 24 h, followed by a 24 h incubation in fresh media. Orange: FA-***728***-DOPS-DMPE-nlsEGFP; Blue: control conjugates without helper lipids; Red: PBS treated cell control. B) Mean fluorescence intensities of cells treated with each sample as described in (A). ****p* < 0.001. Data are shown as mean ± SEM (n=3).

Fluorescence microscopy was also used to investigate the nlsEGFP delivery efficiency of FA-***728***-DOPS-DMPE-nlsEGFP. Figure 3.32 A shows that FA-***728***-DOPS-DMPE-nlsEGFP treated cells exhibited homogeneous green fluorescence all over the cells after incubation with nanoparticles for 24 h followed by additional incubation in fresh medium for 24 h. Furthermore, nlsEGFP was apparently also transported into the cell nuclei. More nlsEGFP positive cells were found in the fluorescence microscopy of FA-***728***-DOPS-DMPE-nlsEGFP treated cells compared to the cells treated with ***728***-SS-nlsEGFP as reported before, [144] which is consistent with the cellular internalization results shown in Figure 3.33 A. FA-***728***-DOPS-DMPE-nlsEGFP treated cells presented also a higher mean fluorescence intensity than ***728***-SS-nlsEGFP treated cells (Figure 3.33 B). FA-***728***-DOPS-DMPE-nlsEGFP also displayed a higher cellular association compared with ***728***-SS-nlsEGFP after a 45 min short incubation on ice (Figure 3.34 A). The

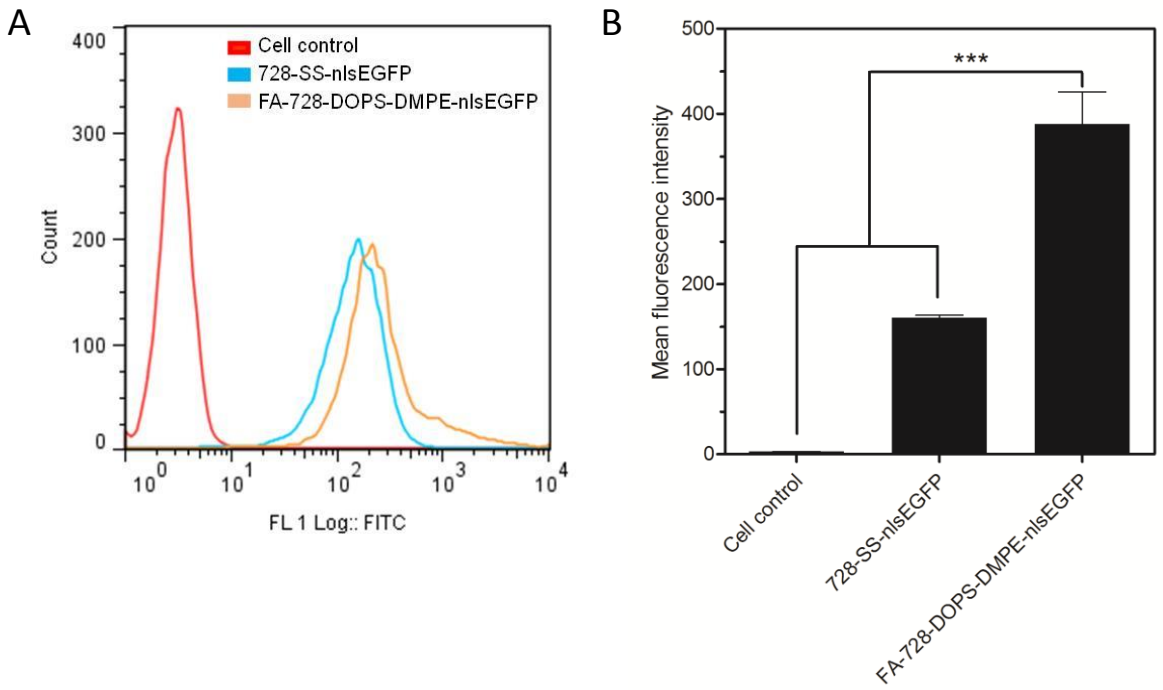

Figure 3.34 A) Cellular association of cells treated with various nlsEGFP nanoparticles (1 µM) on ice for 45 min. Orange: FA-***728***-DOPS-DMPE-nlsEGFP; Blue: control conjugates without helper lipids; Red: PBS treated cell control. B) Mean fluorescence intensities of cells treated with each sample as described in (A). ****p* < 0.001. Data are shown as mean ± SEM (n=3).

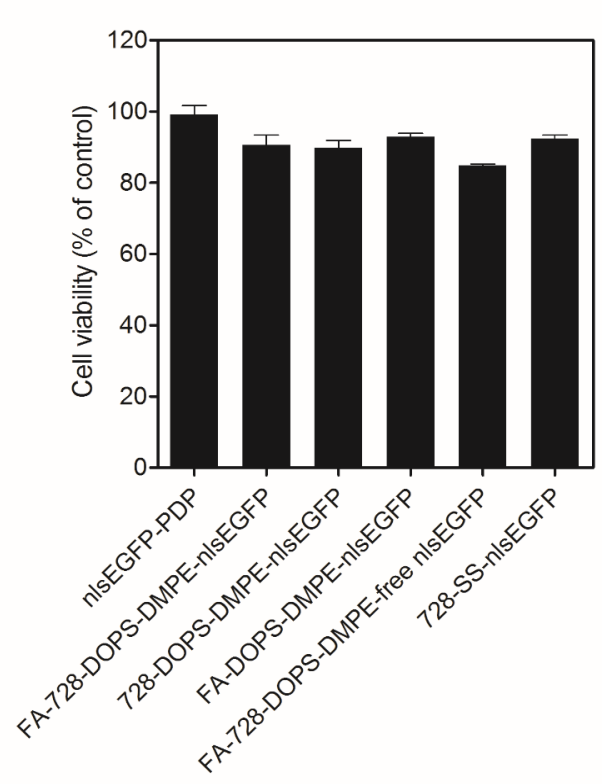

Figure 3.35 Metabolic cell activities (in % of untreated controls) of KB cells treated with 1 µM various nlsEGFP nanoparticles. Data are shown as mean ± SD (n=3).

mean fluorescence intensity of FA-***728***-DOPS-DMPE-nlsEGFP treated cells was higher than that of cells treated with ***728***-SS-nlsEGFP in the cellular association assay (Figure 3.34 B). Oppositely, the SPDP modified nlsEGFP, FA-DOPS-DMPE-nlsEGFP (without ***728***) and FA-***728***-DOPS-DMPE-free nlsEGFP controls did not generate detectable nlsEGFP fluorescence in the representative fluorescence images of treated KB cells. Flow cytometry results further confirmed these findings. SPDP modified nlsEGFP and FA-DOPS-DMPE-nlsEGFP treated cells manifested the same fluorescence intensity as the PBS treated cell control. Cells treated with FA-***728***-DOPS-DMPE-free nlsEGFP (non-covalent protein incorporation) presented only slightly higher fluorescence (Figure 3.32 B). Notably, FA-***728***-DOPS-DMPE-nlsEGFP treated cells displayed a 44-fold higher mean fluorescence intensity than cells treated with FA-***728***-DOPS-DMPE-free nlsEGFP, and a 94-fold higher fluorescence than cells treated with FA-DOPS-DMPE-nlsEGFP (Figure 3.32 C). Encouragingly, none of the tested nlsEGFP nanoparticle formulations showed cytotoxicity (Figure 3.35**)**.

4. Discussion

4.1 Enhanced intracellular protein transduction by sequence defined tetra-oleoyl oligoaminoamides targeted for cancer therapy

Section 4.1 has been adapted from: Peng Zhang, Dongsheng He, Philipp Michael Klein, Xiaowen Liu, Ruth Röder, Markus Döblinger, and Ernst Wagner, Adv. Funct. Mater. 2015, 25, 6627–6636.

Intracellularly active proteins present a therapeutic subclass which due to delivery problems still is in its early stage. The particularly crucial barriers of intracellular protein delivery include specific delivery to the targeted cells, highly efficient cellular internalization, effective endolysosomal escape, timely release of proteins from the delivery system and following subcelluar traffic to specific subcellular sites [54, 58, 61]. Among these barriers, especially endolysosomal entrapment hamper effective protein transduction into the cytosol. Cargo proteins are largely sequestrated and degraded in the endolysosomes without access to the subcellular target sites for subsequent biological actions. Therefore, novel delivery technologies are required to cope with these barriers via combing multiple functions. In our laboratory, using solid-phase synthesis technology, precise sequence-define oligomers have been designed and syntesiyed and contain various moieties and functions.

In this study, from an existing library of more than 900 precise cationic oligoaminoamides, sixteen candidates were chosen for in-depth evaluation of intracellular protein delivery. All oligomers were manufactured by solid-phase supported synthesis to gain precise chemical structures in defined sequences and topologies. Folic acid was conjugated to the cationic backbone for receptor mediated protein transduction through a monodisperse PEG (PEG_{24}) chain, which can help to reduce the unspecific interactions between nanocarriers and the biological environment. The backbones of different oligomers have different topologies, such as

two-arm, three-arm, and four-arm, [114] and consist of novel artificial amino acid building blocks (e.g., Stp, Sph) as basic functional units for endosomal escape. [129] Oleic acids were incorporated into oligomers to enhance endosomal and nanoparticle stabilization [114, 128]. Moreover, natural amino acids were included in these oligomers: lysines were included as branching points (by selective modifi cation both at α- and ε-amino groups), histidines [129] to promote proton sponge effect enhancing endolysosomal escape, tyrosines [154] and cysteines [125, 126] were coupled to facilitate association of conjugates by aromatic ring interactions or reducible disulfide bonds, respectively. Cysteines also act as bioreducible attachment sites for the cargo proteins. Different substitutes for folic acid (glutamic acid, glutaric acid, alanine) were used in the nontargeted control oligomers (Table 3.1).

Two representative proteins, nlsEGFP and RNase A, were employed to evaluate targeted intracellular protein delivery. Recombinant nlsEGFP [121] contains a nuclear localization sequence (NLS) derived from SV40 large T-antigen which can help nlsEGFP in migrating from cytosol into the nucleus by natural mechanisms. Hence, based on this property, nlsEGFP can be utilized to characterize endolysosomal escape and subcellular nuclear transport by fluorescence microscopy. Meanwhile, RNase A [66] when internalized into the cytosol of cancer cells can degrade the cellular RNA and induce cell killing. Biologically reducible SPDP linkers were utilized to covalently attach oligomers to nlsEGFP or RNase A through disulfide bonds. Following endolysosomal escape, the formed disulfide linkages are supposed to be cleaved by cytosolic reducing glutathione (GSH). As a result, oligomer free nlsEGFP or RNase A will be obtained.

SDS-PAGE results proved the successful modification of nlsEGFP and RNase A with representative oligomers and the modification of proteins with oligomers by disulfide bonds is biologically reversible at physiological conditions (Figure 3.2). The formation of slightly smaller and more positively charged nanoparticles by RNase A conjugates

compared to the nlsEGFP conjugates (Table 3.2, 3.3) may be explained by the intrinsic properties of RNase A (smaller, more basic protein). The discrepancy between TEM (10 nm, Figure 3.3) and the larger (25 nm) size of ***729***-SS-RNase A conjugates measured by DLS may be explained by the extended worm-like shape and because TEM was performed in vacuum state where conjugate size would shrink.

All the nlsEGFP conjugates showed nice cellular association and internalization already after a short incubation. The two-arm targeted oligomer conjugates, ***715*** and ***729***, manifested efficient folate receptor specificity. However, the four-arm oligomer conjugates presented lower specificity, which can be well explained by their higher numbers of positive charges and/or more disulfide crosslinks. The high positive charge can induce unspecific association on cells and more crosslinks may prevent folate acid arising on conjugates surface.

Furthermore, the fluorescence intensity was investigated after a long incubation of cells with nlsEGFP conjugates, the fluorescence intensity was supposed to be reduced because of cell proliferation and/or degradation of nlsEGFP by proteases in lysosomes if entrapped. Only cells treated with ***712, 713, 728, 729, 794*** and ***795*** nlsEGFP conjugates remained EGFP fluorescence-positive. Compared with ***706*** and ***707***, respectively, ***712*** and ***713*** nlsEGFP conjugates had a higher recovery of EGFP fluorescence.This can be attributed to the histidines in the oligomers which have been reported to increase the buffer capacity, enhancing endosomal escape or postponing the lysosomal acidification required for protease bioactivities. These effects of histidines may help nlsEGFP to escape from protease degradation. ***729***-SS-nlsEGFP showed the highest percentage of fluorescence-positive cells among all the conjugates, which indicated that 729 may be a potent nanocarrier for targeted protein delivery.

Fluorescence microscopy was performed to confirm the capacity of these oligomers to deliver nlsEGFP into cells, promote endolysosomal escape, and subsequent

subcellular trafficking into the nucleus. ***729***-SS-nlsEGFP and ***728***-SS-nlsEGFP treated cells presented homogeneous fluorescence throughout the cells. This suggests that ***729***-SS-nlsEGFP and ***728***-SS-nlsEGFP successfully escaped from endosomes/lysosomes and were reduced in the cytosol, resulting in oligomer-free nlsEGFP all over the cells. Moreover, nlsEGFP was found imported into the cell nuclei, compared with only cytosolic location (presented by dark appearance of the nuclei) as observed in previous work [121], which also validates the successful endosomal escape of ***729***-SS-nlsEGFP and ***728***-SS-nlsEGFP, the biological reversibility of conjugation, and subsequent nuclear translocation mediated via the NLS signal. The nlsEGFP was not concentrated in the nucleus, which may result from incomplete release of nlsEGFP from the carrier or linker, as the NLS (Pro-Lys-Lys-Lys-Arg-Lys-Val) of nlsEGFP is rich in lysines, it is quite possible that some NLS lysines are irreversibly amidated by the SPDP linker. Such modified NLS would not work as a nuclear localization signal.

The performances of the targeted FolA containing ***729*** conjugate and the nontargeted glutamate-containing ***728*** conjugate can be directly compared by microscopy and flow cytometry. FolA-targeted ***729***-SSnlsEGFP shows more efficient and effective nlsEGFP transduction ability as compared to the nontargeted ***728***-SS-nlsEGFP. Covalent conjugation by disulfide bonds plays a decisive role in the nlsEGFP transfection, which was demonstrated by the ineffectiveness of the mixtures of ***729*** and free nlsEGFP. ***729***-SS-nlsEGFP is the only conjugate presenting nice cellular association, cellular internalization, folate receptor specificity, long-term survival of nlsEGFP activity, and subcellular nuclear import among all the targeted oligomers.

The protein delivery efficiency of oligomers was further compared through conjugating oligomers with RNase A as therapeutic cargo protein. Successful delivery of RNase A into the cytosol was expected to elicit degradation of cytosolic RNA, thereby inducing cell killing. Five targeted oligomers (***707, 713, 729, 733, 795***) and their nontargeted

control oligomers could successfully induce tumor cell killing but the plain oligomers did not induce significant tumor cell killing. The corresponding dose of SPDP linker modified RNase A did also not result in any detectable change of cell viability, which can be attributed to the lack of intracellular delivery for SPDP modified RNase A. Cells treated with the mixtures of free RNase A and oligomers also presented appreciable reduction of metabolic activity. Such an effect of noncovalent mixtures was not observed in the nlsEGFP delivery (Figure 3.7 A) and is presumably based on the special properties of RNase A. The intrinsic positive charge of RNase A (pI 9.6) enables the protein to bind to the negatively charged cell membrane; simultaneous internalization of membrane-bound RNase A with the endosomolytic oligomers, as a result, may indirectly mediate endosomal release into the cytosol, analogously as observed elsewhere [155]. Among all the tested conjugates, ***729***-SS-RNase A (Figure 3.8 A) and its nontargeted ***728*** analog (Figure 3.9) mediated the by far highest cytotoxicity, whereas the toxicity of the free oligomer was negligible.

Interestingly, no significant decrease in cell viability was observed in folate-receptor-negative cells (MCF-7 and Neuro-2a) after incubation with ***729***-SSRNase A conjugate at the same concentrations. It remains to be determined whether the major reasons are (i) reduced cellular uptake due to lack of target receptor or (ii) reduced sensitivity toward internalized RNase A, for example by different levels of natural cytosolic ribonuclease inhibitor [66], the main physiological inhibitor of RNase A. In our previous siRNA delivery work, gene silencing was less challenging in Neuro-2a cells than in KB cells [128, 156, 157], arguing against alternative (i) as exclusive reason. Preference of RNase in killing a series of tumor cells as opposed to normal cells has been reported in the literature, with reasons which go beyond delivery and are still not fully understood [65, 66]. The higher cell internalization efficiency of ***729***-SS-RNase A-FITC than free RNase A-FITC-PDP was also confirmed by fluorescence microscopy and flow cytometry evalution, revealing again that ***729*** is a potent nanocarrier for protein delivery (Figure 3.10).

The key role of oleic acids in oligomer ***729*** was investigated by compared the protein delivery efficiency of ***728*** or ***729*** with their control oligomers (***937, 737***). The control oligomers have the same sequence, functional modules and topology as in ***728*** or ***729*** except the oleic acids. Flow cytometry results suggest that the oleic acids do not have a significantly enhancing effect on cellular binding or uptake of nlsEGFP conjugates (Figure 3.11, 3.12 A). However, after a long incubation, the ***729***-SS-nlsEGFP treated cells showed green fluorescence of nlsEGFP distributed throughout the cytosol and nucleus, whereas no nlsEGFP was observable in the ***737***-SS-nlsEGFP treated cells, which is consistent with the flow cytometry results (Figure 3.12 B, C), indicating that the proteins had been degraded by lysosomal proteases because of endolysosomal entrapment. Considering the similar molecular structure and cell uptake ability of ***729***-SSnlsEGFP and ***737***-SS-nlsEGFP, we concluded that the different protein delivery efficiency may result from the distinct endosomal escape efficacy based on the oleic acid modification. An analogous comparison of the RNase A delivery efficiency of ***729***-SS-RNase A and ***737***-SS-RNase A gave consistent results. Also the oleic acid modified nontargeted oligomer ***728*** presented higher nlsEGFP and RNase A delivery efficiency than the control oligomer ***937***. The far more erythrocyte lysis of oleic acid modified oligomers (***728, 729***) or their protein conjugates further verified this conclusion when compared with the oligomers without oleic acid (***937, 737***) or their protein conjugates, respectively. All these results proved that the oleic acids as the endosomolytic unit in ***729*** play a crucial role in the enhanced intracellular protein delivery.

4.2 Lipo-oligomer nanoformulations for targeted intracellular protein delivery

Section 4.2 has been partly adapted from: Peng Zhang, Benjamin Steinborn, Ulrich Lächelt, Stefan Zahler, and Ernst Wagner, Biomacromolecules DOI: 10.1021/acs.biomac.7b00666.

In this study, novel lipo-oligoaminoamide nanoformulations for targeted intracellular protein delivery are generated by first bioreversibly conjugating a sequence-defined amphiphilic lipo-oligomer ***728*** to the cargo protein via disulfide bonds, followed by formulation of the formed ***728***-SS-protein conjugate with different helper lipids in various compositions. The triblock oligoaminoamide ***728*** contains cysteines for reversible covalent protein conjugation and crosslink-stabilization of formed nanoparticles, polyethylene glycol (PEG) for shielding and providing a hydrophilic domain, eight cationizable succinoyl tetraethylene pentamine (Stp) repeats for endosomal buffering and escape into the cytosol, and a tetra-oleic acid block for hydrophobic stabilization. Three different helper lipids, DOPS (anionic lipid), DOPE (neutral lipid), LinA (fatty acid) were applied to help to form stable nanoparticles and neutralize the positive charges on the nanoparticle surfaces. Cholesterol was applied to stabilize lipid bilayers and enhance the stability of the lipidic protein nanoparticles. Three PEGylated lipids, DMPE-PEG2000, DSPE-PEG2000, or the novel folate-PEGconjugated lipid analog ***1042*** were also used to reduce the zeta potential, enhance the serum stability, and provide optional targeting capacity.

Dynamic light scattering (DLS) measurements showed that the prepared lipo-oligomer nanoformulations had nanoscale sizes varied from 80 nm to 150 nm. The zeta potential of the proteoliposomes nanoparticles varied from 6 mV to 22 mV, strongly depending on the intrinsic properties of proteins (Table 3.6). The RNase A nanoparticles exhibited higher zeta potential than nlsEGFP nanoparticles, this may be attributed to the positive charges of RNase A (a basic protein) at pH 7.4. This also indicated that the covalently attached proteins are at least partly exposed at the

outside surface of nanoparticles. The difference of size and zeta potential between representative lipid-based nanoparticles and nanoparticles formed from lipo-oligomer protein conjugates is clear and validate the effective co-formulations of ***728*** conjugates with helper lipids (Figure 3.20 A, B). Among all tested nanoparticles, only the DOPS group presents relatively obvious charge decreases, which can be attributed to the negative charge of DOPS (Table 3.6). All the tested formulations presented almost full oxidation of free cysteines. The resulting disulfide crosslinkages are supposed to stabilize the formed nanoparticles. The representative FA-***728***-DOPS-DMPE-RNase A or FA-***728***-DOPS-DMPE-nlsEGFP nanoparticles exhibited high stability in 72h (Figure 3.20 D). The size difference of the representative RNase A nanoparticles between DLS and TEM measurements are supposed to derive from the shrink effect of nanoparticles under vacuum state in TEM and the over-emphasized scattering intensity of larger nanoparticles in the DLS measurements.

Hypothetical structures for the protein-containing nanoformulations (namely liposomal or micellar structures) are outlined (Figure 3.17 A). For **728**-SS-protein conjugates without helper lipids, lipid bilayer structures as occurring in liposomes can be excluded based on theoretical considerations [158-162]; for example, 6 molar equivalents of ***728*** (i.e. 24 equivalents of oleic acids, ~4 nm^2 of bilayer) cannot provide sufficient lipidic membrane area compared with the EGFP protein area (~4.5-10 nm^2) [163] for bilayer formation; only worm-like micellar structures, consistent with reported TEM results [144], can be formed. The situation should be different with the added helper lipids; according to the applied molar ratio, the approximately 30 lipid equivalents would be sufficient to support one EGFP molecule. In fact, 15 lipids can supply enough area (~10 nm^2) [158-162] for one attached EGFP molecule (~4.5-10 nm^2) [163], suggesting that liposomal bilayer formation is possible. For that case, proteo-liposomal nanostructures are expected to contain an inner aqueous core,

which was validated by the increased fluorescence in the calclein release assay (Figure 3.22).

In the comparison of cell killing effect of lipo-oligomer RNase A nanoformulations, cell viability reduction was not observed on the SPDP modified RNase A treated KB cells, which may derive from the lack of effective delivery of SPDP modified RNase A into cytosol. Moreover, the cells treated with corresponding nanoparticles without ***728*** presented no cell viability reduction (Figure 3.24 A). This result may derive from the lack of strong association between RNase A and lipid nanoparticles, and the lack of efficient endolysosomal escape, whereas ***728*** is supposed to provide both functions. In contrast, all the targeted RNase A nanoparticles showed significant cell killing, validating efficient intracellular RNase A delivery and bioactivity. Cell treated with the corresponding nanoparticles containing nonconjugated “free RNase A” also exhibited appreciable decrease of cell viability (Figure 3.24 A). This effect may also be attributed to intrinsic property of the RNase A. RNase A (pI 9.6) as a basic protein with positive charge under physiological conditions may bind to the cell membrane and internalize simultaneously with nanoparticles of FA-***728***-DOPS-DMPE, resulting in indirect endolysosomal escape. However, the nanoparticles conjugated with RNase A via disulfide linkage always presented higher cytotoxicity compared with the noncovalent formulations, which may result from the increased protein loading efficiency upon covalent attachment and the higher resistance against dissociation between proteins and nanoparticles under serum containing conditions. Among all the tested targeted RNase A nanoparticles, FA-***728***-DOPS-DMPE-RNase A mediated the highest cytotoxicity. This effect may be attributed to relatively higher serum stability, as shown in the turbidity assay (Figure 3.23). Among the tested targeted RNase A nanoparticles, FA-***728***-DOPS-DMPE-RNase A showed highest resistance against aggregation. The relatively low zeta potential of FA-***728***-DOPS-DMPE-RNase A may contribute to this. The cytotoxicity of FA-***728***-DOPS-DMPE-RNase A is RNase A protein concentration-dependent. FA-***728***-DOPS-DMPE-RNase A also presented

effective targeting ability as proved by the higher folate-receptor-positive KB cells killing than the non-targeted control and free folic acid competiton control, as well as the effective killing of folate-receptor-positive L1210 cells but without killing the folate-receptor-negative cells Neuro 2A or MCF-7.

FA-***728***-DOPS-DMPE-RNase A presented similar cell killing as the non-targeted control or the ***728***-SS-RNase A conjugate (not significant) after incubation in 0% FBS containing medium, but presented substantial higher KB cell killing activity than the non-targeted formulation or ***728***-SS-RNase A after treating KB cells with the nanoformulations in 20% FBS containing medium, which may result from the targeting ability of FA-***728***-DOPS-DMPE-RNase A and higher serum stability compared with ***728***-SS-RNase A (Figure 3.23). Also, the dramatic reduction of cytotoxicity of FA-***728***-DOPS-DMPE-free RNase A (containing nonconjugated protein) from 0% FBS containing medium treatment to 20% FBS containing medium treatment (Figure 3.29) validates the importance of covalent attachment to enhance serum stability. Both in 0% FBS and 20% FBS containing serum, the ***728***-lacking control FA-DOPS-DMPE-RNase A did not present any cytotoxicity, which further proves the key role of ***728*** in the lipo-oligomer nanoformulation.

Furthermore, using nlsEGFP as cargo protein, FA-***728***-DOPS-DMPE-nlsEGFP presented higher cellular association and cellular internalization, as well as higher mean fluorescence intensity than the non-targeted control ***728***-DOPS-DMPE-nlsEGFP, evidencing the targeting nlsEGFP delivery ability of FA-***728***-DOPS-DMPE-nlsEGFP nanoparticles. Both formulations presented effective nlsEGFP persistence after a long incubation, validating efficient resistance to protease degradation if entrapped in lysosomes.

FA-***728***-DOPS-DMPE-nlsEGFP treated cells exhibited homogeneous green fluorescence all over the cells under fluorescence microscopy. This presented that FA-***728***-DOPS-DMPE-nlsEGFP underwent successful endolysosomal escape and

nlsEGFP was released from the nanoparticles in the reducible cytosolic environment, resulting in oligomer-free nlsEGFP throughout the cells. Furthermore, nlsEGFP was apparently also transported into the cell nuclei, which further validated the effective endolysosomal escape of FA-***728***-DOPS-DMPE-nlsEGFP, the bioreversibility of disulfide linkage, and the following nuclear localization of nlsEGFP via the NLS sequence. More nlsEGFP positive cells were found in the fluorescence microscopy of FA-***728***-DOPS-DMPE-nlsEGFP treated cells compared to the cells treated with ***728***-SS-nlsEGFP as reported before [144], which is consistent with the cellular internalization and mean fluorescence intensity results shown in Figure 3.33. These results proved that introduction of helper lipids significantly enhanced the targeted intracellular transduction of nlsEGFP. The ineffectiveness of FA-DOPS-DMPE-nlsEGFP and FA-***728***-DOPS-DMPE-free nlsEGFP further proved that ***728*** and bioreversible covalent attachment of GFP via disulfide linkages play a crucial role in the intracellular protein delivery. These results are consistent with corresponding RNase A transfection results (Figure 3.24).

5. Summary

Protein therapeutics present great potency in the treatment of various diseases because of their higher functional specificity and less adverse effects over small-molecule drugs. Since the introduction of human insulin as the first recombinant protein therapeutic in 1982, numerous protein therapeutics have been developed and widely applied in disease therapy, such as diabetes, hepatitis, haemophilia, and malignant tumors. However, clinically applied protein therapeutics are largely limited to those exerting their bioactivity extracellularly. Protein biologics which perform functions in the cytosol have not been widely applied in clinical trials due to the lack of efficient intracellular delivery technology. The particular crucial barriers include specific delivery to the targeted cells, highly efficient cellular internalization, effective endolysosomal escape, timely release of proteins from the delivery system and following subcelluar traffic to specific subcellular sites. Among these barriers, especially endolysosomal entrapment hamper effective protein transduction into the cytosol. Cargo proteins are largely sequestrated and degraded in the endolysosomes without access to the subcellular target sites for subsequent biological actions. Therefore, novel delivery technologies are required to cope with these barriers via combing multiple functions. Precise sequence-define oligomers have been designed and syntesiyed and contain various moieties and functions in our laboratory using solid-phase synthesis technology. Here, the thesis further expanded the application of sequence-define oligomers for targeted intracellular protein transduction and cancer therapy with effective endosomal escape and further improved the efficiency and stability of targeted intracellular protein delivery nanoformulations through incorporation of lipids.

In the first part, based on our former work, which established a library of more than 900 precise sequence-defined oligoaminoamide oligomers, we further expand their application for targeted intracellular protein transduction and cancer therapy.

Screening a small library of selected candidates, we identified sequence defined oligomers comprising PEG as hydrophilic shielding agent and optionally folic acid as targeting ligand as potent intracellular transduction agents for proteins covalently conjugated via bioreversible disulfide bonds. All evaluated oligomers present encouraging cellular association and internalization of protein as evidenced by nlsEGFP delivery. However, only the two-arm oligomers which were terminally modified with oleic acids showed both efficient cytosolic and nuclear delivery, and intracellular persistence of nlsEGFP. The oleic acid modification was a molecular requirement in conjugates for nanoparticle formation with medium small size of 25–35 nm, for destabilizing target lipid membranes enhancing cytosolic delivery, and altogether for efficient protein transduction. Folate-containing receptor targeted oligomer conjugates presented superior nlsEGFP transfection efficiency over the nontargeted control oligomer conjugates. Furthermore, choosing RNase A as a cargo protein for cancer therapy, the oleic acid modified two-arm oligomers again showed the most significant antitumoral effect. These results demonstrate the oleic acid modified sequence defined oligoaminoamide oligomers as a novel and promising nanocarrier for targeted intracellular protein delivery and cancer therapy.

In the second part, a novel targeted intracellular protein delivery system was developed by bioreversible coupling of cargo protein with the sequence defined amphiphilic triblock lipo-oligoaminoamide ***728*** followed by self-assembly with a variety of helper lipids (DOPS; DOPE; or linoleic acid), cholesterol, PEGylated lipids (DMPE-PEG2000 or DSPE-PEG2000) and optionally a folic acid-PEG conjugated lipid analog ***1042*** for targeting. Protein cargos RNase A or nlsEGFP were covalently coupled to lipo-oligomer ***728*** via disulfide linkages before nanoformulation. The disulfide bonds are supposed to be reduced in the cytosol after cellular uptake and endosomal escape, resulting in the release of oligomer-free proteins. Optimized protein nanoparticles including ***728***, DOPS, cholesterol, DMPE-PEG2000 and ***1042*** presented particle sizes of ~100 nm by DLS and ~50 nm by TEM, and a decreased

zeta potential compared to the control conjugates without helper lipids. They display a high colloidal stability in various conditions including high serum-containing medium, and mediated improved targeted cytosolic delivery of RNase A and nlsEGFP compared with the ***728***-SS-protein conjugates, resulting in the highest RNase A-induced cell killing on folate-receptor-positive KB cells, effective cell killing even under higher serum conditions, and effective delivery of nlsEGFP into the nucleus. In sum, the bioreversible lipo-oligomer protein conjugation combined with helper lipid nanoformulation presents a promising platform for intracellular protein delivery.

6. Abbreviations

ACN	Acetonitrile
BCA	Bicinchoninic acid assay
Boc	*tert*-Butoxycarbonyl
BSA	Bovine serum albumin
CPP	Cell-penetrating peptide
D_2O	Deuterium oxide
DAPI	4',6-Diamidino-2-phenylindole
DCM	Dichloromethane
Dde	1-(4,4-Dimethyl-2,6-dioxocyclohex-1-ylidene)-3-ethyl
DIPEA	*N,N*-Diisopropylethylamine
DLS	Dynamic laser-light scattering
DMEM	Dulbecco's modified Eagle's medium
DMF	*N,N*-Dimethylformamide
DMSO	Dimethylsulfoxide
DODT	3,6-Dioxa-1,8-octanedithiol
DOPE	1,2-dioleoyl-sn-glycero-3-phosphoethanolamine
DOPS	1,2-dioleoyl-sn-glycero-3-phospho-L-serine
DMPE-PEG2000	1,2-dimyristoyl-sn-glycero-3-phosphoethanolamine-N-[methoxy(polyethylene glycol)-2000]
DSPE-PEG2000	1,2-distearoyl-*sn*-glycero-3-phosphoethanolamine-N-[methoxy(polyethylene glycol)-2000]
DTNB	5,5'-Dithio-bis(2-nitrobenzoic acid)
DTT	DL-Dithiothreitol
EDTA	Ethylendiaminetetraacetic acid

EGFP	Enhanced green fluorescent protein
FBS	Fetal bovine serum
FDA	Food and Drug Administration
FITC	Fluorescein isothiocyanate
Fmoc	Fluorenylmethoxycarbonyl
FolA	Folic acid
FR	Folate receptor
HCl	Hydrochloric acid
HEPES	N-(2-hydroxethyl) piperazine-N‘-(2-ethansulfonic acid)
HIV	Human immunodeficiency virus
HOBt	1-Hydroxybenzotriazole
IPTG	Isopropyl β-D-1-thiogalactopyranoside
KCN	Potassium cyanide
LinA	Linoleic acid
MTBE	Methyl tert-butyl ether
MTT	3-(4,5-Dimethylthiazol-2-yl)-2,5-diphenyltetrazolium bromide
MWCO	Molecular Weight Cut Off
NaOH	Sodium hydroxide
NLS	Nuclear localization signal
nlsEGFP	Nuclear localization signal tagged EGFP
NMR	Nuclear magnetic resonance
OleA	Oleic acid
PBS	Phosphate buffered saline
PDI	Polydispersity index

PEG	Polyethylene glycol
PyBOP	Benzotriazol-1-yloxy-tripyrrolidinophosphonium hexafluorophosphate
RP-HPLC	Reversed-phase high performance liquid chromatography
RPMI	Roswell Park Memorial Institute medium
RNA	Ribonucleic acid
RNase A	Ribonuclease A
RT	Room temperature
SEC	Size-exclusion chromatography
SPDP	N-succinimidyl 3-(2-pyridyldithio) propionate
Sph	Succinoyl-pentaethylene hexamine
SPS	Solid-phase synthesis
Stp	Succinoyl-tetraethylene pentamine
TEPA	Tetraethylene pentamine
TEM	Transmission electron microscopy
TFA	Trifluoroacetic acid
TIS	Triisopropylsilane

7. References

[1] Leader B, Baca QJ, Golan DE. Protein therapeutics: A summary and pharmacological classification. Nature Reviews Drug Discovery 2008;7:21-39.
[2] Walsh G. Biopharmaceutical benchmarks 2014. Nature Biotechnology 2014;32:992-1000.
[3] Ford KG, Souberbiele BE, Darling D, Farzaneh F. Protein transduction: an alternative to genetic intervention? Gene Therapy 2001;8:1-4.
[4] Leavy O. Therapeutic antibodies: past, present and future FOREWORD. Nature Reviews Immunology 2010;10:297-.
[5] Ecker DM, Jones SD, Levine HL. The therapeutic monoclonal antibody market. Mabs-Austin 2015;7:9-14.
[6] Hurwitz H, Fehrenbacher L, Novotny W, Cartwright T, Hainsworth J, Heim W, et al. Bevacizumab plus irinotecan, fluorouracil, and leucovorin for metastatic colorectal cancer. New Engl J Med 2004;350:2335-42.
[7] Ferrara N, Hillan KJ, Gerber HP, Novotny W. Discovery and development of bevacizumab, an anti-VEGF antibody for treating cancer. Nature Reviews Drug Discovery 2004;3:391-400.
[8] Yang JC, Haworth L, Sherry RM, Hwu P, Schwartzentruber DJ, Topalian SL, et al. A randomized trial of bevacizumab, an anti-vascular endothelial growth factor antibody, for metastatic renal cancer. New Engl J Med 2003;349:427-34.
[9] Kabbinavar F, Hurwitz HI, Fehrenbacher L, Meropol NJ, Novotny WF, Lieberman G, et al. Phase II, randomized trial comparing bevacizumab plus fluorouracil (FU) leucovorin (LV) with FU/LV alone in patients with metastatic colorectal cancer. Journal of Clinical Oncology 2003;21:60-5.
[10] Olsen NJ, Stein CM. Drug therapy - New drugs for rheumatoid arthritis. New Engl J Med 2004;350:2167-79.
[11] Weinblatt ME, Keystone EC, Furst DE, Moreland LW, Weisman MH, Birbara CA, et al. Adalimumab, a fully human anti-tumor necrosis factor a monoclonal antibody, for the treatment of rheumatoid arthritis in patients taking concomitant methotrexate - The ARMADA trial (vol 48, pg 35, 2003). Arthritis and Rheumatism 2003;48:855-.
[12] Domling A, Holak TA. Programmed Death-1: Therapeutic Success after More than 100 Years of Cancer Immunotherapy. Angew Chem Int Edit 2014;53:2286-8.
[13] Finfer S, Bellomo R, Boyce N, French J, Myburgh J, Norton R, et al. A comparison of albumin and saline for fluid resuscitation in the intensive care unit. New Engl J Med 2004;350:2247-56.
[14] Raghu G, Brown KK, Bradford WZ, Starko K, Noble PW, Schwartz DA, et al. A placebo-controlled trial of interferon gamma-1b in patients with idiopathic pulmonary fibrosis. New Engl J Med 2004;350:125-33.

[15] Key LL, Rodriguiz RM, Willi SM, Wright NM, Hatcher HC, Eyre DR, et al. Long-Term Treatment of Osteopetrosis with Recombinant Human Interferon-Gamma. New Engl J Med 1995;332:1594-9.
[16] Ezekowitz RAB, Dinauer MC, Jaffe HS, Orkin SH, Newburger PE. Partial Correction of the Phagocyte Defect in Patients with X-Linked Chronic Granulomatous-Disease by Subcutaneous Interferon-Gamma. New Engl J Med 1988;319:146-51.
[17] Baron S, Tyring SK, Fleischmann WR, Coppenhaver DH, Niesel DW, Klimpel GR, et al. The Interferons - Mechanisms of Action and Clinical-Applications. Jama-J Am Med Assoc 1991;266:1375-83.
[18] Key LL, Ries WL, Rodriguiz RM, Hatcher HC. Recombinant Human Interferon-Gamma Therapy for Osteopetrosis. J Pediatr-Us 1992;121:119-24.
[19] Out HJ, Driessen SGAJ, Mannaerts BMJL, Coelingh Bennink HJT. Recombinant follicle-stimulating hormone (follitropin beta, Puregon) yields higher pregnancy rates in in vitro fertilization than urinary gonadotropins. Fertility and Sterility 1997;68:138-42.
[20] Westergaard LW, Bossuyt PMM, Van der Veen F, van Wely M. Human menopausal gonadotropin versus recombinant follicle stimulation hormone for ovarian stimulation in assisted reproductive cycles. Cochrane Db Syst Rev 2003.
[21] Rao DB, Sane PG, Georgiev EL. Collagenase in the treatment of dermal and decubitus ulcers. J Am Geriatr Soc 1975;23:22-30.
[22] Boxer AM, Gottesman N, Bernstein H, Mandl I. Debridement of Dermal Ulcers and Decubiti with Collagenase. Geriatrics 1969;24:75-+.
[23] Greinacher A, Volpel H, Janssens U, Hach-Wunderle V, Kemkes-Matthes B, Eichler P, et al. Recombinant hirudin (lepirudin) provides safe and effective anticoagulation in patients with heparin-induced thrombocytopenia: a prospective study. Circulation 1999;99:73-80.
[24] Eriksson BI, WilleJorgensen P, Kalebo P, Mouret P, Rosencher N, Bosch P, et al. A comparison of recombinant hirudin with a low-molecular-weight heparin to prevent thromboembolic complications after total hip replacement. New Engl J Med 1997;337:1329-35.
[25] Szmuness W, Stevens CE, Harley EJ, Zang EA, Oleszko WR, William DC, et al. Hepatitis-B Vaccine - Demonstration of Efficacy in a Controlled Clinical-Trial in a High-Risk Population in the United-States. New Engl J Med 1980;303:833-41.
[26] Crosnier J, Jungers P, Courouce AM, Laplanche A, Benhamou E, Degos F, et al. Randomised placebo-controlled trial of hepatitis B surface antigen vaccine in French haemodialysis units: I, Medical staff. Lancet 1981;1:455-9.
[27] Ranke MB, Gruhler M, Rosskamp R, Brügmann G, Attanasio A, Blum WF, et al. Testing with growth hormone-releasing factor (GRF(1–29)NH2) and somatomedin C measurements for the evaluation of growth hormone deficiency. European Journal of Pediatrics 1986;145:485-92.

[28] Ghigo E, Aimaretti G, Gianotti L, Bellone J, Arvat E, Camanni F. New approach to the diagnosis of growth hormone deficiency in adults. Eur J Endocrinol 1996;134:352-6.
[29] Urnovitz HB, Sturge JC, Gottfried TD. Increased sensitivity of HIV-1 antibody detection. Nature Medicine 1997;3:1258-.
[30] Vandeperre P, Simonon A, Msellati P, Hitimana DG, Vaira D, Bazubagira A, et al. Postnatal Transmission of Human-Immunodeficiency-Virus Type-1 from Mother to Infant - a Prospective Cohort Study in Kigali, Rwanda. New Engl J Med 1991;325:593-8.
[31] Busch MP, Eble BE, Khayambashi H, Heilbron D, Murphy EL, Kwok S, et al. Evaluation of Screened Blood Donations for Human-Immunodeficiency-Virus Type-1 Infection by Culture and DNA Amplification of Pooled Cells. New Engl J Med 1991;325:1-5.
[32] Noguchi H, Matsushita M, Kobayashi N, Levy MF, Matsumoto S. Recent Advances in Protein Transduction Technology. Cell Transplant 2010;19:649-54.
[33] Wang M, Zuris JA, Meng FT, Rees H, Sun S, Deng P, et al. Efficient delivery of genome-editing proteins using bioreducible lipid nanoparticles. Proc Natl Acad Sci U S A 2016;113:2868-73.
[34] Wang M, Alberti K, Sun S, Arellano CL, Xu QB. Combinatorially Designed Lipid-like Nanoparticles for Intracellular Delivery of Cytotoxic Protein for Cancer Therapy. Angew Chem Int Edit 2014;53:2893-8.
[35] Zuris JA, Thompson DB, Shu Y, Guilinger JP, Bessen JL, Hu JH, et al. Cationic lipid-mediated delivery of proteins enables efficient protein-based genome editing in vitro and in vivo. Nature Biotechnology 2015;33:73-80.
[36] Tang R, Kim CS, Solfiell DJ, Rana S, Mout R, Velazquez-Delgado EM, et al. Direct Delivery of Functional Proteins and Enzymes to the Cytosol Using Nanoparticle-Stabilized Nanocapsules. ACS Nano 2013;7:6667-73.
[37] Ray M, Tang R, Jiang ZW, Rotello VM. Quantitative Tracking of Protein Trafficking to the Nucleus Using Cytosolic Protein Delivery by Nanoparticle-Stabilized Nanocapsules. Bioconjugate Chemistry 2015;26:1004-7.
[38] Yan M, Du JJ, Gu Z, Liang M, Hu YF, Zhang WJ, et al. A novel intracellular protein delivery platform based on single-protein nanocapsules. Nat Nanotechnol 2010;5:48-53.
[39] Gu Z, Yan M, Hu BL, Joo KI, Biswas A, Huang Y, et al. Protein Nanocapsule Weaved with Enzymatically Degradable Polymeric Network. Nano Letters 2009;9:4533-8.
[40] Liu GJ, Ma SB, Li SK, Cheng R, Meng FH, Liu HY, et al. The highly efficient delivery of exogenous proteins into cells mediated by biodegradable chimaeric polymersomes. Biomaterials 2010;31:7575-85.
[41] Li X, Yang WJ, Zou Y, Meng FH, Deng C, Zhong ZY. Efficacious delivery of protein drugs to prostate cancer cells by PSMA-targeted pH-responsive chimaeric polymersomes. Journal of Controlled Release 2015;220:704-14.

[42] Li S, Zhang J, Deng C, Meng FH, Yu L, Zhong ZY. Redox-Sensitive and Intrinsically Fluorescent Photoclick Hyaluronic Acid Nanogels for Traceable and Targeted Delivery of Cytochrome c to Breast Tumor in Mice. ACS applied materials & interfaces 2016;8:21155-62.
[43] Chen J, Zou Y, Deng C, Meng FH, Zhang J, Zhong ZY. Multifunctional Click Hyaluronic Acid Nanogels for Targeted Protein Delivery and Effective Cancer Treatment in Vivo. Chem Mater 2016;28:8792-9.
[44] Anraku Y, Kishimura A, Kamiya M, Tanaka S, Nomoto T, Toh K, et al. Systemically Injectable Enzyme-Loaded Polyion Complex Vesicles as In Vivo Nanoreactors Functioning in Tumors. Angew Chem Int Edit 2016;55:560-5.
[45] Lee Y, Ishii T, Kim HJ, Nishiyama N, Hayakawa Y, Itaka K, et al. Efficient Delivery of Bioactive Antibodies into the Cytoplasm of Living Cells by Charge-Conversional Polyion Complex Micelles. Angew Chem Int Edit 2010;49:2552-5.
[46] Nischan N, Herce HD, Natale F, Bohlke N, Budisa N, Cardoso MC, et al. Covalent Attachment of Cyclic TAT Peptides to GFP Results in Protein Delivery into Live Cells with Immediate Bioavailability. Angew Chem Int Edit 2015;54:1950-3.
[47] Dinca A, Chien WM, Chin MT. Intracellular Delivery of Proteins with Cell-Penetrating Peptides for Therapeutic Uses in Human Disease. Int J Mol Sci 2016;17:263.
[48] Myrberg H, Lindgren M, Langel U. Protein delivery by the cell-penetrating peptide YTA2. Bioconjug Chem 2007;18:170-4.
[49] Walsh CT, Garneau-Tsodikova S, Gatto GJ. Protein posttranslational modifications: The chemistry of proteome diversifications. Angew Chem Int Edit 2005;44:7342-72.
[50] Buckholz RG, Gleeson MAG. Yeast Systems for the Commercial Production of Heterologous Proteins. Bio-Technol 1991;9:1067-72.
[51] Terpe K. Overview of bacterial expression systems for heterologous protein production: from molecular and biochemical fundamentals to commercial systems. Appl Microbiol Biot 2006;72:211-22.
[52] Lai T, Yang Y, Ng SK. Advances in Mammalian cell line development technologies for recombinant protein production. Pharmaceuticals 2013;6:579-603.
[53] Pisal DS, Kosloski MP, Balu-Iyer SV. Delivery of Therapeutic Proteins. J Pharm Sci-Us 2010;99:2557-75.
[54] Lu Y, Sun WJ, Gu Z. Stimuli-responsive nanomaterials for therapeutic protein delivery. Journal of Controlled Release 2014;194:1-19.
[55] Yu MY, Wu J, Shi JJ, Farokhzad OC. Nanotechnology for protein delivery: Overview and perspectives. Journal of Controlled Release 2016;240:24-37.
[56] Schellekens H. Bioequivalence and the immunogenicity of biopharmaceuticals. Nat Rev Drug Discov 2002;1:457-62.
[57] Lu YJ, Yang J, Sega E. Issues related to targeted delivery of proteins and peptides. Aaps Journal 2006;8:E466-E78.

[58] Gu Z, Biswas A, Zhao MX, Tang Y. Tailoring nanocarriers for intracellular protein delivery. Chemical Society Reviews 2011;40:3638-55.
[59] Bareford LA, Swaan PW. Endocytic mechanisms for targeted drug delivery. Advanced Drug Delivery Reviews 2007;59:748-58.
[60] Ganta S, Devalapally H, Shahiwala A, Amiji M. A review of stimuli-responsive nanocarriers for drug and gene delivery. J Control Release 2008;126:187-204.
[61] Fu AL, Tang R, Hardie J, Farkas ME, Rotello VM. Promises and Pitfalls of Intracellular Delivery of Proteins. Bioconjugate Chemistry 2014;25:1602-8.
[62] Pai LH, Wittes R, Setser A, Willingham MC, Pastan I. Treatment of advanced solid tumors with immunotoxin LMB-1: an antibody linked to Pseudomonas exotoxin. Nat Med 1996;2:350-3.
[63] Kreitman RJ, Stetler-Stevenson M, Margulies I, Noel P, Fitzgerald DJ, Wilson WH, et al. Phase II trial of recombinant immunotoxin RFB4(dsFv)-PE38 (BL22) in patients with hairy cell leukemia. J Clin Oncol 2009;27:2983-90.
[64] Schirrmann T, Krauss J, Arndt MA, Rybak SM, Dubel S. Targeted therapeutic RNases (ImmunoRNases). Expert opinion on biological therapy 2009;9:79-95.
[65] Qiao M, Zu LD, He XH, Shen RL, Wang QC, Liu MF. Onconase downregulates microRNA expression through targeting microRNA precursors. Cell research 2012;22:1199-202.
[66] Leland PA, Raines RT. Cancer chemotherapy--ribonucleases to the rescue. Chem Biol 2001;8:405-13.
[67] Shlyakhovenko VA. Ribonucleases in tumor growth. Experimental oncology 2009;31:127-33.
[68] Gu Z, Biswas A, Zhao M, Tang Y. Tailoring nanocarriers for intracellular protein delivery. Chem Soc Rev 2011;40:3638-55.
[69] Choi SO, Kim YC, Lee JW, Park JH, Prausnitz MR, Allen MG. Intracellular Protein Delivery and Gene Transfection by Electroporation Using a Microneedle Electrode Array. Small 2012;8:1081-91.
[70] Daugimont L, Baron N, Vandermeulen G, Pavselj N, Miklavcic D, Jullien MC, et al. Hollow Microneedle Arrays for Intradermal Drug Delivery and DNA Electroporation. J Membrane Biol 2010;236:117-25.
[71] Jo J, Hong S, Choi WY, Lee DR. Cell-penetrating peptide (CPP)-conjugated proteins is an efficient tool for manipulation of human mesenchymal stromal cells. Scientific Reports 2014;4:4378.
[72] Ramakrishna S, Dad AK, Beloor J, Gopalappa R, Lee SK, Kim H. Gene disruption by cell-penetrating peptide-mediated delivery of Cas9 protein and guide RNA. Genome Research 2014;24:1020-7.
[73] Sawant R, Torchilin V. Intracellular transduction using cell-penetrating peptides. Mol Biosyst 2010;6:628-40.
[74] Liu J, Gaj T, Patterson JT, Sirk SJ, Barbas Iii CF. Cell-Penetrating Peptide-Mediated Delivery of TALEN Proteins via Bioconjugation for Genome Engineering. PLoS One 2014;9:e85755.

[75] Lindgren M, Hallbrink M, Prochiantz A, Langel U. Cell-penetrating peptides. Trends PharmacolSci 2000;21:99-103.
[76] Patel LN, Zaro JL, Shen WC. Cell penetrating peptides: Intracellular pathways and pharmaceutical perspectives. Pharmaceutical Research 2007;24:1977-92.
[77] Green I, Christison R, Voyce CJ, Bundell KR, Lindsay MA. Protein transduction domains: are they delivering? Trends in Pharmacological Sciences;24:213-5.
[78] Peer D, Karp JM, Hong S, FaroKHzad OC, Margalit R, Langer R. Nanocarriers as an emerging platform for cancer therapy. Nat Nanotechnol 2007;2:751-60.
[79] Shi JJ, Votruba AR, Farokhzad OC, Langer R. Nanotechnology in Drug Delivery and Tissue Engineering: From Discovery to Applications. Nano Letters 2010;10:3223-30.
[80] Faraji AH, Wipf P. Nanoparticles in cellular drug delivery. Bioorgan Med Chem 2009;17:2950-62.
[81] Gao JH, Xu B. Applications of nanomaterials inside cells. Nano Today 2009;4:37-51.
[82] Chou LYT, Ming K, Chan WCW. Strategies for the intracellular delivery of nanoparticles. Chemical Society Reviews 2011;40:233-45.
[83] Gaberc-Porekar V, Zore I, Podobnik B, Menart V. Obstacles and pitfalls in the PEGylation of therapeutic proteins. Curr Opin Drug Disc 2008;11:242-50.
[84] Kabanov AV, Vinogradov SV. Nanogels as Pharmaceutical Carriers: Finite Networks of Infinite Capabilities. Angewandte Chemie International Edition 2009;48:5418-29.
[85] Stuart MA, Huck WT, Genzer J, Muller M, Ober C, Stamm M, et al. Emerging applications of stimuli-responsive polymer materials. Nat Mater 2010;9:101-13.
[86] Solaro R. Targeted delivery of proteins by nanosized carriers. Journal of Polymer Science Part A: Polymer Chemistry 2008;46:1-11.
[87] Saito N, Usui Y, Aoki K, Narita N, Shimizu M, Hara K, et al. Carbon nanotubes: biomaterial applications. Chemical Society Reviews 2009;38:1897-903.
[88] Liguori L, Marques B, Villegas-Mendez A, Rothe R, Lenormand JL. Liposomes-mediated delivery of pro-apoptotic therapeutic membrane proteins. Journal of Controlled Release 2008;126:217-27.
[89] Chatin B, Mevel M, Devalliere J, Dallet L, Haudebourg T, Peuziat P, et al. Liposome-based Formulation for Intracellular Delivery of Functional Proteins. Mol Ther Nucleic Acids 2015;4:e244.
[90] Muratori C, Bona R, Federico M. Lentivirus-Based Virus-Like Particles as a New Protein Delivery Tool. In: Federico M, editor. Lentivirus Gene Engineering Protocols: Second Edition. Totowa, NJ: Humana Press; 2010. p. 111-24.
[91] Kaczmarczyk SJ, Sitaraman K, Young HA, Hughes SH, Chatterjee DK. Protein delivery using engineered virus-like particles. Proc Natl Acad Sci U S A 2011;108:16998-7003.

[92] Zhao Q, Chen W, Chen Y, Zhang L, Zhang J, Zhang Z. Self-assembled virus-like particles from rotavirus structural protein VP6 for targeted drug delivery. Bioconjug Chem 2011;22:346-52.
[93] Lim YT, Cho MY, Lee JM, Chung SJ, Chung BH. Simultaneous intracellular delivery of targeting antibodies and functional nanoparticles with engineered protein G system. Biomaterials 2009;30:1197-204.
[94] Shi Kam NW, Jessop TC, Wender PA, Dai H. Nanotube Molecular Transporters: Internalization of Carbon Nanotube−Protein Conjugates into Mammalian Cells. Journal of the American Chemical Society 2004;126:6850-1.
[95] Medintz IL, Pons T, Delehanty JB, Susumu K, Brunel FM, Dawson PE, et al. Intracellular delivery of quantum dot-protein cargos mediated by cell penetrating peptides. Bioconjug Chem 2008;19:1785-95.
[96] Ghosh P, Yang X, Arvizo R, Zhu Z-J, Agasti SS, Mo Z, et al. Intracellular Delivery of a Membrane-Impermeable Enzyme in Active Form using Functionalized Gold Nanoparticles. Journal of the American Chemical Society 2010;132:2642-5.
[97] Slowing, II, Trewyn BG, Lin VS. Mesoporous silica nanoparticles for intracellular delivery of membrane-impermeable proteins. J Am Chem Soc 2007;129:8845-9.
[98] Bale SS, Kwon SJ, Shah DA, Banerjee A, Dordick JS, Kane RS. Nanoparticle-mediated cytoplasmic delivery of proteins to target cellular machinery. ACS Nano 2010;4:1493-500.
[99] Chorny M, Hood E, Levy RJ, Muzykantov VR. Endothelial delivery of antioxidant enzymes loaded into non-polymeric magnetic nanoparticles. Journal of controlled release : official journal of the Controlled Release Society 2010;146:144-51.
[100] Kam NWS, Dai H. Carbon Nanotubes as Intracellular Protein Transporters: Generality and Biological Functionality. Journal of the American Chemical Society 2005;127:6021-6.
[101] Furuhata M, Kawakami H, Toma K, Hattori Y, Maitani Y. Intracellular Delivery of Proteins in Complexes with Oligoarginine-Modified Liposomes and the Effect of Oligoarginine Length. Bioconjugate Chemistry 2006;17:935-42.
[102] Sarker SR, Hokama R, Takeoka S. Intracellular delivery of universal proteins using a lysine headgroup containing cationic liposomes: deciphering the uptake mechanism. Mol Pharm 2014;11:164-74.
[103] Tang R, Jiang Z, Ray M, Hou S, Rotello VM. Cytosolic delivery of large proteins using nanoparticle-stabilized nanocapsules. Nanoscale 2016;8:18038-41.
[104] Discher BM, Won Y-Y, Ege DS, Lee JC-M, Bates FS, Discher DE, et al. Polymersomes: Tough Vesicles Made from Diblock Copolymers. Science 1999;284:1143-6.
[105] Discher DE, Eisenberg A. Polymer Vesicles. Science 2002;297:967-73.
[106] Discher DE, Ortiz V, Srinivas G, Klein ML, Kim Y, Christian D, et al. Emerging Applications of Polymersomes in Delivery: from Molecular Dynamics to Shrinkage of Tumors. Prog Polym Sci 2007;32:838-57.

[107] Lee Y, Ishii T, Cabral H, Kim HJ, Seo JH, Nishiyama N, et al. Charge-conversional polyionic complex micelles-efficient nanocarriers for protein delivery into cytoplasm. Angew Chem Int Ed Engl 2009;48:5309-12.
[108] Cronican JJ, Thompson DB, Beier KT, McNaughton BR, Cepko CL, Liu DR. Potent Delivery of Functional Proteins into Mammalian Cells in Vitro and in Vivo Using a Supercharged Protein. ACS Chemical Biology 2010;5:747-52.
[109] Cronican JJ, Beier KT, Davis TN, Tseng J-C, Li W, Thompson DB, et al. A Class of Human Proteins That Deliver Functional Proteins Into Mammalian Cells In Vitro and In Vivo. Chemistry & biology 2011;18:833-8.
[110] Thompson DB, Cronican JJ, Liu DR. Engineering and Identifying Supercharged Proteins for Macromolecule Delivery into Mammalian Cells. Methods in enzymology 2012;503:293-319.
[111] Abbing A, Blaschke UK, Grein S, Kretschmar M, Stark CM, Thies MJ, et al. Efficient intracellular delivery of a protein and a low molecular weight substance via recombinant polyomavirus-like particles. J Biol Chem 2004;279:27410-21.
[112] Lachelt U, Wagner E. Nucleic Acid Therapeutics Using Polyplexes: A Journey of 50 Years (and Beyond). Chemical Reviews 2015;115:11043-78.
[113] Zhang P, Wagner E. History of Polymeric Gene Delivery Systems. Topics in Current Chemistry 2017;375:26.
[114] Schaffert D, Troiber C, Salcher EE, Frohlich T, Martin I, Badgujar N, et al. Solid-phase synthesis of sequence-defined T-, i-, and U-shape polymers for pDNA and siRNA delivery. Angew Chem Int Ed Engl 2011;50:8986-9.
[115] Lächelt U, Wagner E. Nucleic Acid Therapeutics Using Polyplexes: A Journey of 50 Years (and Beyond). Chem Rev 2015.
[116] Salcher EE, Kos P, Frohlich T, Badgujar N, Scheible M, Wagner E. Sequence-defined four-arm oligo(ethanamino)amides for pDNA and siRNA delivery: Impact of building blocks on efficacy. J Control Release 2012;164:380-6.
[117] Schaffert D, Badgujar N, Wagner E. Novel Fmoc-polyamino acids for solid-phase synthesis of defined polyamidoamines. Org Lett 2011;13:1586-9.
[118] Schaffert D, Troiber C, Wagner E. New Sequence-Defined Polyaminoamides with Tailored Endosomolytic Properties for Plasmid DNA Delivery. Bioconjug Chem 2012;23:1157-65.
[119] Lachelt U, Wittmann V, Muller K, Edinger D, Kos P, Hohn M, et al. Synthetic Polyglutamylation of Dual-Functional MTX Ligands for Enhanced Combined Cytotoxicity of Poly(I:C) Nanoplexes. Mol Pharm 2014;11:2631-9.
[120] Maier K, Martin I, Wagner E. Sequence Defined Disulfide-Linked Shuttle for Strongly Enhanced Intracellular Protein Delivery. Molecular Pharmaceutics 2012;9:3560-8.
[121] Maier K, Wagner E. Acid-labile traceless click linker for protein transduction. J Am Chem Soc 2012;134:10169-73.

[122] Feener EP, Shen WC, Ryser HJ. Cleavage of disulfide bonds in endocytosed macromolecules. A processing not associated with lysosomes or endosomes. J Biol Chem 1990;265:18780-5.
[123] Saito G, Swanson JA, Lee KD. Drug delivery strategy utilizing conjugation via reversible disulfide linkages: role and site of cellular reducing activities. AdvDrug DelivRev 2003;55:199-215.
[124] Kellogg BA, Garrett L, Kovtun Y, Lai KC, Leece B, Miller M, et al. Disulfide-linked antibody-maytansinoid conjugates: optimization of in vivo activity by varying the steric hindrance at carbon atoms adjacent to the disulfide linkage. Bioconjug Chem 2011;22:717-27.
[125] Klein PM, Muller K, Gutmann C, Kos P, Krhac Levacic A, Edinger D, et al. Twin disulfides as opportunity for improving stability and transfection efficiency of oligoaminoethane polyplexes. J Control Release 2015;205:109-19.
[126] Klein PM, Wagner E. Bioreducible polycations as shuttles for therapeutic nucleic acid and protein transfection. Antioxidants & redox signaling 2014;21:804-17.
[127] Kaiser E, Colescott RL, Bossinger CD, Cook PI. Color test for detection of free terminal amino groups in the solid-phase synthesis of peptides. Anal Biochem 1970;34:595-8.
[128] Frohlich T, Edinger D, Klager R, Troiber C, Salcher E, Badgujar N, et al. Structure-activity relationships of siRNA carriers based on sequence-defined oligo (ethane amino) amides. J Control Release 2012;160:532-41.
[129] Lachelt U, Kos P, Mickler FM, Herrmann A, Salcher EE, Rodl W, et al. Fine-tuning of proton sponges by precise diaminoethanes and histidines in pDNA polyplexes. Nanomedicine 2014;10:35-44.
[130] Leader B, Baca QJ, Golan DE. Protein therapeutics: a summary and pharmacological classification. Nat Rev Drug Discov 2008;7:21-39.
[131] Walsh G. Biopharmaceutical benchmarks 2014. Nat Biotech 2014;32:992-1000.
[132] Murthy N, Thng YX, Schuck S, Xu MC, Frechet JM. A novel strategy for encapsulation and release of proteins: hydrogels and microgels with acid-labile acetal cross-linkers. JAmChem Soc 2002;124:12398-9.
[133] Ray M, Tang R, Jiang Z, Rotello VM. Quantitative Tracking of Protein Trafficking to the Nucleus Using Cytosolic Protein Delivery by Nanoparticle-Stabilized Nanocapsules. Bioconjug Chem 2015;26:1004-7.
[134] Lee Y, Ishii T, Kim HJ, Nishiyama N, Hayakawa Y, Itaka K, et al. Efficient delivery of bioactive antibodies into the cytoplasm of living cells by charge-conversional polyion complex micelles. Angew Chem Int Ed Engl 2010;49:2552-5.
[135] Wang M, Alberti K, Sun S, Arellano CL, Xu Q. Combinatorially Designed Lipid-like Nanoparticles for Intracellular Delivery of Cytotoxic Protein for Cancer Therapy. Angewandte Chemie 2014;126:2937-42.

[136] Kaczmarczyk SJ, Sitaraman K, Young HA, Hughes SH, Chatterjee DK. Protein delivery using engineered virus-like particles. Proceedings of the National Academy of Sciences of the United States of America 2011;108:16998-7003.
[137] Liu X, Zhang P, He D, Rodl W, Preiss T, Radler JO, et al. pH-Reversible Cationic RNase A Conjugates for Enhanced Cellular Delivery and Tumor Cell Killing. Biomacromolecules 2016;17:173-82.
[138] Roder R, Helma J, Preiss T, Radler JO, Leonhardt H, Wagner E. Intracellular Delivery of Nanobodies for Imaging of Target Proteins in Live Cells. Pharm Res 2017;34:161-74.
[139] Postupalenko V, Desplancq D, Orlov I, Arntz Y, Spehner D, Mely Y, et al. Protein Delivery System Containing a Nickel-Immobilized Polymer for Multimerization of Affinity-Purified His-Tagged Proteins Enhances Cytosolic Transfer. Angewandte Chemie International Edition 2015;54:10583-6.
[140] Postupalenko V, Sibler A-P, Desplancq D, Nominé Y, Spehner D, Schultz P, et al. Intracellular delivery of functionally active proteins using self-assembling pyridylthiourea-polyethylenimine. Journal of Controlled Release 2014;178:86-94.
[141] June RK, Gogoi K, Eguchi A, Cui XS, Dowdy SF. Synthesis of a pH-Sensitive Nitrilotriacetic Linker to Peptide Transduction Domains To Enable Intracellular Delivery of Histidine Imidazole Ring-Containing Macromolecules. Journal of the American Chemical Society 2010;132:10680-2.
[142] Nischan N, Herce HD, Natale F, Bohlke N, Budisa N, Cardoso MC, et al. Covalent attachment of cyclic TAT peptides to GFP results in protein delivery into live cells with immediate bioavailability. Angew Chem Int Ed Engl 2015;54:1950-3.
[143] Kos P, Lachelt U, Herrmann A, Mickler FM, Doblinger M, He D, et al. Histidine-rich stabilized polyplexes for cMet-directed tumor-targeted gene transfer. Nanoscale 2015;7:5350-62.
[144] Zhang P, He DS, Klein PM, Liu XW, Roder R, Doblinger M, et al. Enhanced Intracellular Protein Transduction by Sequence Defined Tetra-Oleoyl Oligoaminoamides Targeted for Cancer Therapy. Adv Funct Mater 2015;25:6627-36.
[145] Klein PM, Wagner E. Bioreducible Polycations as Shuttles for Therapeutic Nucleic Acid and Protein Transfection. Antioxidants & redox signaling 2013;21:804-17.
[146] Lachelt U, Kos P, Mickler FM, Herrmann A, Salcher EE, Rodl W, et al. Fine-tuning of proton sponges by precise diaminoethanes and histidines in pDNA polyplexes. Nanomedicine 2013.
[147] Raines RT. Ribonuclease A. Chem Rev 1998;98:1045-66.
[148] Adlakha-Hutcheon G, Bally MB, Shew CR, Madden TD. Controlled destabilization of a liposomal drug delivery system enhances mitoxantrone antitumor activity. Nat Biotechnol 1999;17:775-9.
[149] Chang CW, Barber L, Ouyang C, Masin D, Bally MB, Madden TD. Plasma clearance, biodistribution and therapeutic properties of mitoxantrone encapsulated in

conventional and sterically stabilized liposomes after intravenous administration in BDF1 mice. Br J Cancer 1997;75:169-77.
[150] Akbarzadeh A, Rezaei-Sadabady R, Davaran S, Joo SW, Zarghami N, Hanifehpour Y, et al. Liposome: classification, preparation, and applications. Nanoscale research letters 2013;8:102.
[151] Sharma A, Sharma US. Liposomes in drug delivery: Progress and limitations. International Journal of Pharmaceutics 1997;154:123-40.
[152] Shimanouchi T, Walde P, Gardiner J, Mahajan YR, Seebach D, Thomae A, et al. Permeation of a β-heptapeptide derivative across phospholipid bilayers. Biochimica et Biophysica Acta (BBA) - Biomembranes 2007;1768:2726-36.
[153] Allen TM, Cleland LG. Serum-induced leakage of liposome contents. Biochim Biophys Acta 1980;597:418-26.
[154] Troiber C, Edinger D, Kos P, Schreiner L, Klager R, Herrmann A, et al. Stabilizing effect of tyrosine trimers on pDNA and siRNA polyplexes. Biomaterials 2013;34:1624-33.
[155] Erazo-Oliveras A, Najjar K, Dayani L, Wang TY, Johnson GA, Pellois JP. Protein delivery into live cells by incubation with an endosomolytic agent. Nat Methods 2014;11:861-7.
[156] Dohmen C, Frohlich T, Lachelt U, Rohl I, Vornlocher H-P, Hadwiger P, et al. Defined Folate-PEG-siRNA Conjugates for Receptor-specific Gene Silencing. Mol Ther Nucleic Acids 2012;1:e7.
[157] Dohmen C, Edinger D, Frohlich T, Schreiner L, Lachelt U, Troiber C, et al. Nanosized Multifunctional Polyplexes for Receptor-Mediated SiRNA Delivery. ACS Nano 2012;6:5198-208.
[158] White SH, King GI. Molecular packing and area compressibility of lipid bilayers. Proc Natl Acad Sci U S A 1985;82:6532-6.
[159] Edholm O, Nagle JF. Areas of molecules in membranes consisting of mixtures. Biophys J 2005;89:1827-32.
[160] Petrache HI, Dodd SW, Brown MF. Area per lipid and acyl length distributions in fluid phosphatidylcholines determined by (2)H NMR spectroscopy. Biophys J 2000;79:3172-92.
[161] Lewis BA, Engelman DM. Lipid bilayer thickness varies linearly with acyl chain length in fluid phosphatidylcholine vesicles. J Mol Biol 1983;166:211-7.
[162] Petrache HI, Tristram-Nagle S, Gawrisch K, Harries D, Parsegian VA, Nagle JF. Structure and fluctuations of charged phosphatidylserine bilayers in the absence of salt. Biophys J 2004;86:1574-86.
[163] Ormo M, Cubitt AB, Kallio K, Gross LA, Tsien RY, Remington SJ. Crystal structure of the Aequorea victoria green fluorescent protein. Science 1996;273:1392-5.

8. Publications

Original articles

Zhang P, He DS, Klein PM, Liu XW, Röder R, Doblinger M, Wagner E (2015) Enhanced Intracellular Protein Transduction by Sequence Defined Tetra-Oleoyl Oligoaminoamides Targeted for Cancer Therapy. *Advanced Functional Materials* 25 (42):6627-6636.

Zhang P, Steinborn B, Lächelt U, Zahler S, Wagner E (2017) Lipo-Oligomer Nanoformulations for Targeted Intracellular Protein Delivery. *Biomacromolecules* DOI: 10.1021/acs.biomac.7b00666

Liu X*, **Zhang P***, Rödl W, Maier K, Lächelt U, Wagner E (2017) Toward Artificial Immunotoxins: Traceless Reversible Conjugation of RNase A with Receptor Targeting and Endosomal Escape Domains. *Molecular Pharmaceutics* 14 (5):1439-1449. (*equal contribution)

Liu X, **Zhang P**, He D, Rodl W, Preiss T, Radler JO, Wagner E, Lächelt U (2016) pH-Reversible Cationic RNase A Conjugates for Enhanced Cellular Delivery and Tumor Cell Killing. *Biomacromolecules* 17 (1):173-182.

Review

Zhang P, Wagner E (2017) History of Polymeric Gene Delivery Systems. *Topics in Current Chemistry* 375 (2):26.

Poster presentations

Zhang P, He DS, Klein PM, Liu XW, Roder R, Doblinger M, Wagner E. Enhanced Intracellular Protein Transduction by Sequence Defined Tetra-Oleoyl Oligoaminoamides Targeted for Cancer Therapy. 1st LMU-ChAN (Ludwig-Maximilians

-Universität - China Academic Network) Scientific Forum, Munich, Germany, November 13-15, 2015. (Poster)

Zhang P, He DS, Klein PM, Liu XW, Roder R, Doblinger M, Wagner E. Enhanced Intracellular Protein Transduction by Sequence Defined Tetra-Oleoyl Oligoaminoamides Targeted for Cancer Therapy. Tokyo-LMU Symposium, Munich, Germany, October 28-29, 2015. (Poster)

9. Acknowledgements

Time flies! At the end of my PhD study, I would like to express my gratitude to all people supporting me during the past four years.

First of all, I would like to thank my supervisor Prof. Dr. Ernst Wagner for giving me the opportunity to do my PhD in his research group. I greatly appreciate his scientific support and professional guidance. I have learned a lot from not only the informative discussions with him but also the email communications with him even after midnight.

I would like to thank Dr. Dongsheng He, Dr. Ulrich Lächelt, Philipp Klein and Benjamin Steinborn for their generous supply with oligomers. Special thanks to Dongsheng for introducing me into the field of oligomer synthesis. I also want to thank Xiaowen for the kind collaboration and many discussions, and Ruth for the help in the protein project. Special thanks to Wei for numerous scientific discussions and great help in the experiments. Many thanks to Eva and Sarah for the trials in the animal experiments. I would also like to thank Markus Döblinger and Susanne Kempter for their help with TEM, as well as Rafal and Prof. Dr. Joachim O. Rädler for helpful discussions. I want to thank Petra and Miriam for their instructions on cell culture at the beginning of my PhD, Andi for the safety instructions, as well as Katharina and Ruth for keeping the cell culture room tidy and clean. I am very grateful to Wolfgang for solving the computer and equipment problems, as well as Anna, Ursula, Melinda, Marus and Olga for keeping the lab running.

Many thanks to Dr. Martina Rüffer and now Uli for preparing the traditional Weißwurst, St. Nicholas chocolate and Glühwein, as well as Ines, Jasmin and Dominik for the organization of lab activities, especially the impressive and great music played by our Christmas band, Dominik, Philipp H. and Ines. I would also like to thank our lunch group, Dongsheng, Xiaowen, Dian-Jang, Wei, Xiudong, Jie and Yanfang for the interesting and extensive discussions, also the basketball games with Dian-Jang,

Sören, Philipp K., Philipp H. and Stephan for the exciting moments of making a goal. Thanks also to my neighbor Adam for the helpful discussions, and to Ana, Bojan and Jonathan for the funny time especially in my first and only skiing trip. Many thanks to all the AK Wagner members for the nice atmosphere and unforgettable time we spent together.

Special thanks to China Scholarship Council for supporting my study and life in Munich. I also want to thank the international office of LMU and my CSC scholarship colleagues for making my first step in Germany easier. Many thanks to all my friends for helping and caring me all the time.

Finally, I want to express my gratitude to my parents and parents-in-law for their constant support and trust in my life. I would also like to thank my older sister for always being there for me. Whenever I'm in trouble, it always makes me calm and optimistic that I know I can count on my family.

Last but not least, I want to express my deepest gratitude to my beloved wife Mingqian for her sincere love and continuous support. We have been through a lot together, we will experience more in the future, no matter what will happen, with you, my life will be always beautiful.